NASA Contractor Report 191521

System Identification for Space Station Freedom Using Observer/Kalman Filter Markov Parameters

Michael Papadopoulos
Robert H. Tolson

Joint Insitute for Advancement of Flight Sciences
The George Washington University
Langley Research Center, Hampton, VA

Grant NAG1-1416
August 1993

National Aeronautics and Space Administration

Langley Research Center
Hampton, Virginia 23681-0001

ABSTRACT

The Modal Identification Experiment (MIE) is a proposed experiment to define the dynamic characteristics of Space Station Freedom. Previous studies have emphasized free-decay modal identification. The feasibility of using a forced response method (Observer/Kalman Filter Identification (OKID)) is addressed. The interest in using OKID is to (1) determine the input mode shape matrix which can be used for controller design or control-structure interaction analysis, and (2) investigate if forced response methods may aid in separating closely space modes. A model of the SC-7 configuration of Space Station Freedom was excited using simulated control system thrusters to obtain acceleration output. It is shown that an 'optimum' number of outputs exist for OKID. To recover global mode shapes, a modified method, called Global-Local OKID, was developed. This study shows that using data from a long forced response followed by free-decay leads to the 'best' modal identification. Twelve out of the thirteen target modes were identified for such an output. In contrast, five, six, and six target modes were recovered from the three individual twenty second forced simulations. In addition, the 'on-off' commands to the thrusters can be used to produce step inputs for system identification.

NOMENCLATURE

n	System order
A_c	Continuous system (state) matrix
B_c	Continuous control input matrix
C	Output matrix
D	Direct transmission matrix
A	Discrete system (state) matrix
B	Discrete control input matrix
$\bar{A}$	Observer system (state) matrix
$\bar{B}$	Observer control input matrix
p	Observer decay
No	Number of outputs (measurements)
Ni	Number of inputs (excitations)
l	Data length
l^*	Observer data length
u	Input data matrix
y	Output data matrix
Y	System Markov Parameter matrix
$\bar{Y}$	Observer Markov Parameter matrix

V	Discrete observability matrix and/or Observer input matrix
W	Discrete controllability matrix
$H(k-1)$	(k-1)th time shift Hankel data matrix
P_n	Truncated left matrix of singular vectors
D_n	Truncated diagonal matrix of singular values
Q_n	Truncated right matrix of singular vectors
G	Observer gain
No^*	Independent output subset in OKID
$\bar{No}$	Remaining output subset ($No - No^*$)
C^*	Output matrix for No^*
D^*	Direct transmission matrix for No^*
$\bar{C}$	Output matrix for $\bar{No}$
$\bar{D}$	Direct transmission matrix for $\bar{No}$

TABLE OF CONTENTS

I. INTRODUCTION

Space structures (e.g., Space Station Freedom (SSF)) are becoming increasingly complex. To mathematically model such structures requires high-fidelity finite element methods, which may necessarily increase cost (time, money, etc.). Component mode synthesis (CMS) techniques can be used to circumvent this dilemma. These techniques discretize a structure into components and analyses are done component by component. Component results are then truncated and combined to form a complete system model. But even CMS, while computationally efficient, has its drawbacks, namely, it is highly susceptible to modal truncation errors.[1] Consequently, any finite element or continuum model, for that matter, will be in error primarily due to modeling issues. These models, therefore, require validation or correction before they can be used for control design or control-structure interaction analysis, for example. One method which accomplishes this task is linear system identification. Linear system identification is the process of using experimental data to obtain a linear model and, if unknown, the data's noise characteristics. The data can be obtained from either ground-based or operational testing. However, this process is also not without difficulties.[2,3] Some of the challenging issues include extrapolation from a one-g to a zero-g environment if ground-based data is used, high modal density, low frequency range of interest, nonlinearity, non-classical damping, and limited excitation and measurement capabilities.[4] In the end, a model based as much on theory as on experiment is required for any meaningful analysis.

The Modal Identification Experiment (MIE) is a proposed experiment to determine the dynamic characteristics of the SSF in orbit. While MIE is not required in the Space

Station Freedom Program, it is an extension of the structure verification effort and there are numerous benefits. The first benefit is to improve the finite element modeling techniques for large space structures. In particular, damping estimates for these structures are still basically unknown. Good estimates are necessary because the steady state vibration amplitude near a resonance frequency is inversely proportional to the damping. Another benefit is to provide improvements in second-generation design of equipment.[5]

Many methods exist in the linear system identification area.[6] Some work in time and others in the frequency domain. This study considers only time-domain methods since they were found to be superior to the frequency domain methods on the SSF due to the wide frequency range of interest.[4] In particular, the Eigensystem Realization Algorithm (ERA)[7] is one such method which can use free-decay for modal identification. However, it may be difficult to identify closely spaced modes because of their similarity in modal amplitudes. In addition, one mode may decay faster than the other and may not be identified. A forced response method may provide better identification since both modes will be varying in amplitude and phase during the excitation.

Recently, the Observer/Kalman Filter Identification Method (OKID)[8] was developed for application to forced response data. Previous studies have addressed methods for determining the modal characteristics using free response data.[4] This study addresses the feasibility of using the OKID method. One issue is the knowledge of the input forces since there is no plan to measure the forces on the SSF in orbit. In particular, the actual inputs produced by the ACS (attitude control system) jets are known to have a rise and

fall time, whereas, the commanded inputs are step inputs. The effect of this on the system identification using OKID is investigated. Another issue is the limited amount of forced response data. That is, the baseline experiment length is 120 seconds with only 20 seconds of forcing.

II. FORMULATION OF EIGENSYSTEM REALIZATION ALGORITHM (ERA)

The equations of motion for a linear structure are often written as a set of finite-dimensional, linear, second-order differential equations

$$M(t)\ddot{q}(t) + C_v(t)\dot{q}(t) + K(t)q(t) = f(t) \tag{2.1}$$

where the square matrices $M(t)$ and $K(t)$ are mass and stiffness and $C_v(t)$ represents the damping mechanism, which is assumed to be viscous. The vector $q(t)$ contains the generalized displacements and $f(t)$ is the load vector.

With

$$x(t) = \begin{Bmatrix} q(t) \\ \dot{q}(t) \end{Bmatrix}$$

Eq. (2.1) can be equivalently put into state-variable or fundamental form

$$\begin{aligned} \dot{x}(t) &= A_c(t)x(t) + B_c(t)u(t) \\ y(t) &= C(t)x(t) + D(t)u(t) \end{aligned} \tag{2.2}$$

where subscript c denotes a continuous time matrix. The matrix A_c represents the mass, damping, and stiffness, and B_c characterizes the input $u(t)$, that is, it contains the input locations and could also contain conversion factors if $u(t)$ is, for example, voltage. The measurement matrix C selects the proper terms from the state vector $x(t)$ and finally, D is the direct transmission matrix where the input appears directly in the measurement vector $y(t)$ and exists only if the measurements are acceleration.

A solution to Eqs. (2.2) exists if $A_c(t)$ and $B_c(t)$ do not vary with time (in which case $C(t)$ and $D(t)$ also do not vary with time) and is written

$$x(t) = e^{A_c(t-t_0)}x(t_0) + \int_{t_0}^{t} e^{A_c(t-\tau)}B_c u(\tau)\,d\tau \tag{2.3}$$

Without loss of generality, let t_0=0. Then Eq. (2.3) becomes

$$x(t) = e^{A_c t}x(0) + \int_{0}^{t} e^{A_c(t-\tau)}B_c u(\tau)\,d\tau \tag{2.4}$$

Eq. (2.4) should be discretized in time to reflect the fact that in practice measurements are available at discrete times only. Therefore, if we assume a sampling rate of Δt then

$$t = k\Delta t$$
$$x(k\Delta t) = e^{A_c k\Delta t}x(0) + \int_{0}^{k\Delta t} e^{A_c(k\Delta t-\tau)}B_c u(\tau)\,d\tau \quad , \quad k=1,\ldots,\infty \tag{2.5}$$

If k is increased by 1 to k+1 we obtain

$$x([k+1]\Delta t) = e^{A_c \Delta t}x(k\Delta t) + \int_{k\Delta t}^{(k+1)\Delta t} e^{A_c([k+1]\Delta t-\tau)}B_c u(\tau)\,d\tau \ , \quad k=0,\ldots,\infty \tag{2.6}$$

Eq. (2.6) is cumbersome to use in practice because of the need to integrate for each value of k. However, if we assume that the input $u(s)$ is constant over the interval $[k\Delta t,(k+1)\Delta t)$, that is, $u(s)=u(k\Delta t)$ for all s when $k\Delta t \le s < (k+1)\Delta t$ (which is often done in digital control applications where the input is generated by computer), then it can be shown that Eq. (2.6) becomes

$$\begin{aligned} x([k+1]\Delta t) &= Ax(k\Delta t) + Bu(k\Delta t) \\ y(k\Delta t) &= Cx(k\Delta t) + Du(k\Delta t) \end{aligned} \quad , \quad k=0,1,\ldots,\infty \qquad (2.7)$$

where

$$A = e^{A_c \Delta t} = \sum_{m=0}^{\infty} \frac{A_c^m (\Delta t)^m}{m!}$$

$$B = \left[\int_0^{\Delta t} e^{A_c \tau} d\tau \right] B_c = \left[\sum_{m=0}^{\infty} \frac{A_c^m (\Delta t)^{m+1}}{m!} \right] B_c$$

Dropping the notation $k\Delta t$ in favor of k, realizing that when we say k we mean $k\Delta t$, we obtain the discrete state-variable equations

$$\begin{aligned} x(k+1) &= Ax(k) + Bu(k) \\ y(k) &= Cx(k) + Du(k) \end{aligned} \quad , \quad k=0,1,\ldots,\infty \qquad (2.8)$$

The matrix $A \epsilon \Re(n,n)$, where $\Re(n,n)$ is the set of real n x n matrices, $B \epsilon \Re(n,Ni)$, $C \epsilon \Re(No,n)$, and $D \epsilon \Re(No,Ni)$ where No and Ni are the number of outputs and inputs, respectively, and n is the system order (equal to twice the number of vibration modes). Eqs. (2.8) represent a recursive algorithm for computing the measurement responses (e.g., position, velocity, or acceleration) at the sampling instances without the need for integration. The only assumption is that the input is constant over the sampling time. This assumption is called a zero-order hold and will be discussed further in section 8.3.

The output can be calculated from Eqs. (2.8) but requires the state vector. An explicit solution (depending only on the input) can be obtained by carrying out a few operations from Eqs. (2.8). Assuming $x(0)=0$

$$
\begin{aligned}
x(1) &= Bu(0) \\
x(2) &= ABu(0) + Bu(1) \\
x(3) &= A^2Bu(0) + ABu(1) + Bu(2) \\
&\vdots
\end{aligned}
$$

$$
\begin{aligned}
y(0) &= Du(0) \\
y(1) &= CBu(0) + Du(1) \\
y(2) &= CABu(0) + CBu(1) + Du(2) \\
y(3) &= CA^2Bu(0) + CABu(1) + CBu(2) + Du(3) \\
&\vdots
\end{aligned}
$$

From above, the solution can then be written as

$$
y(k) = \sum_{i=0}^{k} Y_{k-i} u(i) \tag{2.9}
$$

where

$$
Y_j = \begin{cases} D & j=0 \\ CA^{j-1}B & j>0 \end{cases}
$$

$Y_j, j \geq 0$ are called the Markov Parameters or pulse response functions and are the solution to Eqs. (2.8) when a unit pulse is applied, i.e.,

$$
u(k) = \begin{cases} 1 & k=0 \\ 0 & k>0 \end{cases}
$$

It should be pointed out that the Markov Parameters are unique while $\{A, B, C, D\}$ need not be unique. That is, there exists many sets of $\{A, B, C, D\}$ that give the same pulse response. To see this, let T represent a non-singular coordinate transformation ($z = Tx$), then

$$A' = T^{-1}AT$$

$$B' = T^{-1}B$$

$$C' = CT$$

The Markov Parameters under this transformation are

$$Y'_k = C'A'^{k-1}B' = (CT)(T^{-1}AT)^{k-1}(T^{-1}B) \tag{2.10}$$

But since $(T^{-1}AT)^{k-1} = T^{-1}A^{k-1}T$ (Appendix A), Eq. (2.10) becomes

$$Y'_k = CA^{k-1}B = Y_k$$

Since there are an infinite number of coordinate transformations, there are an infinite number of realizations that give the same Markov Parameters.

For a linear system with zero-order hold inputs, the Markov Parameters contain all the information about the system (i.e., A, B, C, D). The purpose of minimum realization theory is to find state-space matrices $\{A, B, C, D\}$ given the sequence of Markov Parameters Y_k, $0 \le k < \infty$ such that the dimension of A is as small as possible.

To realize the state-space matrices from test data we make use of the following result from Ho and Kalman[9]:

> The sequence Y_k has a finite-dimensional realization if and only if there is an integer n and constants $(\alpha_1, \alpha_2, \ldots, \alpha_n)$ such that
>
> $$Y_{n+j} = \sum_{i=1}^{n} \alpha_i Y_{n-i+j}$$
>
> for all $j > 0$.

Simply put, this mean that there are only n linearly independent Markov Parameters. To test this result, and as an application to be used later, let us form the $rNo \times cNi$ block data matrix

$$H(k-1) = \begin{bmatrix} Y_k & Y_{k+1} & Y_{k+2} & \cdots & Y_{k+c-1} \\ Y_{k+1} & Y_{k+2} & Y_{k+3} & \cdots & Y_{k+c} \\ \vdots & \vdots & \vdots & \ddots & \vdots \\ Y_{k+r-1} & Y_{k+r} & Y_{k+r+1} & \cdots & Y_{k+r+c-2} \end{bmatrix} \quad , \quad k \geq 1 \qquad (2.11)$$

$H(k-1)$ is called a generalized Hankel matrix where No and Ni are the number of measurements (outputs) and inputs, respectively. In theory, we have the following result

$$\lim_{r,c \to \infty} rank[H(k-1)] = n$$

In practice, however, $H(k-1)$ is usually full rank for all values of r and c due to noise.

Eq. (2.11) is composed of pulse response data where each Markov Parameter, of size $No \times Ni$, represents the response at a particular time instant. Each Markov Parameter can be partitioned as follows

$$Y_j = \begin{bmatrix} Y_{11} & Y_{12} & \cdots & Y_{1Ni} \\ Y_{21} & Y_{22} & \cdots & Y_{2Ni} \\ \vdots & \vdots & \ddots & \vdots \\ Y_{No1} & Y_{No2} & \cdots & Y_{NoNi} \end{bmatrix} \quad , \quad j = k, k+1, \ldots, k+r+c-2$$

where the first column represents the response at the No outputs due to a pulse input at the first input, keeping all other inputs at zero. Likewise, the last column is the response at the No outputs due to a pulse input at the $Ni'th$ input, keeping all other inputs at zero.

Notice that the Hankel matrix consists of Markov Parameters that are incremented equally in the row and column directions. This does not have to be the case but will not be discussed further.

Eq. (2.11) can also be written in the form

$$H(k-1) = \begin{bmatrix} CA^{k-1}B & CA^{k}B & CA^{k+1}B & \cdots & CA^{k+c-2}B \\ CA^{k}B & CA^{k+1}B & CA^{k+2}B & \cdots & CA^{k+c-3}B \\ \vdots & \vdots & \vdots & \ddots & \vdots \\ CA^{k+r-2}B & CA^{k+r-1}B & \cdots & \cdots & CA^{k+r+c-3}B \end{bmatrix} \tag{2.12}$$

or more simply as

$$H(k-1) = VA^{k-1}W \tag{2.13}$$

where

$$V = \begin{bmatrix} C \\ CA \\ CA^2 \\ \vdots \\ CA^{r-1} \end{bmatrix} \quad , \quad W = \begin{bmatrix} B & AB & A^2B & \cdots & A^{c-1}B \end{bmatrix}$$

V and W are the discrete observability and controllability matrices and are of sizes $rNo\,x\,n$ and $n\,x\,cNi$, respectively.

Let us briefly discuss the significance of these two matrices. The state vector in Eqs. (2.8) can be succinctly written as

$$x(p)-A^p x(0) = \begin{bmatrix} B & AB & A^2B & \cdots & A^{p-1}B \end{bmatrix} \begin{bmatrix} u(p-1) \\ u(p-2) \\ \vdots \\ u(0) \end{bmatrix} = W_p U_p \qquad (2.14)$$

for $p>0$. Eq. (2.14) suggests an important question. That is, can the state be driven to any arbitrary state from an initial state by a proper selection of the input? We can then define the following

> The system (Eqs. 2.8) is (completely) state controllable if any state can be reached from any initial state in a finite time interval by some finite control action (input).

Obviously, this controllability is related to the matrix W_p. In particular, the solution for the control action becomes

$$U_p = W_p^+ [x(p)-A^p x(0)]$$

where + denotes the pseudoinverse. For the input to affect the state $[x(p)]$, W_p has to be full row rank. The size of W_p is $n \times pNi$. If we assume that $n>pNi$, then there exists more equations than unknowns and a least squares solution can be performed, in which case it is not possible to exactly reach an arbitrarily selected state because an error term will always exist (i.e. we can only minimize the error term). However, if we assume that $n \leq pNi$, then although a non-unique solution for $n<pNi$ exists, we can exactly reach the state. Therefore, $p \geq integer\left[\frac{n}{Ni}\right]$ and because W_p has to be full row rank, the state is controllable if $rank[W_p]=n$. A physical interpretation of this is that

there are n basis vectors of W_p that span the set of controllable states.

To examine observability, consider the output from Eqs. (2.8). The observability matrix is

$$V_p = \begin{bmatrix} C \\ CA \\ CA^2 \\ \vdots \\ CA^{p-1} \end{bmatrix}$$

and must be full column rank. Like controllability, we can define the following

> The system (Eqs. 2.8) is (completely) state observable if the knowledge of the input $u(k)$ and the output $y(k)$ completely determines the state $x(p)$ where $0 \leq k \leq p$.

From Kalman's duality theorem[10], the corresponding statements for observability follow from the previous controllability discussion. That is, the state is observable if $rank[V_p] = n$.

The concepts of observability and controllability play an important role in system identification. This is important because it can be shown that a minimum realization exists if and only if a system is observable and controllable[11].

It is now necessary to condense the Hankel matrix in Eq. (2.11). The three most common data reduction algorithms are least squares, transformations, and coherent averaging[12]. We will consider only the transformation algorithms, in particular, the singular value decomposition (SVD). Simply put, the SVD allows the determination of

the rank of a matrix (Appendix B). The Hankel matrix for k=1 is decomposed as follows

$$H(0)_{rNo\,x\,cM} = P_{rNo\,x\,rNo}\, D_{rNo\,x\,cM}\, Q^{T}_{cM\,x\,cM}$$

Theoretically, the number of non-zero singular values in D is taken as the rank of $H(0)$. Practically, all singular values will be non-zero due to measurement noise, computer round-off, etc. The problem then is how to select a cut-off. If the singular values decrease significantly then rank selection is simple. This case is shown by the top graph of Figure 2.1. The clean data (noise free) represents a three-degree-of-freedom (order=six) simulation (discussed in section 6.2). Because the system has order six there should, theoretically, be only six non-zero singular values. The non-zero singular values beyond six are due to round-off errors. If, however, they transition smoothly (which almost always occurs for real data) one is at a loss, as shown in the bottom graph of Figure 2.1. This noisy data was obtained from simulation results on the SC-7 configuration of SSF (discussed in chapter 9). Typical rank selection methods include keeping all singular values above a prescribed tolerance or choosing where there is a sudden change in slope of successive singular values[12]. It should be noted that this rank will represent only the strong modes (highly excited). There will often be modes (weakly or not at all excited) which may not appear in the decomposition. Denoting this rank by n, truncate $H(0)$ such that

$$H(0)_{rNo\,x\,cM} \approx P_{rNo\,x\,n}\, D_{n\,x\,n}\, Q^{T}_{n\,x\,cM} \qquad (2.15)$$

where we have selected the first n columns of P and Q and the first n columns and

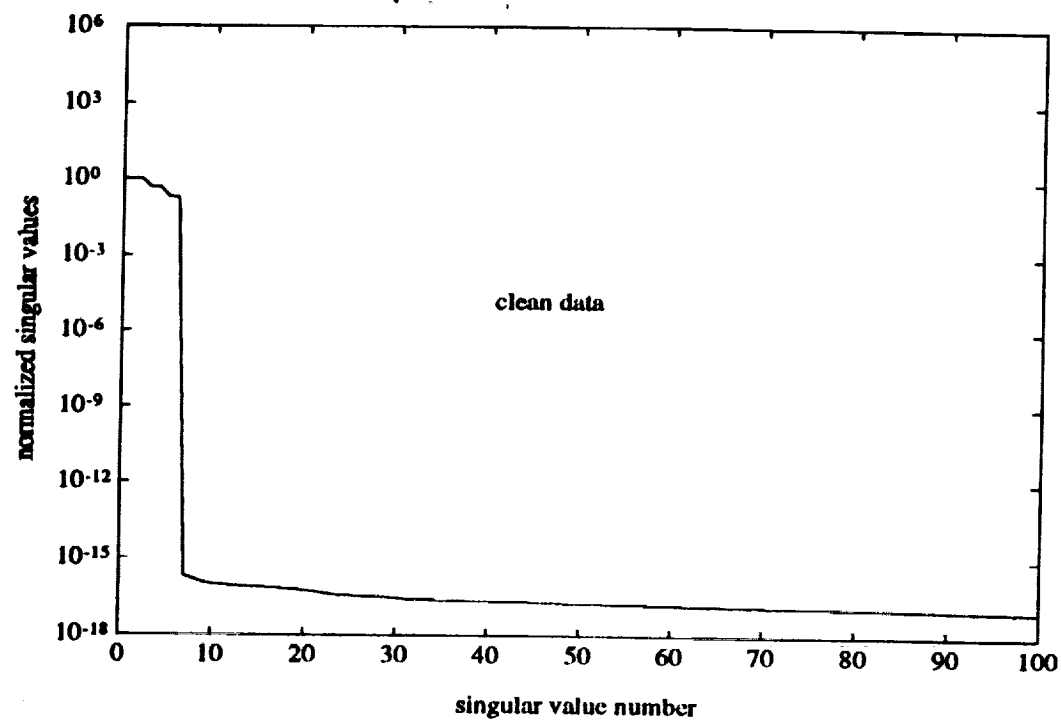

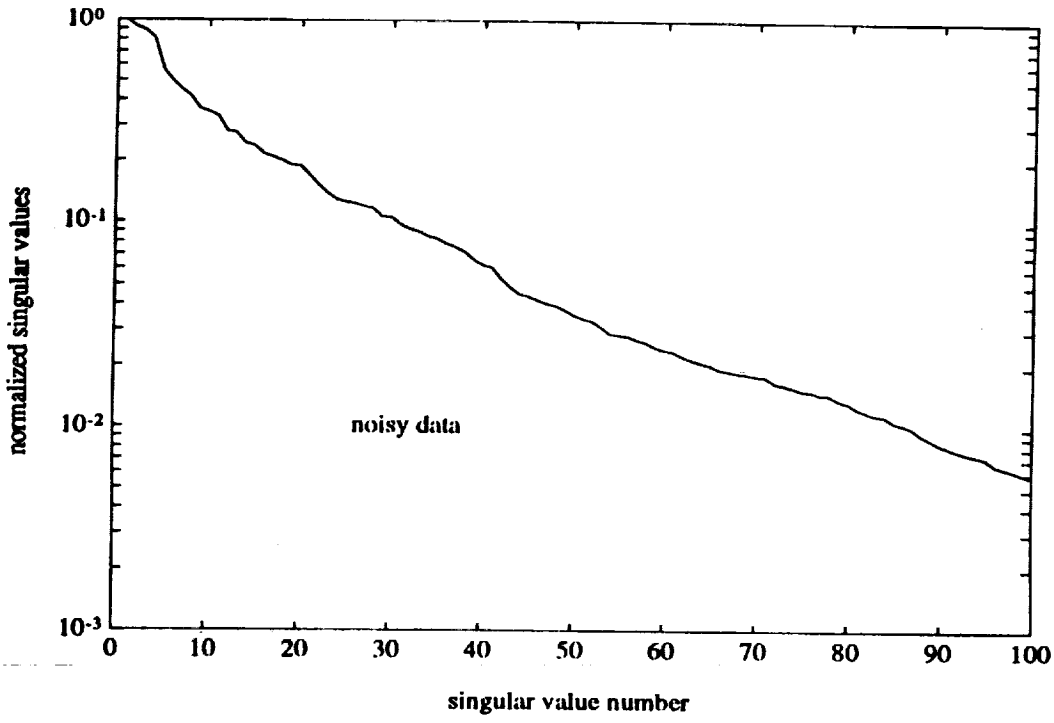

Figure 2.1 Singular value distribution for data without and with noise

rows of D. Hereafter, denote the truncated versions of P, D, Q as P_n, D_n, Q_n.

Equating Eq. (2.15) and (2.13), remembering that k=1

$$P_n D_n Q_n^T = VW \tag{2.16}$$

There are three natural ways to partition Eq. (2.16). The input normal form is

$$V = P_n D_n$$
$$W = Q_n^T$$

The output normal form is

$$V = P_n$$
$$W = D_n Q_n^T$$

The internally balanced form is

$$V = P_n D_n^{1/2}$$
$$W = D_n^{1/2} Q_n^T \tag{2.17}$$

It has been shown by Juang[13] that while there is really no essential numerical difference between the three forms, the internally balanced form is slightly better conditioned and will therefore be used in this development.

From Eqs. (2.13) and (2.17), we immediately have

$$C = E_{No} V = E_{No} P_n D_n^{1/2}$$
$$B = WE_{Ni} = D_n^{1/2} Q_n^T E_{Ni}$$

E_{No} and E_{Ni} are selection matrices and denote

$$E_{No} = \left[I_{No} \;\; 0_{No} \;\; 0_{No} \;\; \cdots \;\; 0_{No} \right] \quad (No \, x \, rNo) \qquad , \qquad E_{Ni} = \begin{bmatrix} I_{Ni} \\ 0_{Ni} \\ 0_{Ni} \\ \vdots \\ 0_{Ni} \end{bmatrix} \quad (cNi \, x \, Ni)$$

where 0_{No} and 0_{Ni} are zero square matrices. These matrices are used as a notational device rather than computationally. The A matrix may be obtained from Eq. (2.13) with k=2

$$H(1) = VAW$$

Since V is full row rank and W full column rank

$$A = (V^T V)^{-1} V^T H(1) W^T (WW^T)^{-1}$$

But making use of the orthogonality of V and W and Eqs. (2.17)

$$(V^T V)^{-1} V^T = (D_n^{1/2} P_n^T P_n D_n^{1/2})^{-1} D_n^{1/2} P_n^T = D_n^{-1/2} P_n^T$$

$$W^T (WW^T) = Q_n D_n^{1/2} (D_n^{1/2} Q_n^T Q_n D_n^{1/2})^{-1} = Q_n D_n^{-1/2}$$

Therefore,

$$A = D_n^{-1/2} P_n^T H(1) Q_n D_n^{-1/2}$$

and a minimum realization (of order n) exists and is given by

$$\begin{aligned} C &= E_{No} P_n D_n^{1/2} \\ A &= D_n^{-1/2} P_n^T H(1) Q_n D_n^{-1/2} \\ B &= D_n^{1/2} Q_n^T E_{Ni} \end{aligned} \qquad (2.18)$$

An eigendecomposition on the discrete matrix A such that

$$A\varphi = \varphi z$$

allows for the determination of the discrete eigenvalues located along the diagonal of the z matrix. Transform the discrete eigenvalues to continuous space by

$$\lambda_i = \frac{\ln(z_i)}{\Delta t} \qquad , \qquad i=1,...,n$$

if $k=1$ is used in Eq. (2.11), $Re(\lambda_i) = -\zeta_i w_{n_i}$ and $Im(\lambda_i) = w_{d_i} = w_{n_i}\sqrt{1-\zeta_i^2}$; w_{d_i} is the damped natural frequency. The system natural frequency and damping are then

$$w_{n_i} = |\lambda_i|$$

$$\zeta_i = \frac{-Re(\lambda_i)}{w_{n_i}}$$

where | | denotes magnitude. The output and input mode shapes (usually referred to as mode shapes and modal participation factors, respectively) can then be determined from $C\varphi$ and $\varphi^{-1}B$. This is the formulation of the ERA. Free-decay, instead of pulse response data, can also be used in the Hankel matrix since it can be shown that they have the same structure as the Markov Parameters.[14] In summary, the computational steps are

1) Obtain pulse response or free-decay data

2) Form Hankel matrices $H(0)$ and $H(1)$; Eq. (2.11)

3) Perform the SVD on $H(0)$ and truncate keeping only the significant modes; Eq. (2.15)

4) Compute $\{A,B,C,D\}$; Eqs. (2.18). If using pulse response, D obtained from first $Ni'th$ columns of Y matrix. If using free-decay, D does not exist

III. FORMULATION OF OBSERVER/KALMAN IDENTIFICATION (OKID)

The following formulation parallels the development presented in Ref. 8. We start with the familiar state-variable equations,

$$\begin{aligned} x(k+1) &= Ax(k) + Bu(k) \\ y(k) &= Cx(k) + Du(k) \end{aligned} \quad , \quad k \geq 0 \tag{3.1}$$

Assuming that this system is initially at rest (x(0)=0), the input/output histories can be represented in matrix form as

$$y_{No\,x\,l} = Y_{No\,x\,Ml}\; U_{Ml\,x\,l} \tag{3.2}$$

where

$$y = \begin{bmatrix} y(0) & y(1) & \cdots & y(l-1) \end{bmatrix}$$

$$Y = \begin{bmatrix} D & CB & CAB & \cdots & CA^{l-2}B \end{bmatrix}$$

$$U = \begin{bmatrix} u(0) & u(1) & u(2) & \cdots & u(l-1) \\ & u(0) & u(1) & \cdots & u(l-2) \\ & & u(0) & \cdots & u(l-3) \\ & & & \ddots & \vdots \\ & & & & u(0) \end{bmatrix}$$

Y represents the pulse response matrix (whose block elements are known as Markov Parameters) and is of dimension $No\ x\ Nl$ where l is the number of data points, y is the known output data matrix, and U is the known input data matrix in upper block triangular form.

A comment should be made regarding Eq. (3.2). For a full rank input data matrix U, Y can be solved from Eq. (3.2) for $m=1$ since the number of equations is equal to the number of unknowns. A number of problems quickly arise with this course of

action. The size of U would be considerable since a large l is usually required for 'good' identification. This presents computer memory limitations. Furthermore, if sufficiently rich inputs are not used, U^{-1} becomes ill-conditioned. And lastly, one input may be inadequate to identify all the structural modes regardless of the number of outputs. For $m>1$, Y will not be unique, whereas it is known that it must be unique for a finite-dimensional linear system. That is, we cannot know *the* solution for Y out of an infinite number of solutions.

If we assume that A is asymptotically stable, that is, $A^k \approx 0$ $k \geq p$, then Eq. (3.2) can be written as

$$y_{No\,x\,l} \approx Y_{No\,x\,Ni(p+1)}\, U_{Ni(p+1)\,x\,l} \tag{3.3}$$

where

$$y = \begin{bmatrix} y(0) & y(1) & \cdots & y(l-1) \end{bmatrix}$$

$$Y = \begin{bmatrix} D & CB & CAB & \cdots & CA^{p-1}B \end{bmatrix}$$

$$U = \begin{bmatrix} u(0) & u(1) & u(2) & \cdots & u(p) & \cdots & u(l-1) \\ & u(0) & u(1) & \cdots & u(p-1) & \cdots & u(l-2) \\ & & u(0) & \cdots & u(p-2) & \cdots & u(l-3) \\ & & & & \vdots & \ddots & \vdots \\ & & & & u(0) & \cdots & u(l-p-1) \end{bmatrix}$$

We realize that as p increases the approximation in Eq. (3.3) becomes more exact. Unfortunately, a large p is required for lightly damped structures. We now face the same problem we had in trying to solve for Y in Eq. (3.2), namely, the large size of U. This dilemma can be solved, however, if we feed the output to the state equation. This

will transform the state in Eqs. (3.1) to what appears as an observer state. An observer determines state estimates from a dynamic system for the state of another system. Eqs. (3.1) can then be solved because it will artificially increase the system damping due to the arbitrariness of the observer gain. The observer model is constructed from Eqs. (3.1) by adding and subtracting a state term, $Gy(k)$, where G is the observer gain, to give

$$\begin{aligned} x(k+1) &= Ax(k) + Bu(k) + Gy(k) - Gy(k) \\ y(k) &= Cx(k) + Du(k) \end{aligned}$$

or by substituting $y(k)$ from the above equation

$$\begin{aligned} x(k+1) &= Ax(k) + Bu(k) + G[Cx(k) + Du(k)] - Gy(k) \\ &= (A + GC)x(k) + (B + GD)u(k) - Gy(k) \end{aligned}$$

Now introduce the following notation

$$\bar{A} = A + GC$$

$$\bar{B} = [B + GD \ , \ -G]$$

$$v(k) = \begin{bmatrix} u(k) \\ y(k) \end{bmatrix}$$

to yield the linear observer model

$$\begin{aligned} \bar{x}(k+1) &= \bar{A}\bar{x}(k) + \bar{B}v(k) \\ y(k) &= C\bar{x}(k) + Du(k) \end{aligned} \quad , \quad k \geq 0 \qquad (3.4)$$

The matrix representation of the input/output histories of Eqs. (3.4) is

$$y_{No \times l} = \bar{Y}_{No \times [(Ni+No)(l-1)+Ni]} \, V_{[(Ni+No)(l-1) \times Ni] \times l} \qquad (3.5)$$

where

$$y = \begin{bmatrix} y(0) & y(1) & y(2) & \cdots & y(l-1) \end{bmatrix}$$

$$\bar{Y} = \begin{bmatrix} D & C\bar{B} & C\bar{A}\bar{B} & \cdots & C\bar{A}^{l-2}\bar{B} \end{bmatrix}$$

$$V = \begin{bmatrix} u(0) & u(1) & u(2) & \cdots & u(l-1) \\ & v(0) & v(1) & \cdots & v(l-2) \\ & & v(0) & \cdots & v(l-3) \\ & & & \ddots & \vdots \\ & & & & v(0) \end{bmatrix}$$

$\bar{Y}$ will be referred to as the Observer Markov Parameter matrix because it is the matrix of Markov Parameters of an observer system. Note that the size of V is even larger than U because we have included the outputs in the input matrix. As before, if we assume that $\bar{A}$ is asymptotically stable, $\bar{A}^k \approx 0 \; k \geq p$, then Eq. (3.5) becomes

$$y_{q \times l} = \bar{Y}_{q \times [(m+q)p + m]} \; V_{[(m+q)p + m] \times l} \tag{3.6}$$

where

$$y = \begin{bmatrix} y(0) & y(1) & y(2) & \cdots & y(l-1) \end{bmatrix}$$

$$\bar{Y} = \begin{bmatrix} D & C\bar{B} & C\bar{A}\bar{B} & \cdots & C\bar{A}^{p-1}\bar{B} \end{bmatrix}$$

$$V = \begin{bmatrix} u(0) & u(1) & u(2) & \cdots & u(p) & \cdots & u(l-1) \\ & v(0) & v(1) & \cdots & v(p-1) & \cdots & v(l-2) \\ & & v(0) & \cdots & v(p-2) & \cdots & v(l-3) \\ & & & & \vdots & \ddots & \vdots \\ & & & & v(0) & \cdots & v(l-p-1) \end{bmatrix}$$

The next objective is to compute the system Markov Parameters from the Observer Markov Parameters. Since $Y_k = CA^{k-1}B$, let $\bar{Y}_k = C\bar{A}^{k-1}\bar{B}$ and define the following

$$Y = \left[Y_0 \;\; Y_1 \;\; Y_2 \;\; \cdots \;\; Y_{l-1}\right] = \left[D \;\; CB \;\; CAB \;\; \cdots \;\; CA^{l-2}B\right]$$

$$\bar{Y} = \left[\bar{Y}_0 \;\; \bar{Y}_1 \;\; \bar{Y}_2 \;\; \cdots \;\; \bar{Y}_{l-1}\right] = \left[D \;\; C\bar{B} \;\; C\bar{A}\bar{B} \;\; \cdots \;\; C\bar{A}^{l-2}\bar{B}\right]$$

$$\bar{Y}_k = \left[\bar{Y}_k^{(1)} \;,\; \bar{Y}_k^{(2)}\right] \qquad , \qquad k = 1, \ldots, \infty$$

Then, the relationship between the Observer Markov Parameters and the system Markov Parameters can be shown to be[8]

$$Y_k = \bar{Y}_k^{(1)} + \sum_{i=1}^{k} \bar{Y}_i^{(2)} Y_{k-i} \qquad , \qquad k \geq 1 \tag{3.7}$$

$$Y_o = \bar{Y}_o = D$$

Note that for $k \geq p+1$, $\bar{Y}_k$ and therefore $\bar{Y}_k^{(1)}$ and $\bar{Y}_k^{(2)}$ are considered to be zero. Therefore, Eqs. (3.7) can be written as

$$\begin{aligned} Y_k &= \bar{Y}_k^{(1)} + \sum_{i=1}^{k} \bar{Y}_i^{(2)} Y_{k-i} \qquad , \qquad k = 1, \ldots, p \\ Y_k &= \sum_{i=1}^{p} \bar{Y}_i^{(2)} Y_{k-i} \qquad , \qquad k = p+1, \ldots, \infty \end{aligned} \tag{3.8}$$

Observe from Eqs. (3.8) that by the choice of p, there will be only p independent Markov and Observer Markov Parameters and consequently the maximum system order is $(No)p$ (see Eq. (2.11)). Solve Eq. (3.6) for $\bar{Y}$ and use Eqs. (3.8) to recover Y. It is important to realize that the inputs and outputs must be as linearly independent as possible to prevent any numerical ill-conditioning of the V matrix in Eq. (3.6).[8] A state space model, (A,B,C,D), may then be realized from the sequence Y_k using ERA[7].

IV. FORMULATION OF GLOBAL-LOCAL OKID (GLOKID)

4.1 Introduction

It has been shown that the OKID uses general input/output data to compute the pulse response of an asymptotically stable observer. The Markov Parameters of the original system are then determined recursively from the Markov Parameters of the observer system from which a realization can be obtained. However, this method may have difficulties if a limited amount of data is available for the identification process and limited capability to perform repeated experiments. This will be true of orbiting structures such as the Space Station. Also, since these vehicles are becoming more complex, e.g., high modal density, it may be necessary to use many outputs and inputs. In addition, spatial information may be lost if not all the measurements are used and there may be numerical ill-conditioning problems when the measurements are not all independent.

Section 4.2 presents a new version of OKID suited for these purposes. This modified method (GLOKID) considers a subset of outputs from which 'system' frequencies and damping are obtained. The global mode shapes are then formed by appending two local mode shapes, one from OKID and the other from a least squares process on the remaining measurement set (i.e., the set not used in OKID).

4.2 Problem Formulation

GLOKID begins with the premise that only a few outputs should be used for determination of $\bar{Y}$. Letting No^* represent this reduced output set and renaming l to

l^* where l^* is the number of observer data points, then

$$y_{No^* \times l^*} = \bar{Y}_{No^* \times [(Ml+No^*)p \times Ml]} \; V_{[(Ml+No^*)p \times Ml] \times l^*} \tag{4.1}$$

After solving for $\bar{Y}$ from Eq. (4.1), recover Y and use ERA to realize a state-space model of the system (A, B, C^*, D^*). Note that C^* and D^* are only valid for No^* outputs and A and B are assumed independent of the number of observations (outputs). $\bar{C}$ and $\bar{D}$ may be recovered for the remaining outputs $(\bar{No})$ by the following algebraic manipulations

$$y_{\bar{No} \times l} = Y_{\bar{No} \times Ml} \; U_{Ml \times l}$$

$$y = \begin{bmatrix} \bar{D} & \bar{C}B & \bar{C}AB & \cdots & \bar{C}A^{l-2}B \end{bmatrix} \begin{bmatrix} u(0) & u(1) & u(2) & \cdots & u(l-1) \\ & u(0) & u(1) & \cdots & u(l-2) \\ & & u(0) & \cdots & u(l-3) \\ & & & \ddots & \vdots \\ & & & & u(0) \end{bmatrix}$$

$$y = \bar{D}\,u + \bar{C}\begin{bmatrix} B & AB & \cdots & A^{l-2}B \end{bmatrix} \begin{bmatrix} 0 & u(0) & u(1) & u(2) & \cdots & u(l-2) \\ & & u(0) & u(1) & \cdots & u(l-3) \\ & & & u(0) & \cdots & u(l-4) \\ & & & & \ddots & \vdots \\ & & & & & u(0) \end{bmatrix}$$

or

$$y_{\bar{No} \times l} = \begin{bmatrix} \bar{D} & \bar{C} \end{bmatrix} \begin{bmatrix} u \\ U^* \end{bmatrix} = \begin{bmatrix} \bar{D} & \bar{C} \end{bmatrix} \bar{U} \tag{4.2}$$

where

$$\bar{U} = \begin{bmatrix} u \\ U^* \end{bmatrix}$$

$$U^* = \begin{bmatrix} B & AB & \cdots & A^{l-2}B \end{bmatrix} \begin{bmatrix} 0 & u(0) & u(1) & u(2) & \cdots & u(l-2) \\ & & u(0) & u(1) & \cdots & u(l-3) \\ & & & u(0) & \cdots & u(l-4) \\ & & & & \ddots & \vdots \\ & & & & & u(0) \end{bmatrix}$$

Eq. (4.2) can be solved for $\bar{C}$ and $\bar{D}$ from

$$\begin{bmatrix} \bar{D} & \bar{C} \end{bmatrix} = y\bar{U}^+ = y\bar{U}^T(\bar{U}\bar{U}^T)^{-1} \tag{4.3}$$

It should be noted that the A matrix must be truncated after the eigendecomposition process to keep all 'system' frequencies and damping before evaluation of the $\bar{C}$ and $\bar{D}$ matrices. This truncation can be done by transforming A and B into modal space

$$\Lambda = \varphi^{-1}A\varphi$$
$$B_m = \varphi^{-1}B$$

where φ is the matrix of eigenvectors of A. In this form computational modes can be eliminated in a consistent manner. That is, if the 1st row and column of Λ is deleted then the 1st row of B_m is deleted. Maintaining the same notation after model reduction we now want to transform Λ to real block diagonal form.[13] This is done to allow the least squares process to work with real numbers. Let T be the similarity transformation that makes Λ real such that

$$\Lambda_R = T\Lambda T^{-1}$$

then B_m can be transformed to the real form by

$$B_R = TB_m$$

Eq. (4.2) can then be used again with $A=\Lambda_R$ and $B=B_R$ to get $\bar{C}$ and $\bar{D}$. Note that it is not necessary to perform the multiplication indicated in the U^* expression. The columns of U^* can be recursively calculated from

$$U^*(k+1) = AU^*(k) + Bu(k) \quad , \quad k \geq 0 \tag{4.4}$$

where $U^*(0)=0_{n\,x\,1}$. The global C and D matrices can then be obtained from

$$C = \begin{bmatrix} (C^*T^{-1})_{No^*\,x\,n} \\ \bar{C}_{\bar{No}\,x\,n} \end{bmatrix}$$
$$D = \begin{bmatrix} D^*_{No^*\,x\,Ni} \\ \bar{D}_{\bar{No}\,x\,Ni} \end{bmatrix} \tag{4.5}$$

In summary, the computational steps are

1) Select sensor subset No^* and perform OKID-ERA

2) Transform A and B to real form

3) Calculate $\bar{U}$; Eqs. (4.2) and (4.4)

4) Calculate $\bar{D}$ and $\bar{C}$ for the remaining outputs; Eq. (4.3)

5) Append $\bar{D}$ and $\bar{C}$ to C^*T^{-1} and D^*; Eqs. (4.5)

V. CRITERIA FOR MODE SELECTION

5.1 Introduction

Spurious modes will appear since it is not possible to identify the correct model order, which necessitates the use of mode indicators. A number of indicators are available, including modal amplitude coherence[7], modal phase collinearity[7], consistent mode indicator[15], extended mode amplitude coherence[15], mode singular value[16], mode strength ratio[15], modal monophasicity coefficient[17], and frequency and damping variance[16], to name a few. Only three indicators (mode singular value, modal monophasicity coefficient, and modal amplitude coherence) are used in this study and are discussed in sections 5.2, 5.3, and 5.4, respectively.

5.2 Mode Singular Value (msv)[16]

The Markov Parameters in modal coordinate form are written as

$$Y_m = \left[Y_{m_1}\ Y_{m_2}\ \cdots\ Y_{m_l}\right] = \left[C_m B_m\ C_m \Lambda B_m\ \cdots\ C_m \Lambda^{l-1} B_m\right] \tag{5.1}$$

where

$$B_m = \begin{bmatrix} b_1 \\ b_2 \\ \vdots \\ b_n \end{bmatrix} \quad , \quad C_m = \left[c_1\ c_2\ \cdots\ c_n\right]$$

The vectors in B_m are 1 x *Ni* row vectors, C_m contains *No* x 1 column vectors, and Λ is a diagonal matrix of eigenvalues. Consider the first and second terms in Y_m,

$$Y_{m_1} = C_m B_m = [c_1 c_2 \ldots c_n] \begin{bmatrix} b_1 \\ b_2 \\ \vdots \\ b_n \end{bmatrix} = \sum_{i=1}^{n} c_i b_i$$

$$Y_{m_2} = C_m \Lambda B_m = \sum_{i=1}^{n} c_i \lambda_i b_i$$

From above, we can conclude that $Y_{m_k} = \sum_{i=1}^{n} c_i \lambda_i^{k-1} b_i \quad , \quad k = 1, \ldots, l$. Therefore Eq. (5.1) can be rewritten as

$$Y_m = \left[\sum_{i=1}^{n} c_i b_i \quad \sum_{i=1}^{n} c_i \lambda_i b_i \quad \cdots \quad \sum_{i=1}^{n} c_i \lambda_i^{l-1} b_i \right]$$

The mode singular value is then defined as

$$msv_i = \sqrt{|c_i||b_i| / (1 - |\lambda_i|)} \qquad , \qquad i = 1, \ldots, n$$

when l is sufficiently long. A larger *msv* means a higher contribution to the recovered pulse response (Markov Parameters). For obvious reasons, the mode singular value should be computed only for stable eigenvalues. When normalized by the maximum singular value *msv* will range between 0 and 1.

5.3 Modal Monophasicity Coefficient (mmc)

The following development follows Ref. 17. The mmc begins with the idea of a monophase mode. That is, a mode that has the same phase (within a multiple of 180°) at all output points. For example, each output will reach its respective maximum displacement at the same time. Theoretically, all modes will be monophase if they are normal. Practically, a mode will be monophase if the damping is light.

Consider the identified mode shape matrix

$$\Phi = \left[\bar{\phi}_1 \; \bar{\phi}_2 \; \cdots \; \bar{\phi}_n\right]$$

Let the angle necessary to make $\bar{\phi}_k$ real be θ_k so we have

$$\phi_k = \bar{\phi}_k e^{i\theta_k} \qquad , \qquad k=1,\ldots,n \tag{5.2}$$

where ϕ_k is a real vector and $i=\sqrt{-1}$. However, ϕ_k cannot be exactly real due to errors in the identification of Φ and the fact that $\bar{\phi}_k$ is not truly normal. But it is possible to minimize the imaginary component in a mean square sense.

Let

$$\bar{\phi}_k = \begin{Bmatrix} r_{k1} e^{i\bar{\theta}_{k1}} \\ r_{k2} e^{i\bar{\theta}_{k2}} \\ \vdots \\ r_{kq} e^{i\bar{\theta}_{kq}} \end{Bmatrix}$$

where q is the number of outputs. Therefore Eq. (5.2) becomes

$$\phi_k = \begin{Bmatrix} r_{k1} e^{i\bar{\theta}_{k1}} \\ r_{k2} e^{i\bar{\theta}_{k2}} \\ \vdots \\ r_{kq} e^{i\bar{\theta}_{kq}} \end{Bmatrix} e^{i\theta_k}$$

The problem can now be stated as follows:

Find the angle θ_k such that

$$J_k = \sum_{j=1}^{q} \left(Im\left[r_{kj} e^{i(\bar{\theta}_{kj} + \theta_k)} \right] \right)^2 \quad , \quad k = 1, \ldots, n$$

is minimized.

The necessary condition becomes $\frac{\partial J_k}{\partial \theta_k} = 0$, therefore

$$\tan(2\theta_k) = \frac{2\sum_{j=1}^{q} r_{kj}^2 \sin(\bar{\theta}_{kj}) \cos(\bar{\theta}_{kj})}{\sum_{j=1}^{q} r_{kj}^2 (\sin^2(\theta_{kj}) - \cos^2(\theta_{kj}))} \quad , \quad k = 1, \ldots, n$$

but since $r_{kj} e^{i\bar{\theta}_{kj}} = x_{kj} + i y_{kj}$

$$\tan(2\theta_k) = \frac{2\sum_{j=1}^{q} x_{kj} y_{kj}}{\sum_{j=1}^{q} \left(y_{kj}^2 - x_{kj}^2 \right)} \quad , \quad k = 1, \ldots, n$$

However, there will remain some imaginary components since we can only minimize J_k. To measure this deviation calculate J_k, i.e.,

$$J_k = \sum_{j=1}^{q} \left(y_{kj}^2 + (x_{kj}^2 - y_{kj}^2) \sin^2(\theta_k) + x_{kj} y_{kj} \sin(2\theta_k) \right) \quad , \quad k = 1, \ldots, n$$

Since $(I_{xx})_k + (I_{yy})_k$ is invariant for any orthogonal transformation, we can define a parameter which measures the degree of monophasicity, namely

$$mmc_k = 1 - \frac{J_k}{(I_{xx})_k + (I_{yy})_k} \quad , \quad k = 1, \ldots, n$$

where $(I_{xx})_k = \sum_{j=1}^{q} x_{kj}^2$ and $(I_{yy})_k = \sum_{j=1}^{q} y_{kj}^2$. The *mmc* ranges between 0 and 1, where unity

means a monophase mode and zero means a mode with no phase coherence.

5.4 Modal Amplitude Coherence (γ)[7]

The following is taken from Ref. 7. The modal amplitude coherence is defined as the coherence between the modal amplitude history and an ideal one formed by extrapolating the initial value of the history to later points using the identified eigenvalue. The modal amplitude obtained from the Hankel decomposition is

$$\varphi^{-1} D_n^{1/2} Q_n^T = [q_1, q_2, ..., q_n]^*$$

where * denotes complex conjugate transpose and φ is the eigenvector matrix. The idealized modal amplitude history is obtained from

$$\bar{q}_i^* = \left[b_i^*, e^{(s_i \Delta t s_i)} b_i^*, ..., e^{(s_{m-1} \Delta t s_i)} b_i^*\right] \qquad , \qquad i = 1, ..., n$$

where s_i represents the continuous eigenvalues and b_i are the rows of the control input matrix. The coherence parameter (γ) for the ith mode is defined as

$$\gamma_i = \frac{\left|\bar{q}_i^* q_i\right|}{\left[\left(\bar{q}_i^* \bar{q}_i\right)\left(q_i^* q_i\right)\right]^{1/2}}$$

where | | represents magnitude. If γ_i is unity, the approximate mode matches the 'exact' mode identified from the data; if it equals zero, the approximate mode is orthogonal to the 'exact' mode. It should be mentioned that it is better to use the extended mode amplitude coherence and/or consistent mode indicator since γ does not work very well.

VI. ISSUES IN APPLICATION OF OKID-ERA

6.1 Introduction

Now that we have presented the OKID-ERA method, several questions are raised. First, how many data points per unknown are required in the least squares solution for the Observer Markov Parameters? Second, what is a proper p value? And last, what is an appropriate size of the Hankel matrix? These questions can be answered by considering the numerical example presented in section 6.2.

6.2 Role of parameters in OKID-ERA

To illustrate the behavior of the OKID-ERA method as p, l, and size of $H(0)$ are varied, results from a three-degree-of-freedom system (n=6) will be presented.[8] The system is a single input/two output (SIMO) case with the following discrete model

$$A = diag\left[\begin{Bmatrix} 0.9856 & 0.1628 \\ -0.1628 & 0.9856 \end{Bmatrix}, \begin{Bmatrix} 0.8976 & 0.4305 \\ -0.4305 & 0.8976 \end{Bmatrix}, \begin{Bmatrix} 0.8127 & 0.5690 \\ -0.5690 & 0.8127 \end{Bmatrix}\right]$$

$$B = \begin{bmatrix} 0.0011 & 0.0134 & -0.0016 & 0.0072 & 0.0011 & 0.0034 \end{bmatrix}^T$$

$$C = \begin{bmatrix} 1.5119 & 0.0000 & 2.0000 & 0.0000 & 1.5119 & 0.0000 \\ 1.3093 & 0.0000 & 0.0000 & 0.0000 & -1.3093 & 0.0000 \end{bmatrix}$$

$$D = \begin{bmatrix} 0 \\ 0 \end{bmatrix}$$

The displacement response of the system to a random input with standard deviation of 20 was generated and corrupted with process and measurement noise having the covariances

$$Q = diag[0.0242 \;\; 3.592 \;\; 0.0534 \;\; 1.034 \;\; 0.0226 \;\; 0.2279]x10^{-4}$$

$$R = diag[2.785 \;\; 2.785]x10^{-2}$$

The sample interval is 0.1 seconds. The natural frequencies are 0.261, 0.712, and 0.972 Hz with modal damping of 0.639, 1.01, and 1.30%. The resulting data sequences were then analyzed by OKID-ERA.

The results are shown in Table 6.1 for varying number of data points per unknown ($l/(Ni+No)p+Ni$), p values, and dimensions of the $H(0)$ matrix. It is clear from Table 6.1 that the frequency and damping are poor when the p value is equal to the system order (=6). This poor identification is expected since the Observer Markov Parameters, $\bar{Y}_k$, are not zero for $k>p$ when p is low due to the noise. When p is increased to $2n$ (=12), the results improve dramatically except the damping. However, notice that the results have begun to stabilize when the number of columns of the Hankel matrix are greater than the number of rows. That is, the frequency and damping do not change much when the number of columns equals two, three, or four times the number of rows. The bias in the damping is largely removed when p is set to $5n$ (=30). Stability with increasing Hankel matrix size is again evident. When the number of data points per unknown is increased to four, the damping estimates for mode 1 improve for p=30 as compared to two data points per unknown. As more data is included in the least squares process for $\bar{Y}$, the recovered Markov Parameters should be better identified.

Table 6.1 Three-degree-of-freedom simulation results using the OKID-ERA method

data per unknown	p	H(0) Matrix Row	H(0) Matrix Col	Mode 1 freq (Hz)	Mode 1 damp (%)	Mode 2 freq (Hz)	Mode 2 damp (%)	Mode 3 freq (Hz)	Mode 3 damp (%)
2	6	12	12	--	--	--	--	0.829	35.74
			24	--	--	--	--	0.850	35.52
			36	--	--	--	--	0.855	35.29
			48	--	--	--	--	0.856	35.25
	12	24	24	0.260	3.47	0.724	3.50	0.969	2.97
			48	0.259	3.97	0.724	3.27	0.970	3.20
			72	0.259	3.92	0.724	3.23	0.970	3.15
			96	0.259	3.88	0.724	3.22	0.970	3.15
	30	60	60	0.263	0.58	0.713	0.99	0.973	1.37
			120	0.262	1.34	0.714	1.04	0.973	1.41
			180	0.261	1.41	0.714	1.02	0.973	1.40
			240	0.261	1.30	0.714	1.02	0.973	1.40
4	6	12	12	0.322	52.84	--	--	0.906	14.43
			24	0.312	46.55	--	--	0.881	11.65
			36	0.318	46.60	--	--	0.875	11.64
			48	0.319	46.60	--	--	0.873	11.61
	12	24	24	0.259	0.93	0.714	1.35	0.975	2.69
			48	0.259	1.08	0.714	1.37	0.977	2.34
			72	0.259	1.11	0.714	1.37	0.977	2.25
			96	0.259	1.11	0.715	1.37	0.977	2.25
	30	60	60	0.261	0.751	0.712	0.946	0.973	1.43
			120	0.260	0.647	0.712	0.939	0.973	1.40
			180	0.260	0.616	0.712	0.939	0.973	1.40
			240	0.260	0.600	0.712	0.939	0.973	1.39
exact				0.261	0.639	0.712	1.01	0.972	1.30

-- indicates negative damping or unidentified mode

To see this consider Figure 6.1. The Markov Parameters for p=30 are compared for two, three, and four data points per unknown. It is clear that the Markov Parameters from three and four data points per unknown are almost identical. While the Markov Parameters for two data points per unknown is different from the others, it contains the essential characteristics, namely, proper phase and frequency.

In summary, the following can be concluded:

1) Frequencies are identified first while damping is more difficult

2) The p value should be 4 or 5 times the number of modes and Nop needs to be at least $>n$

3) A Hankel matrix size whose number of columns are twice the number of rows give acceptable results. That is, it may not be computationally feasible to use three or four times the number of rows when model order is high or for a system with multiple inputs and outputs

4) Two data points per unknown to determine $\bar{Y}$ give acceptable results. As stated in 3), it may not be feasible to use three or four data points per unknown

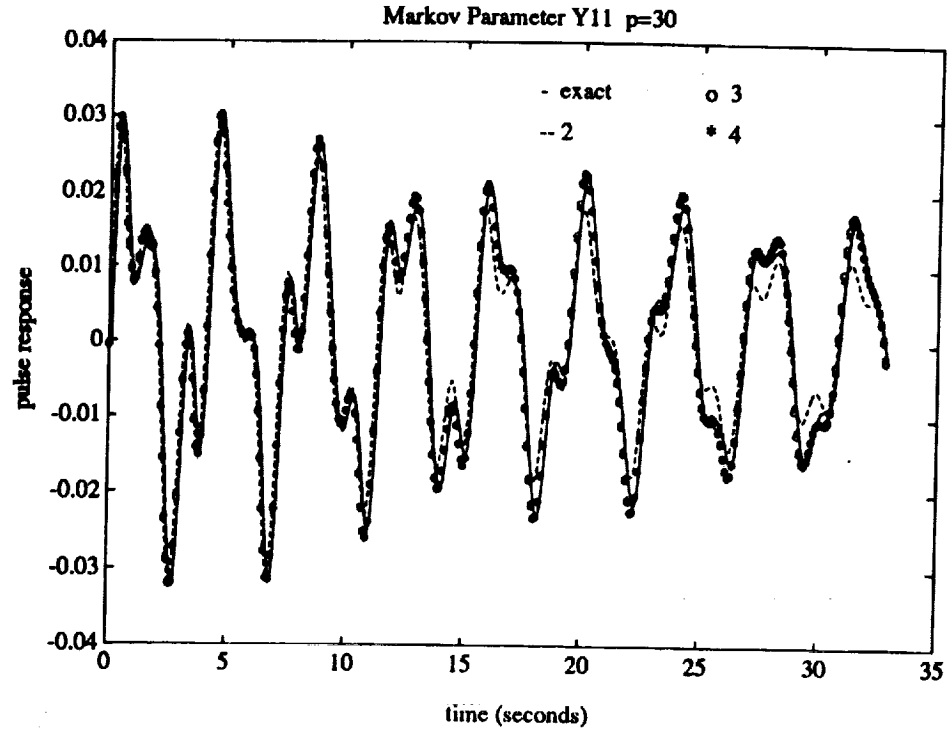

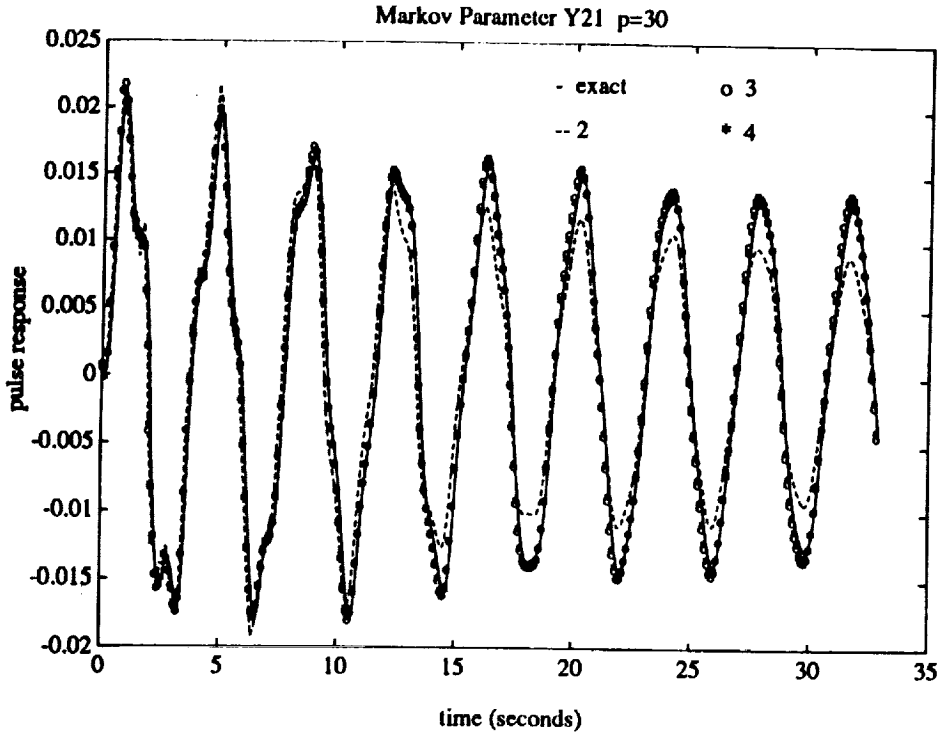

Figure 6.1 Markov Parameters for varying number of data points per unknown

VII. SC-7 Test Structure

The test structure SC-7, shown in Figure 7.1, represents an intermediate configuration of the SSF. This structure is particularly important since it is the first man tended configuration.

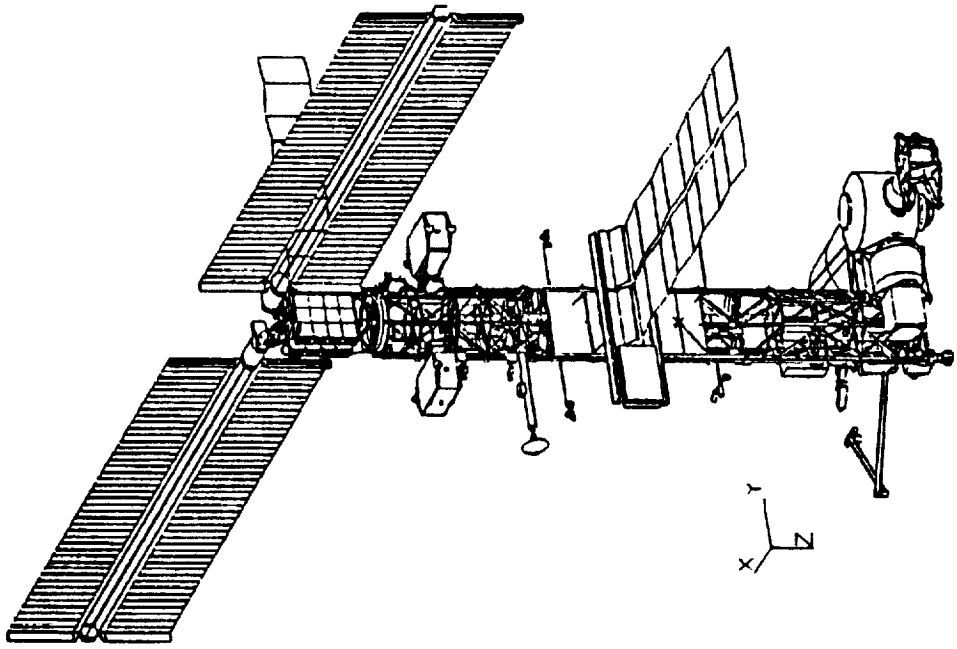

Figure 7.1 SC-7 configuration of SSF

The mass properties of the model are shown in Table 7.1.

Table 7.1 Mass properties of study configuration

Weight (lbs)		261129
Center of mass (in)	x	-10.8
	y	267.4
	z	71.7
Mass Moments of Inertia ($lb\text{-}sec^2\text{-}in$)	Ixx	237×10^6
	Iyy	41.1×10^6
	Izz	246×10^6
	Ixy	0.90×10^6
	Ixz	0.46×10^6
	Iyz	26.7×10^6

The SC-7 model consists of 207 modes (including the six rigid body modes) between 0 and 5 Hz. Figure 7.2 displays the frequency distribution. Modal damping of 1% was used for all modes. Of the 207 modes, only thirteen were selected as target modes[18] to provide a guide for the MIE design. The selection criteria[18] was as follows

1) All modes which could not be identified in a ground vibration test were included
2) The first and second truss bending modes in the XY and YZ planes and the first torsional mode were included
3) Use of the following indicators
    a) Kinetic energy distribution
    b) Kinetic energy maximum values and location
    c) Percentage of kinetic energy in truss
    d) Ratio of maximum truss deflection to maximum deflection of whole structure
    e) Engineering assessment using MSC/NASTRAN and MATLAB truss mode shape plots

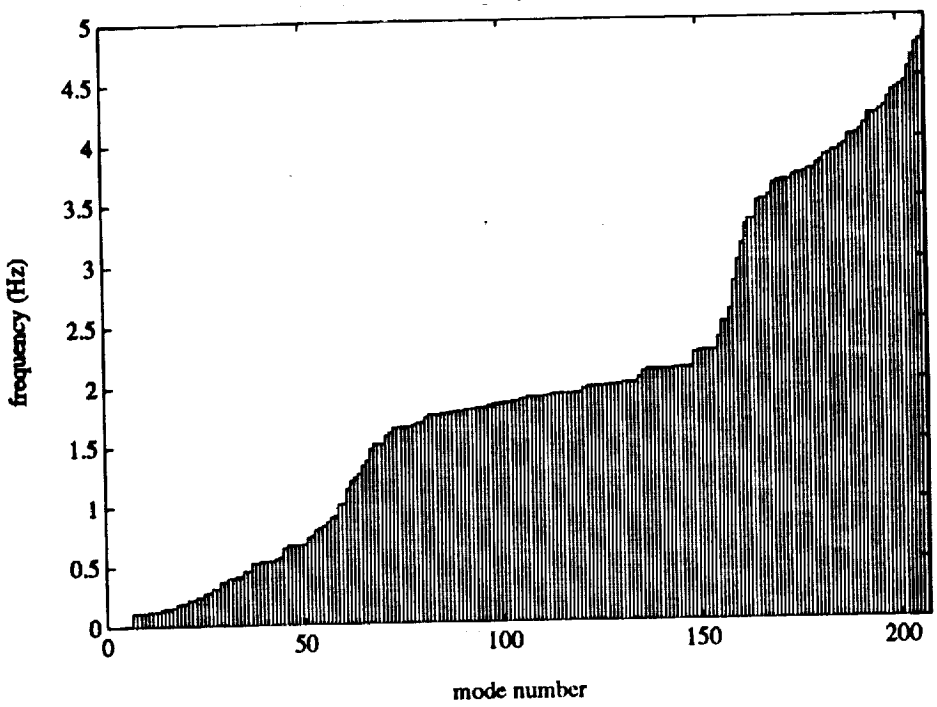

Figure 7.2 SC-7 frequency distribution

The thirteen target modes are shown in Table 7.2. The SSF (and SC-7) will use the ACS (Attitude Control System) and reboost thrusters for attitude control and reboost operations, respectively. These thrusters are located on the two propulsion modules seen in Figure 7.1 (the two boxes near the PV arrays).

Acceleration responses were generated at 61 points on the structure (Figure 7.3) from eight excitation locations (ACS thrusters only; Figure 7.4). Tables 7.3 and 7.4 list the excitation and response grid points with their corresponding directions, respectively.

Table 7.2 The thirteen target modes

freq (Hz)	damp (%)
0.5316749	1.00
0.5669868	1.00
0.7922026	1.00
0.8239532	1.00
0.8604512	1.00
1.133711	1.00
1.222703	1.00
1.367187	1.00
1.465167	1.00
1.502680	1.00
1.741080	1.00
2.029699	1.00
2.085652	1.00

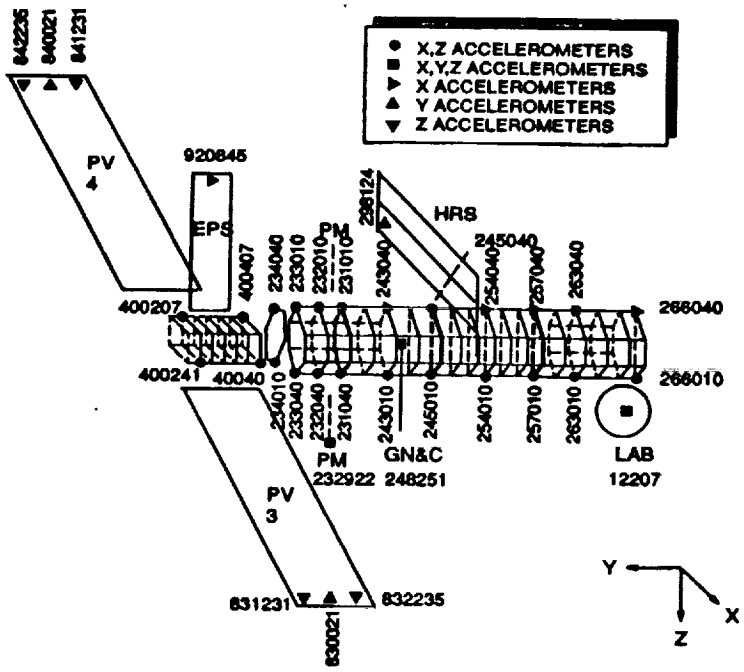

Figure 7.3 SC-7 measurement grid points

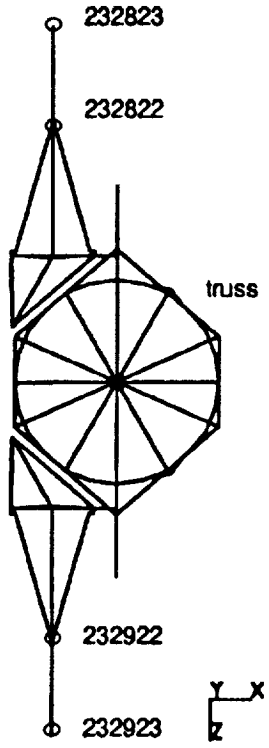

Figure 7.4 SC-7 excitation grid points

Table 7.3 Excitation locations (ACS thrusters) and directions

excitation location	direction
232822 (1)	x
232822 (2)	-x
232922 (3)	x
232922 (4)	-x
232823 (5)	z
232923 (6)	-z
232823 (7)	-y
232923 (8)	-y

( ) identifies input no.

Table 7.4 Measurement locations and directions; ( ) identifies output no.

measurement location	direction	measurement location	direction
12207 (1)	x	243010 (31)	x
12207 (2)	y	243010 (32)	z
12207 (3)	z	248251 (33)	x
231010 (4)	x	248251 (34)	y
231010 (5)	z	248251 (35)	z
231040 (6)	x	254010 (36)	x
231040 (7)	z	254010 (37)	z
233010 (8)	x	254040 (38)	x
233010 (9)	z	263010 (39)	x
233040 (10)	x	263010 (40)	z
233040 (11)	z	263040 (41)	x
234010 (12)	x	263040 (42)	z
234010 (13)	z	266010 (43)	x
234040 (14)	x	266010 (44)	z
234040 (15)	z	266040 (45)	x
243040 (16)	x	298124 (46)	y
245010 (17)	x	830021 (47)	y
245010 (18)	z	831231 (48)	z
245040 (19)	x	832235 (49)	z
245040 (20)	z	840021 (50)	y
257010 (21)	x	841231 (51)	z
257010 (22)	z	842235 (52)	z
257040 (23)	x	920845 (53)	x
232010 (24)	x	400207 (54)	x
232010 (25)	z	400207 (55)	z
232040 (26)	x	400241 (56)	x
232040 (27)	z	400241 (57)	z
232922 (28)	x	400404 (58)	x
232922 (29)	y	400404 (59)	z
232922 (30)	z	400407 (60)	x
		400407 (61)	z

VIII. MODELING OF INPUT FORCE

8.1 Excitation Design

This section was extracted from the work performed by McDonnell Douglas Space Systems Company (Ref. 18). The objective of the input force is to provide the proper excitation to the SC-7 structure so that the measured acceleration responses will be sufficient to identify the thirteen target modes. In orbit, the excitations will be produced by 'on-off' commands to the ACS and reboost thrusters. The ACS and reboost thrusters produce a steady state thrust of 25 and 50 lbs, respectively, with a minimum on-off time of 0.1 and 0.2 seconds. In this study, the ACS thrusters will have an on-off time of 0.2 seconds. However, because these thrusters operate as a blow down system they actually have a variable thrust which ranges from 25 to 9 lbs and 55 to 30 lbs for the ACS and reboost thrusters, respectively. The propulsion modules (which contain the thrusters) therefore have to be replaced periodically. The MIE should then be performed soon after replacement in order to make use of their full force capability (i.e., 25 lbs for ACS jets and 50 lbs for reboost jets).

The excitations will be in the form of randomized pulses which are tailored to excite the lower frequency modes during the earlier portion of the excitation pulse train and the higher frequency modes during the later portion. This arrangement excites the higher frequency modes just prior to the free-decay period, which typically decay quicker. Four sets of linearly independent random forcing functions (RFF) were generated to enhance the ability to identify closely spaced modes and are denoted herein as RFF1, RFF2, RFF3, and RFF4.

Each excitation (consisting of eight inputs) was designed such that it

1) does not continually excite a given frequency
2) maintains SSF within attitude and attitude rate limits (less than five degrees and 0.02 degrees per second, respectively)
3) does not exceed acceleration or load limits
4) provides a minimum modal response of one hundred micro-g for the target modes

The excitations represent five cycles of the lowest important mode (0.532 Hz) with a minimum of twenty seconds in order to provide an adequate number of pulses for exciting the lower frequency modes. A typical simulated ACS excitation is shown in Figure 8.1

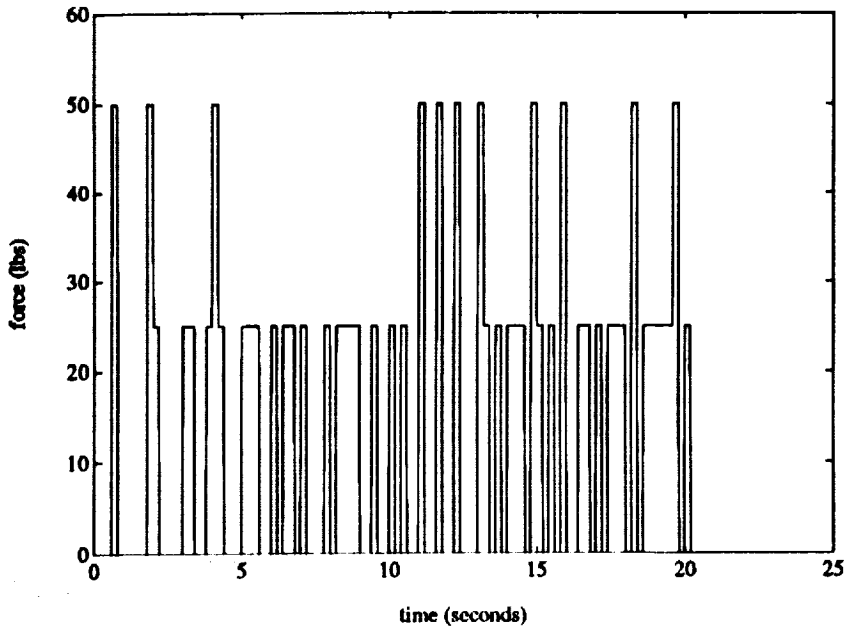

Figure 8.1 Simulated ACS excitation for input 8 of RFF1

8.2 Ramped vs Unramped Input

The unramped input shown in Figure 8.1 cannot be used in MSC/NASTRAN to perform a transient analysis because of a warning against the use of discontinuous excitations. A question then arises as how to model this type of input such that the response from this new input will agree with the response from that which would have been generated with the original input. The model also has to preserve the same characteristics as the original input, namely, it must maintain SSF attitude and attitude rate. A natural choice is to ramp the input making sure to preserve the area under the curve as shown in Figure 8.2.

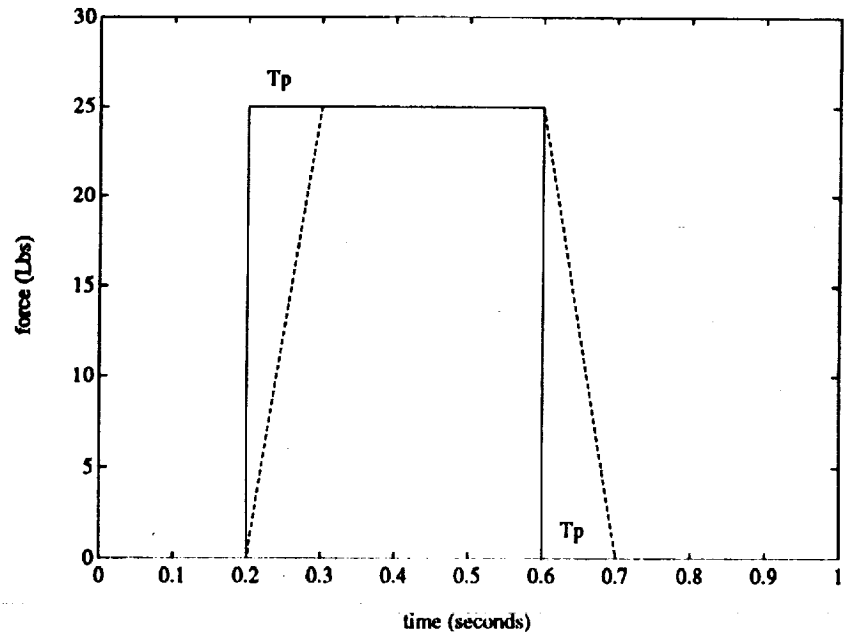

Figure 8.2 Ramped (dashed) and unramped (solid) input

The next question is what rise and fall time to use. It is assumed that the rise and fall times are the same and designated T_p. Tanner (private comm.)[19] showed that rise times of 0.01 and 0.02 produced no significant acceleration response differences while 0.04 showed some difference. T_p was then selected as 0.02. The format for this ramped input is as follows. If an 'on' command was given at 1.2 seconds, for example, the force would be zero at 1.2 seconds and 25 lbs at 1.22 seconds. With an 'off' command at 1.4 seconds, the same 0.02 seconds would be required before the force 'decayed' to zero, i.e., the force is 25 lbs at 1.4 seconds and zero at 1.42 seconds. To produce a 50 lb force the rise time should be the same as the rise time for the 25 lbs force since in this simulation the 50 lbs force was produced from two nearly collocated 25 lb jets (see Figure 7.3).

A Power Spectral Analysis was performed to illustrate the behavior of this model (a ramped input with T_p=0.02 for both 25 and 50 lb forces) to the original input. Figure 8.3 shows the Power Spectral Density of this model and the original unramped input for the first input sequence of RFF1. The solid line represents the original unramped (or square wave) input and the dashed line is the ramped input. As can be seen, there is no difference. This suggests that the ramped input and the original pulse input will excite the same frequencies. The Power Spectral Densities for all sequences show similar results and are given in Appendix C. This ramped input was subsequently used in MSC/NASTRAN to perform a transient analysis. The integration step size was 0.02 for the first 23 seconds (during the force input) and 0.05 seconds thereafter (private comm.: Martinovic)[20].

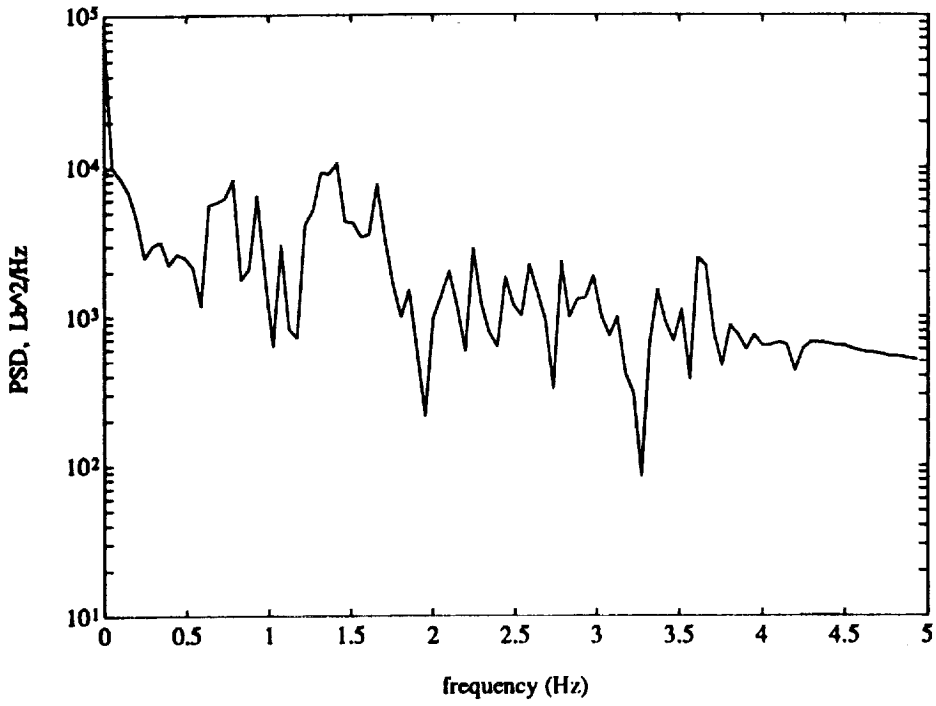

Figure 8.3 PSD of input 1 for ramped (dashed) and square wave (solid) input

8.3 Zero-Order Hold Input Models

While this new ramped input solved the integration problem, it presents another, namely, how to represent a ramped input in a zero-order hold format. The reason for this is that the input must be a zero-order hold since we are using the following discrete system

$$x(k+1) = Ax(k) + Bu(k)$$

One approach is to disregard the rise and fall time and represent the ramped input as an

unramped input (or in the other words, as the original pulse input). Another approach is to preserve the impulse (area) during one sampling interval. Table 8.1 shows the numerical differences between these approaches assuming the force goes from 0 to 25 lbs on the rise and from 25 to 0 lbs on the fall.

Table 8.1. Non-impulse and impulse preserved inputs

time (sec)	zero-order hold input formats	
	model A (impulse not preserved) Force (lbs)	model B (impulse preserved) Force (lbs)
0.1	0.0	0.0
0.2	25.0	22.5
0.3	25.0	25.0
0.4	25.0	25.0
0.5	25.0	25.0
0.6	0.0	2.5
0.7	0.0	0.0

The reason for the decrease in force for the second model is that the force is not 25 lbs at 0.2 seconds but 25 lbs at 0.22 seconds. Both input formats were used separately in an OKID-ERA analysis. Results will be shown with a p of 4, l of 568, and a Hankel matrix size of 244 x 248. Table 8.2 compares the number of identified modes from both models for RFF1c, RFF2c, and RFF4c. RFF1c, for example, refers to noise free (clean) acceleration responses using the RFF1 input sequences. This designation will be used throughout this study. Similarly, RFF1n is polluted (noisy) acceleration responses using

the RFF1 input sequences. Appendix I gives a discussion of the noise model. The recovered modes are listed in Appendix D. These modes were selected (criterion 1) based on 1) frequency error≤1%, 2) damping error≤20%, and 3) mac≥0.9. The mac is the normalized correlation coefficient between a recovered and an exact mode shape.

Table 8.2 Number of recovered modes for impulse and non-impulse preserved

test case	Number of modes	
	impulse preserved	non-impulse preserved
RFF1c	36	37
RFF2c	37	36
RFF4c	36	36

There appears to be little benefit from using the impulse preserved input. In fact, most of the frequencies are identified to at least two decimal places for both zero-order hold models. Also, their Power Spectral Densities are similar as seen in Figure 8.4 for input 1 of RFF1. The complete spectra for all test cases are given in Appendix E. The non-impulse preserved input for this analysis can therefore be used as a zero-order hold input in OKID.

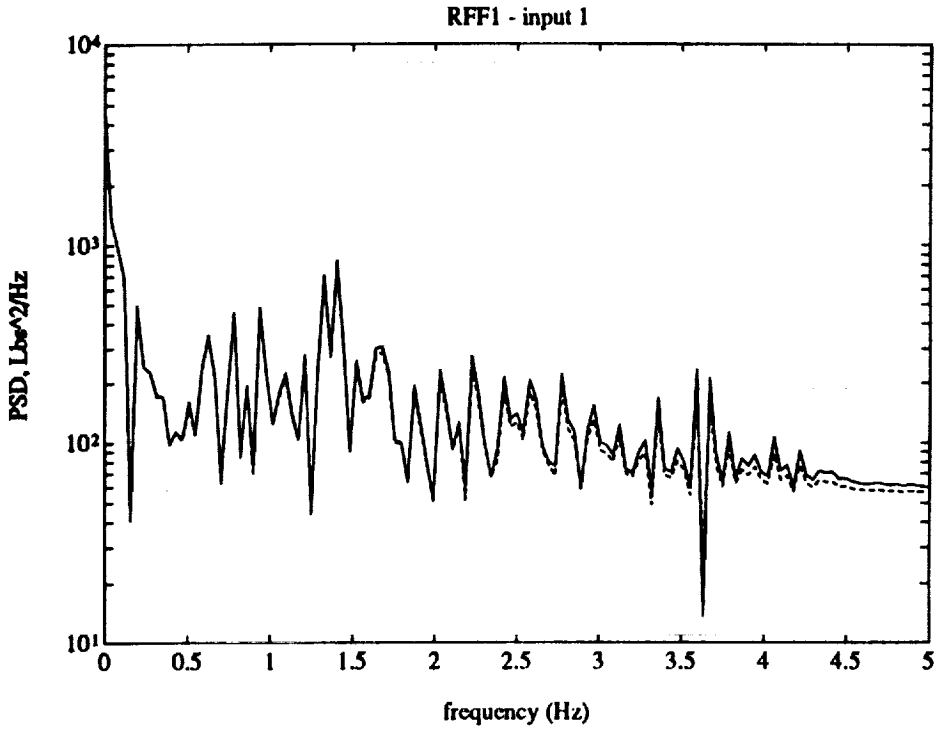

Figure 8.4 PSD of impulse (dashed) and non-impulse (solid) preserved input

8.4 'Exact' Thruster Input

The above analyses are not realistic in the sense that the actual input will neither be ramped nor square wave. A typical thruster firing exhibits a rise and fall time where the fall time will be longer than the rise time (private comm.: Popp)[21]. Also, there will be fluctuations in the force once the force reaches it nominal operating state (i.e., 25 lbs for the ACS jets). In addition, the force does not go to zero as soon as the thrusters are turned off. Figure 8.5 shows a result from an actual ACS thruster ground calibration test firing.[21]

Figure 8.5 Actual ACS thruster input

The horizontal axis plots time (0.05 seconds per block) and the vertical axis plots chamber pressure (psia). The large peak represents the engine running rough with spiking. Normally this spiking would not be seen. While Figure 8.5 represents pressure, the thrust should be in proportion. Acceleration measurements from this input should be obtained to determine if the different zero-order hold inputs (section 8.3) affect identification accuracy. That is, the issue is whether the 'on-off' times with a square wave are a reasonable assumption or will the rise and fall time have to be modeled. Before the integration could be performed, the actual thruster input had to be modeled. Rise and fall times of 0.03 and 0.25 seconds, respectively, with a random fluctuation of $\pm 3.7\%$ of the force at steady state were calculated from Figure 8.5. The fall time here is taken as the time it takes to fall to 1% of the steady state force.

Several models were investigated to represent the rise and fall time. They were the

polynomials, exponentials, and hyperbolic tangents. The polynomials ($n>0$; n=*order*) and exponentials were rejected on the rise because they did not adequately model the rounding of the top left corner of the pulse in Figure 8.5. The hyperbolic tangents and exponentials were rejected on the fall because no rounding was seen at the top right corner of the pulse in Figure 8.5 and they did not exhibit the 'right amount of decay'. The hyperbolic tangent and the polynomial ($n<0$) were finally selected to model the rise and fall, respectively. Again, the reason for having to model the thrust is that it will not be measured.

During the rise the force was modeled by a hyperbolic tangent function of the form

$$F(t) = A\tanh\alpha(t-t_0)+B$$

where

$$t_0 = t_{on}+\frac{T_{rise}}{2}$$

$$\alpha = 150$$

The fall was modeled using an inverse square power law of the following form

$$F(t) = \frac{C}{(t-t_{off}+\delta)^2}$$

A, B and C, δ are determined from the initial conditions (i.e., t_{on}, F_1 and $t_{on}+T_{rise}$, F_2 and t_{off}, F_3 and $t_{off}+T_{fall}$, F_4, respectively). Table 8.3 compares selected values of this input model to actual data. As seen, the model agrees quite well with experiment.

Table 8.3. Input model vs experimental data

	time (sec)	experiment Force (lbs)	model Force (lbs)
rise	0.00	0.00	0.00
	0.01	4.63	4.38
	0.02	20.37	20.62
	0.03	25.00	25.00
fall	0.30	25.00	25.00
	0.31	13.90	13.52
	0.32	8.30	8.50
	0.33	4.60	5.80
	0.40	0.93	1.18
	0.46	0.46	0.55

A transient analysis in MATLAB, a matrix manipulation program, was performed with this input using a constant step size 4th-order Runge-Kutta routine. The 'on-off' commands were obtained from RFF1. The integration step size was 0.002. Note that the input had a random error of ±3.7% of the force at steady state. An OKID-ERA analysis was performed on the clean data using both an impulse and a non-impulse preserved input. Since it is not possible to have an exact representation of the input, an input with no random error was used as the idealized input. The impulse preserved input was obtained from the idealized input and the non-impulse preserved input was the same as model 1 as discussed in section 8.2. The area for the impulse preserved input was calculated with the trapezoidal rule. To do this, data was generated every 0.0005 seconds

using the thruster model above and the area was summed every 0.1 seconds. Power Spectral Densities were compared for both these inputs. Figure 8.6 depicts the spectra for input 1 of RFF1.

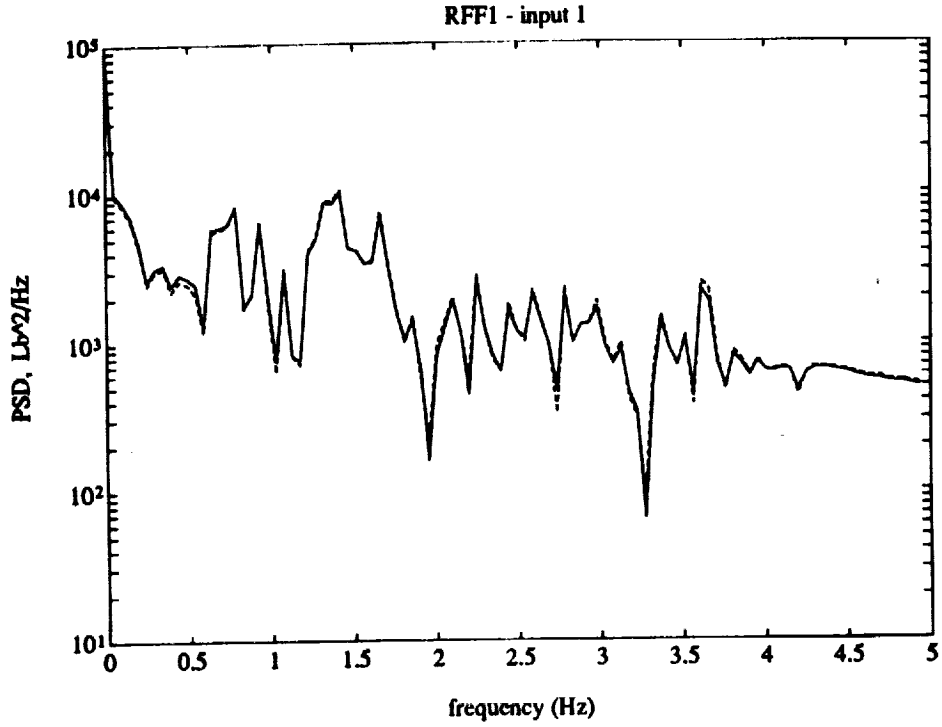

Figure 8.6 PSD of impulse (dashed) and non-impulse (solid) preserved input

The results for all forcing functions are given in Appendix F. It is seen that the impulse preserved input shows no significant difference in spectral content to the non-impulse preserved input. We therefore expect that both inputs will perform equally well in the identification process as was seen in section 8.2. However, these two inputs are different since the non-impulse preserved input will have a zero force when the impulse preserved

input will not. Using the non-impulse preserved input in the identification process assumes that the data will be in free-decay beyond twenty seconds when it is known that, initially, there will be no free-decay region as soon as the thruster is turned off. Rather, a few seconds (1 or 2) should pass before the data can be considered free-decay. Appendix G lists the recovered modes using criterion 1 (section 8.3) for p=5, l =706 and a Hankel matrix size of 305 x 616. As shown in the appendix, while the impulse and non-impulse preserved inputs identified different frequencies (attributed to the difference in power spectra), most of the modes are similar to at least one decimal place. Overall, 43 modes were recovered from the non-impulse preserved input and 42 for the impulse preserved input and because all the impulse preserved spectra are similar to the non-impulse preserved spectra, it can be concluded that there is no need to preserve the impulse and subsequently the 'on-off' commands can be used to produce square wave inputs for the purpose of system identification.

IX. RESULTS

9.1 Independent Measurement Selection

It has already been mentioned that independent inputs and measurements are required to minimize the numerical ill-conditioning of the pseudoinverse of the V matrix. To evaluate the independence, an SVD was performed on the inputs and outputs. As seen in Figure 9.1, the eight inputs are indeed independent since the maximum condition number for RFF1, RFF2, and RFF4 is 1.82. The outputs, however, are not independent as shown in Figure 9.2. That is, the noisy data deviates from the clean data somewhere around 30 outputs, which suggests that the noise dominates beyond at least 40 outputs. The reason why we say all the measurements are not independent is as follows. The rank of the measurement matrix does not change very much past, say, the 40th singular value. This would suggest that only 40 outputs are independent and the remaining 21 outputs are dependent. RFF1, RFF2, RFF3, RFF4, and RFF1 were concatenated in that order to generate an input sequence with a forcing time of 100 seconds. The reason for this will be explained later. This measurement set is called RFF1234n and has outputs which are not independent, as shown in Figure 9.3. The change in slope of the singular values suggest that at most 37 outputs are independent for all test cases.

The question, then, is how to select the independent measurements. The Gram-Schmidt Orthogonalization procedure is used for this purpose. That is, a measurement matrix (outputs listed row wise) was formed and the output with the minimum correlation with the other outputs is used as an initial reference (first output) to start the method. A new measurement matrix (consisting of 60 outputs) was formed after removal of the

minimum correlated output. The Gram-Schmidt procedure was performed (e.g., removal of all dependent components of the 60 outputs from the first output) and another measurement matrix was obtained. The second output then is the maximum magnitude squared (obtained row wise) of this new measurement matrix. This output is removed from the new measurement matrix, all dependent components of the remaining 59 outputs are then removed from the second output, and the third output is the maximum magnitude squared. This procedure is continued for all the outputs. Figures 9.4 and 9.5 plots the output magnitudes. Appendix H lists the ranking of the outputs based on magnitude squared (normalized by the maximum). A range of output cut-offs in the 30's is seen for RFF1n, RFF2n, RFF4n, and RFF1234n, which suggests that those are the only independent measurements.

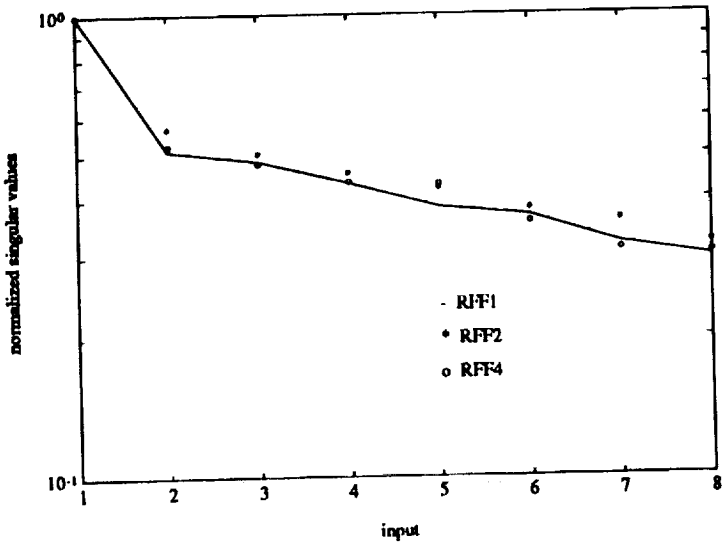

Figure 9.1 Singular value distribution for the eight inputs

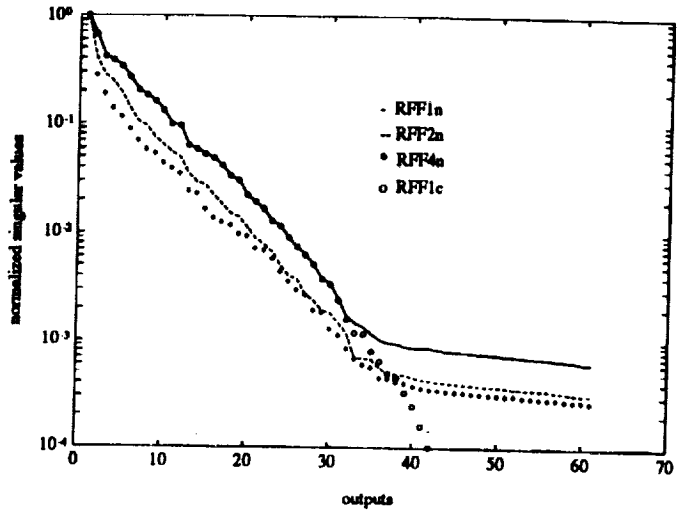

Figure 9.2 Singular value distribution for the outputs

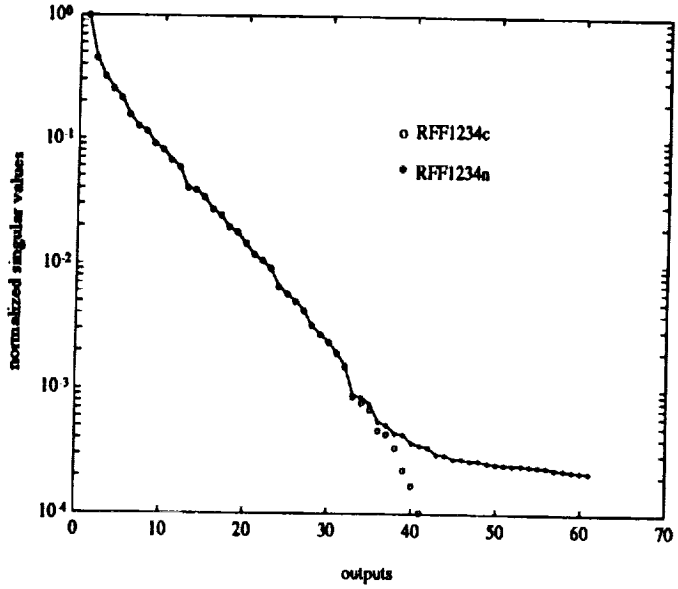

Figure 9.3 Singular value distribution for the outputs

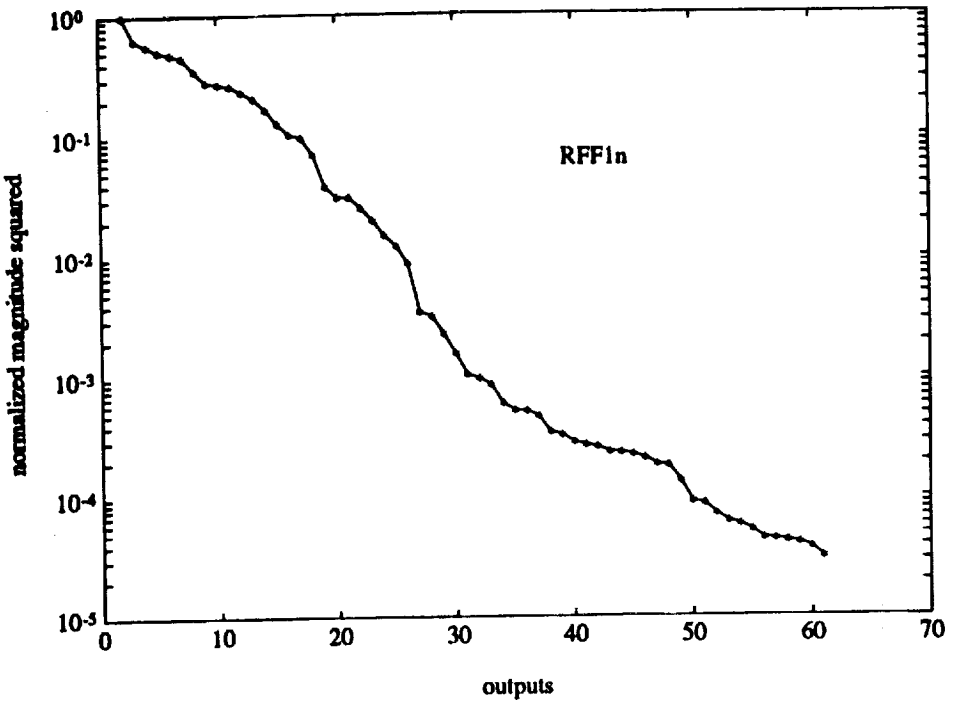

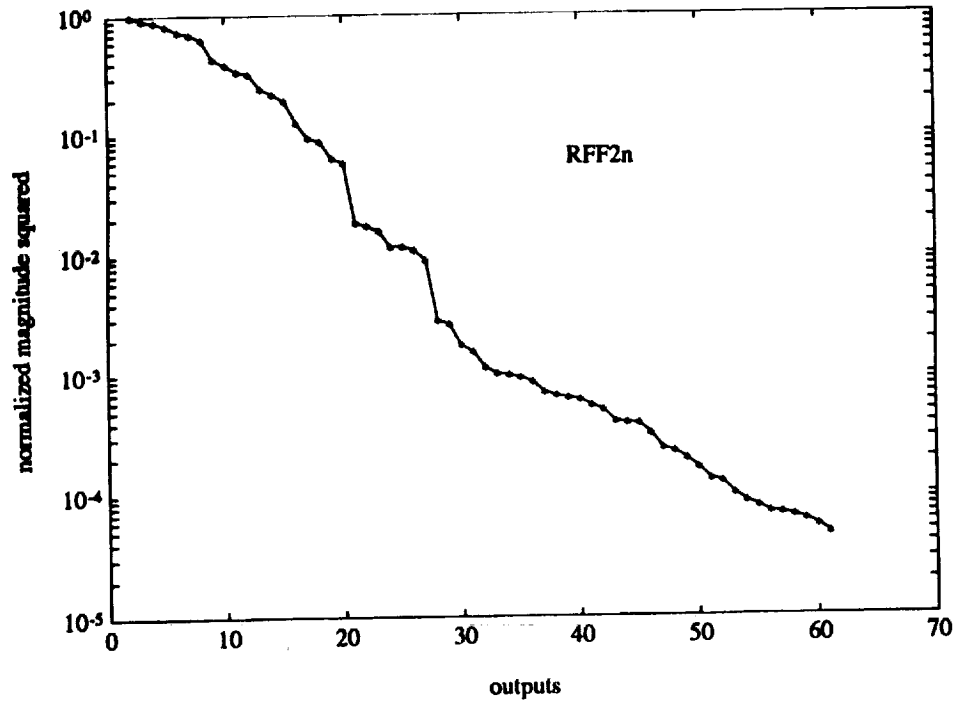

Figure 9.4 Output magnitudes from Gram-Schmidt for RFF1n and RFF2n

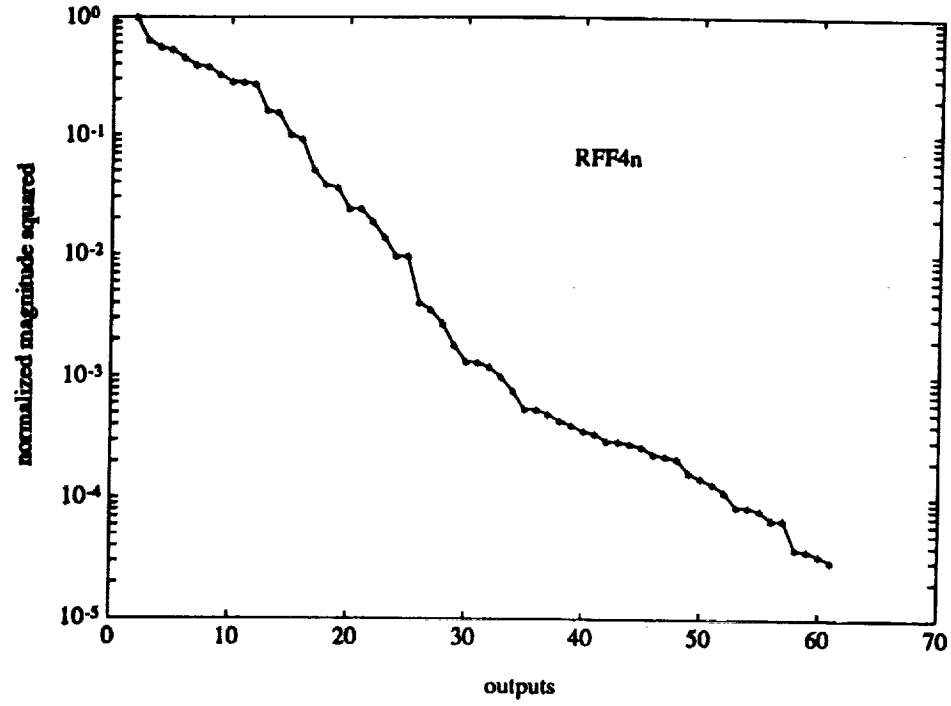

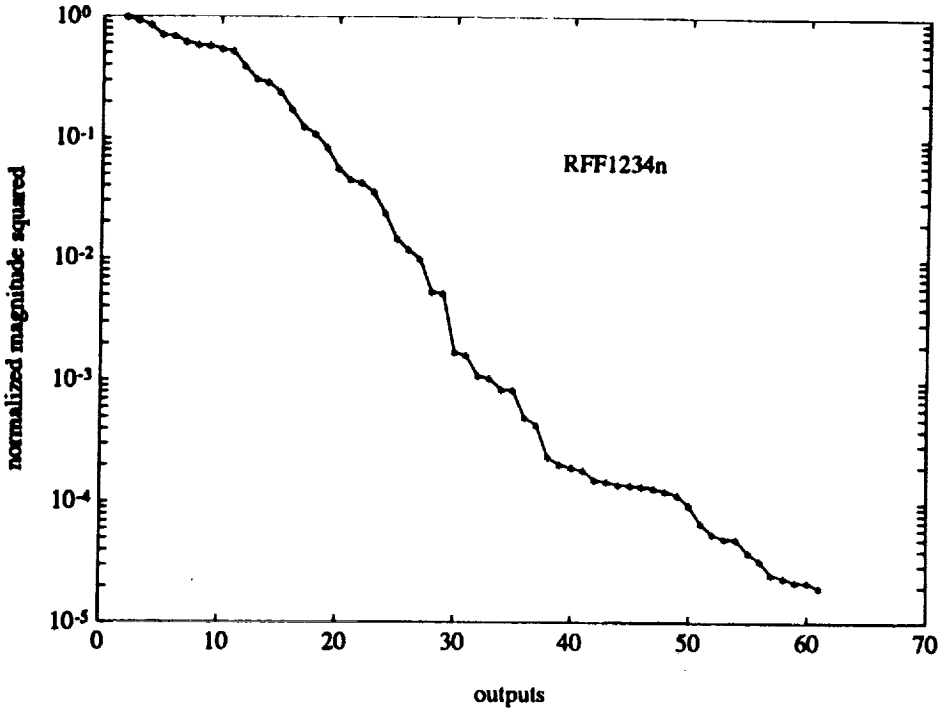

Figure 9.5 Output magnitudes from Gram-Schmidt for RFF4n and RFF1234n

9.2 Variation of Recovered Modes with Number of Outputs

We should investigate the role of the number of outputs in OKID. Figure 9.6 is a plot of the total number of recovered modes versus the number of outputs used in OKID based on a full rank solution of the Hankel matrix decomposition using RFF1234n. The data length was set at two data points per unknown and p was obtained from $floor\left(\frac{492}{No+8}\right)$.

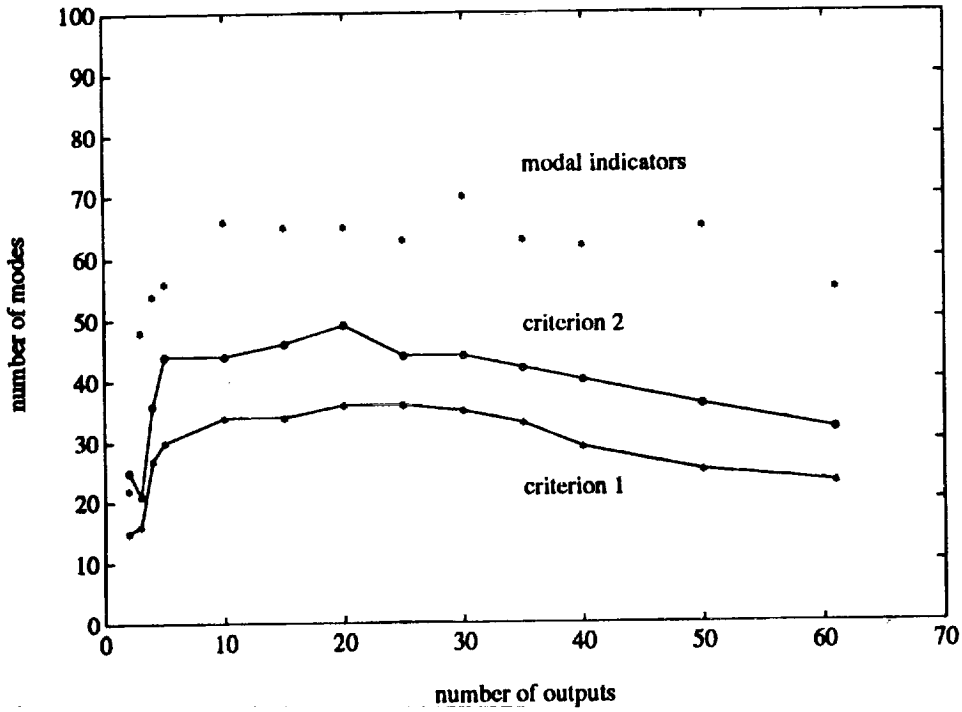

Figure 9.6 Number of recovered modes

Floor is a MATLAB command that rounds to the nearest integer towards minus infinity. The number 492 was obtained by subtracting eight (the number of inputs) from half of

1000 (1000 being the forced data length). The first criterion is criterion 1 (section 8.3). The second criterion (criterion 2), which is less restrictive, identifies all modes with frequency error≤1%, damping error≤40%, and mac≥0.8. In either case, ten to thirty outputs appear to recover the most modes. Notice that although results are presented for 40, 50, and 61 outputs, they represent increasing dependence (i.e., have no new information) and should be avoided since they may cause numerical ill-conditioning. In addition, p decreases as No increases and we expect a poor solution for the Markov Parameters and consequently less or poor mode recovery.

We now discuss the (*) points in Figure 9.6. The above analysis used the known answers. A more objective analysis is to truncate the singular values (e.g., to less than a full rank solution) and use the modal indicators. When the observed order is plotted versus the number of outputs (Figure 9.7), one sees the order stabilizing by 10 outputs. Figure 9.7, therefore, suggests that there are only 100 modes in the data. The decrease in order past 30 outputs is probably, again, due to the measurement dependence. The singular value distribution of $H(0)$ for 30 outputs is shown in Figure 9.8. The (*) in Figure 9.8 indicates the location where truncation was performed. This is how the data in Figure 9.7 was obtained. The rest of the outputs have similar distributions. The points (*) in Figure 9.6 show the number of recovered modes from the modal indicators after singular value truncation based on the order given in Figure 9.7. The optimum numbers are in a range from ten to forty, which is similar to what was obtained with criteria 1 and 2. The difference can be attributed to computational modes that survived the indicator criteria ($mono$≥0.98 or $mono$≥0.9 and msv≥0.02). This is possible since a mode could

be monophase but yet not be a true mode.

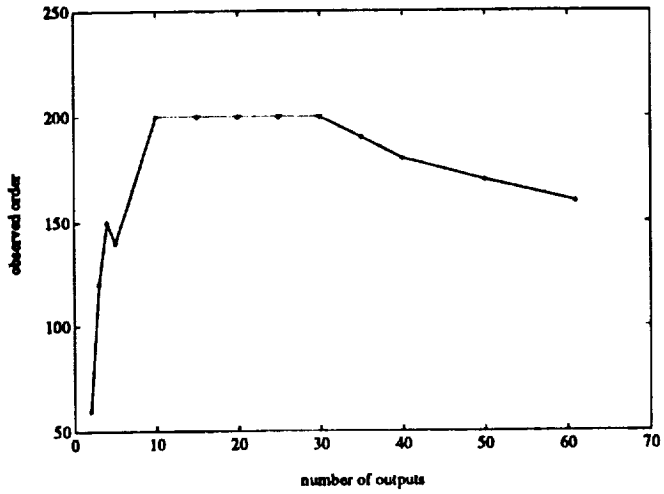

Figure 9.7 Observed order from SVD of H(0) versus number of outputs for RFF1234n

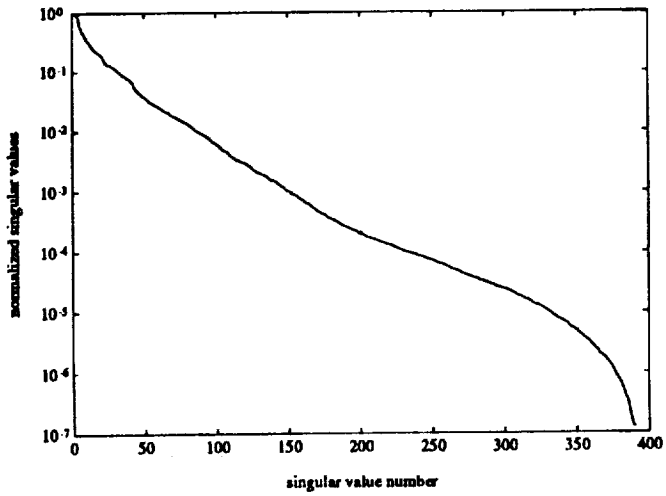

Figure 9.8 Singular values from SVD of H(0) showing location of truncation (*)

All the criteria, however, show the same result. That is, there appears to be an optimum number of outputs which gives the best results. The reason for this can be explained as follows. It is known that for noisy data: (1) $(No)p>n$ and (2) p must be large. If more outputs are used for a fixed data length, then p will decrease. This will satisfy (1) but not (2). If few outputs are used then (2) is satisfied but not (1). There will therefore be a point where both (1) and (2) are optimally satisfied.

9.3 Global-Local OKID Validation

Now that we have established an optimum number of outputs, let us discuss the Global-Local method. Mode shape information will be lost at the other locations if one uses only the independent outputs in OKID. However, there are numerous methods that can be used to solve this dilemma. One approach discussed in this section and already mentioned in section 5 is Global-Local OKID. The remaining methods will be discussed in section 9.5.

There are two natural ways to solve for the D and C matrices in GLOKID. Section 5 presented one method (call it the appending method). Simply put, this method uses the identified D and C matrices from OKID, i.e., D_{OKID} and C_{OKID}, and appends them to the D and C from the least squares solution for the remaining sensors (the sensors that were not used in OKID). The global D and C matrices then become

$$D = \begin{bmatrix} D_{OKID} \\ D_{lsq} \end{bmatrix} \quad , \quad C = \begin{bmatrix} C_{OKID} \\ C_{lsq} \end{bmatrix}$$

Another method (call it the entire method) is to use the entire data set to recover D and C for all the sensors. Obviously, the appending method is computationally more efficient than the entire method. However, to determine which method produces better results, consider the case of No=37 , p=11, and l=1006 on RFF1234n.

Table 9.1 presents the results using both methods. The modes were selected using criterion 1. The fourth column lists the mac for the local mode shapes (No=37). The fifth and sixth columns list the mac using the entire and appending methods. There is a significant improvement in mode shape accuracy of the appending method over the entire method. To visualize this, Figure 9.9 shows the (*) points (appending method) above the solid line (entire method). The (o) points will be discussed later.

Table 9.1 Comparison of methods for determining global mode shapes using GLOKID

damp (%)	freq (Hz)	ex-freq (Hz)	mac (local)	Entire method mac (global)	Appending method mac (global)	Entire method-exact mac (global)
1.0069	0.5670	0.5670	0.9992	0.9840	0.9916	0.9836
1.0660	0.7455	0.7458	0.9957	0.9470	0.9931	0.9562
0.9997	0.7926	0.7922	0.9943	0.9115	0.9753	0.9442
1.1246	0.8060	0.8079	1.0000	0.9858	0.9949	0.9859
1.0252	0.8239	0.8240	0.9941	0.9909	0.9927	0.9947
1.0089	0.8604	0.8605	0.9346	0.9328	0.9496	0.9608
0.9913	0.8966	0.8967	0.9142	0.7463	0.8986	0.7517
0.9905	1.1338	1.1337	0.9999	0.9990	0.9998	0.9991
0.9947	1.2228	1.2227	1.0000	0.9998	0.9999	0.9998
1.0096	1.2553	1.2552	1.0000	0.9997	0.9999	0.9997
1.0438	1.3220	1.3231	0.9999	0.9765	0.9961	0.9781
0.9862	1.3673	1.3672	0.9996	0.9814	0.9981	0.9820
1.0176	1.4651	1.4652	0.9976	0.6700	0.9831	0.6660
1.0087	1.5028	1.5027	0.9996	0.9921	0.9994	0.9925
0.9629	1.6772	1.6781	0.9487	0.8043	0.9374	0.8170
1.1413	1.7409	1.7411	0.9125	0.7082	0.9155	0.6815
1.0791	2.2319	2.2330	0.9886	0.7784	0.8814	0.8056
0.9729	2.2508	2.2515	0.9360	0.4572	0.8850	0.4572
1.0021	2.5889	2.5888	0.9999	0.9977	0.9996	0.9976
1.0029	2.5889	2.5888	0.9999	0.9977	0.9996	0.9976
1.0055	2.8141	2.8142	0.9999	0.9856	0.9980	0.9860
1.0066	2.9891	2.9887	0.9999	0.9560	0.9890	0.9533
1.0009	3.1234	3.1225	0.9993	0.5402	0.9289	0.5466
1.0578	3.2775	3.2788	0.9988	0.6529	0.7449	0.6766

Table 9.1-Continued

1.0144	3.4731	3.4725	0.9912	0.6971	0.9200	0.6822
0.9780	3.5206	3.5206	0.9957	0.5910	0.9540	0.5546
1.1389	3.6164	3.6180	0.9978	0.9653	0.9794	0.9668
1.1360	3.8007	3.8091	0.9984	0.9892	0.9953	0.9887
1.0946	4.4040	4.3812	0.9850	0.9555	0.9013	0.9686
1.1000	4.4502	4.4531	0.9980	0.5174	0.9660	0.8096
1.0807	4.6564	4.6609	0.9954	0.8726	0.9223	0.8900

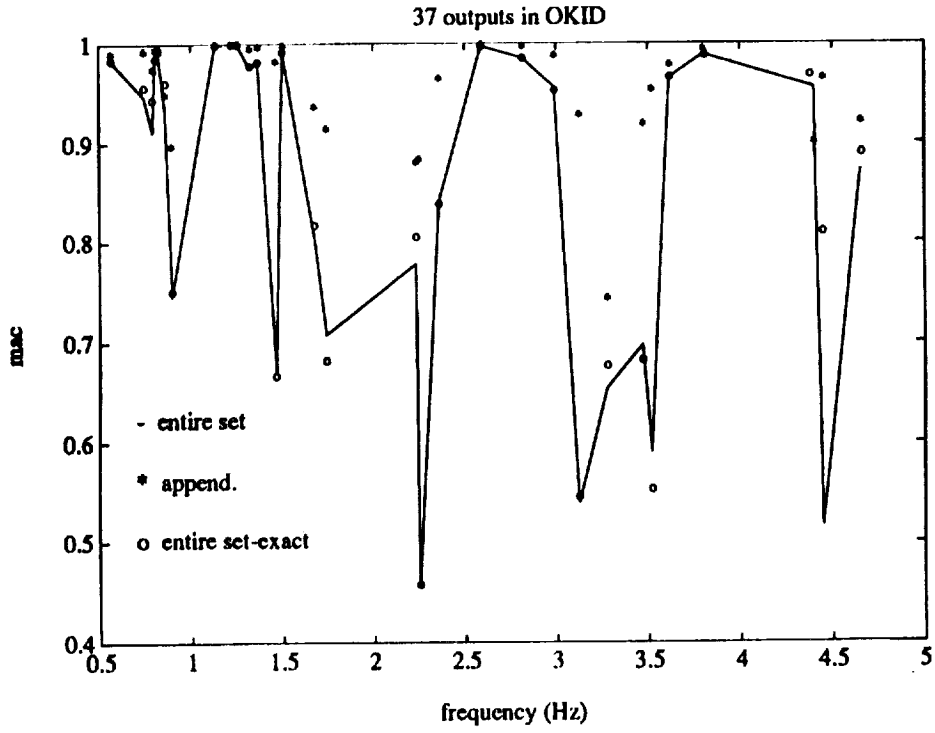

Figure 9.9 Global mode shape determination using GLOKID

An explanation is as follows. Since the mode shape matrix for the sensor subset in OKID was well identified (fourth column), the global mode shapes from the appending method should then be well identified. Notice that these mode shapes are generally of lesser quality than the local mode shapes. There are two possible reasons for this degradation. The first is that the recovered frequency and damping values are not exact and have subsequently affected the least squares process. Since the entire method determines global mode shapes solely from that recovered set, it may be expected to have poor estimates. The first explanation is highly suspicious because the recovered frequencies are within 1% and damping estimates are within 20% of their true values. The second potential reason is that the number of recovered frequencies are more important rather than the errors in frequency and damping (i.e., since not all system frequencies are recovered).

To see which explanation is valid, the identified frequencies and damping values were replaced with their corresponding exact values and the entire method used (call this method the entire-set exact). If the mac's are similar to the previous entire method's mac then the second reason is more plausible. Since the mode shapes in the last column of Table 9.1 are similar to the fifth column, we conclude that the number of recovered frequency and damping values is more important. This is not to say that the quality of the recovered frequency and damping is unimportant. Figure 9.9 shows the (o) points (entire set-exact) closely matching the solid line (entire set) but, in general, the (o) points are above the solid line.

Now, it may be argued that the degradation in mode shape will not be as severe if

the number of outputs used to extrapolate the mode shape (No_{lsq}) is less than the number of outputs used in OKID (the sensor subset), i.e., $No_{OKID}>No_{lsq}$. To see if this is valid consider two analyses. The first uses the 20 optimum number of outputs with p=18. The second uses 37 outputs (determined to be the optimal number of independent outputs) with p=11. Both cases used only the forced response (l=1040). After selection by the modal indicators all modes with frequency error≤1% and mac≥0.8 were kept, as shown in Table 9.2. Figures 9.10 and 9.11 show the mac and damping estimates as a function of frequency, respectively. There does not appear to be any significant difference between the two in terms of mode shape identification. However, the damping estimates for the 20 outputs are better than that for the 37 outputs, as shown in Figure 9.11. To verify this claim, the RMS of the damping for the 20 outputs is 1.1061 while the RMS for the 37 outputs is 1.2871. The better damping values is due to the higher p value.

Table 9.2 Modal parameters for 20 and 37 outputs from GLOKID

37 outputs			20 outputs			
damp (%)	freq (Hz)	mac	damp (%)	freq (Hz)	mac	exact freq (Hz)
3.2116	0.1830	0.8813	1.7939	0.1831	0.9099	0.1815
1.0323	0.5671	0.9995	1.0289	0.5671	0.9991	0.5670
1.0188	0.7455	0.9892	1.0094	0.7459	0.9747	0.7458
1.0209	0.7933	0.9762	1.0015	0.7929	0.9380	0.7922
1.1618	0.8058	0.9970	1.1171	0.8097	0.9964	0.8079
1.1446	0.8230	0.9964	1.0170	0.8243	0.9709	0.8240
1.1301	1.0027	0.9722	0.9931	1.0029	0.9430	1.0033
0.9885	1.1338	0.9999	0.9874	1.1336	0.9999	1.1337
1.4170	1.1999	0.9976	1.2187	1.1956	0.9926	1.1954
0.9845	1.2228	1.0000	0.9912	1.2227	1.0000	1.2227
1.0118	1.2553	1.0000	1.0074	1.2555	1.0000	1.2552
1.1509	1.3225	0.9997	1.2453	1.3233	0.9992	1.3231
1.0162	1.3673	0.9995	0.9597	1.3678	0.9982	1.3672
1.0245	1.4651	0.9951	1.0041	1.4653	0.9904	1.4652
1.0118	1.5027	0.9996	0.9993	1.5029	0.9990	1.5027
1.3234	1.6040	0.9990	0.9645	1.5982	0.9992	1.6017
0.9440	1.6775	0.9543	1.0708	1.6773	0.9672	1.6781
1.1043	2.0337	0.9839	1.3024	2.0336	0.9838	2.0297
1.4358	2.0995	0.9752	1.6590	2.1117	0.9119	2.0956
1.0111	2.2340	0.9755	0.9874	2.2327	0.9466	2.2330
0.9748	2.2510	0.9434	0.9973	2.2502	0.9345	2.2515
1.0283	2.3596	0.9969	1.0045	2.3595	0.9955	2.3591
2.9910	2.4762	0.9310	1.1048	2.4871	0.9627	2.4849
1.0038	2.5889	0.9999	1.0036	2.5889	0.9999	2.5888

Table 9.2-Continued

1.0042	2.8142	0.9994	1.0033	2.8141	0.9990	2.8142
1.0167	2.9891	0.9987	1.0043	2.9889	0.9976	2.9887
1.0000	3.1233	0.9891	1.0189	3.1228	0.9803	3.1225
1.0534	3.2777	0.9320	0.9992	3.2783	0.9258	3.2788
1.0148	3.4735	0.9843	1.0025	3.4739	0.9838	3.4725
0.9771	3.5209	0.9890	0.9716	3.5206	0.9842	3.5206
1.0884	3.6166	0.9911	1.0818	3.6166	0.9887	3.6180
1.0302	3.8048	0.9923	1.2296	3.8029	0.9878	3.8091
1.2540	3.9602	0.8213	0.9609	3.9473	0.8335	3.9236
1.1961	4.0411	0.9218	1.2354	4.0429	0.9377	4.0308
1.4773	4.3264	0.9774	1.4070	4.3199	0.9751	4.3193
1.1393	4.4068	0.8687	0.9099	4.3954	0.9055	4.3812
1.0935	4.4506	0.9695	1.1245	4.4503	0.9835	4.4531
1.0828	4.6571	0.9576	1.0247	4.6621	0.9754	4.6609

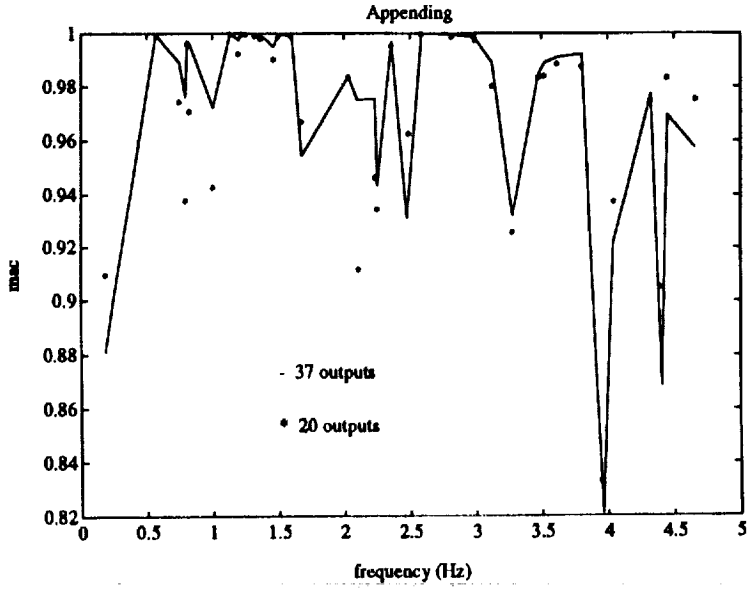

Figure 9.10 Global mode shapes for 20 and 37 outputs

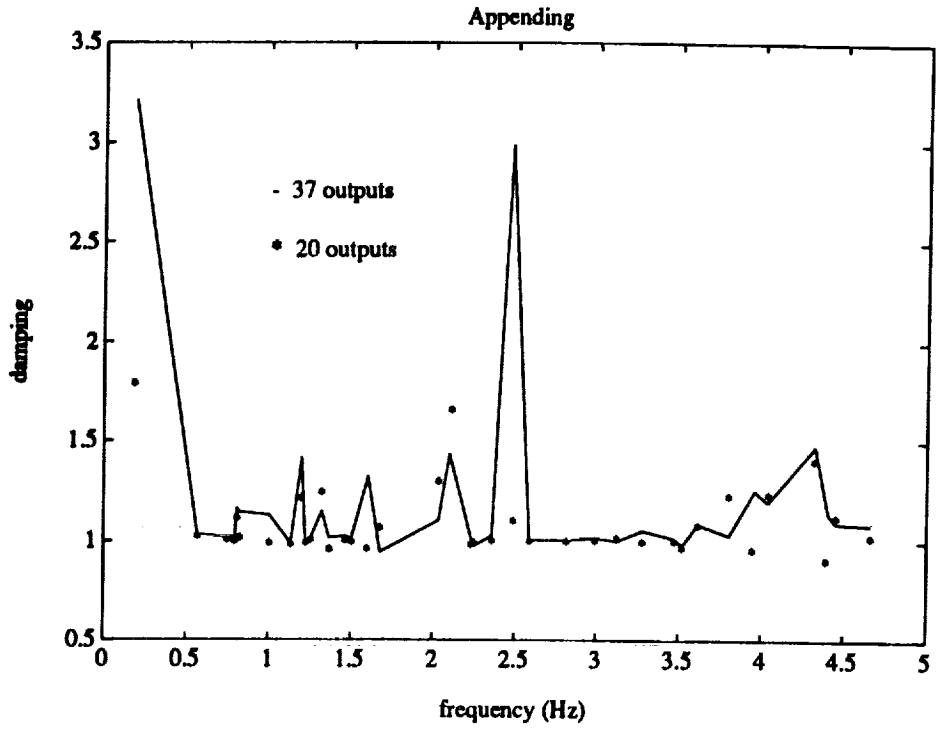

Figure 9.11 Damping estimates for 20 and 37 outputs

9.4 Results for Noisy Measurements (RFF1, RFF2, RFF4)

We now investigate the individual test cases, i.e., RFF1n, RFF2n, and RFF4n, for the total number of recovered modes. RFF3n will not be used due to an error in the input sequence which invalidated the NASTRAN transient analysis. To compare results, the ERA method using free-decay data was used. While the ERA parameters were not optimized they were set to what was deemed reasonable given the computational limitations and data length. The modal indicators for the ERA consisted of the modal amplitude coherence (γ>0.8) in addition to the other two indicators. Table 9.3 presents

results for 20 outputs using OKID-ERA with 60 and 80 seconds and for ERA using 60 seconds. The Hankel matrix size in ERA was 300 x 600. Observe that the ERA generally does better than OKID-ERA (60 seconds) in terms of total and target modes, while OKID-ERA (80 seconds) does somewhat better than ERA in terms of total modes. This is expected since a larger p can be chosen making the Markov Parameters more exact. Also, it is clearly seen that ERA recovered more target modes than either the 60 or 80 second OKID-ERA. It should be pointed out that for RFF1n, for example, 8 target modes were recovered (from criterion 2). The only reason that a five is shown for criterion 1 is that only five modes satisfied criterion 1. For this analysis, the principal difference between criteria is that the first selects all modes with damping error$\leq$20% and the second with damping error$\leq$40%.

Table 9.3 Number of recovered modes (based on local mode shapes)

		Number of modes					
		OKID-ERA				ERA	
		60 sec.		80 sec.		60 sec.	
test cases		Total modes	Target modes	Total modes	Target modes	Total modes	Target modes
RFF1n	crit. 1	15	5	14	6	19	9
	crit. 2	21	8	24	7	22	10
RFF2n	crit. 1	17	7	18	6	18	8
	crit. 2	22	8	26	8	22	10
RFF4n	crit. 1	14	6	21	9	18	9
	crit. 2	18	7	24	9	20	9

Observe also that for RFF1n and RFF2n of criteria 2 and 1, respectively, the number of target modes decrease with an increase in data length which is contrary to the general idea that the longer the data record the better the answers. Although more modes were identified, it was at the expense of losing other modes (in this case a target mode). A possible explanation is that, in this case, more data means more free decay and hence more zeros in the V matrix, which may 'weaken' the effect of the forced data and also produce a poorly conditioned V matrix. This conditioning problem can be seen in the singular values of the V matrix in Figure 9.12.

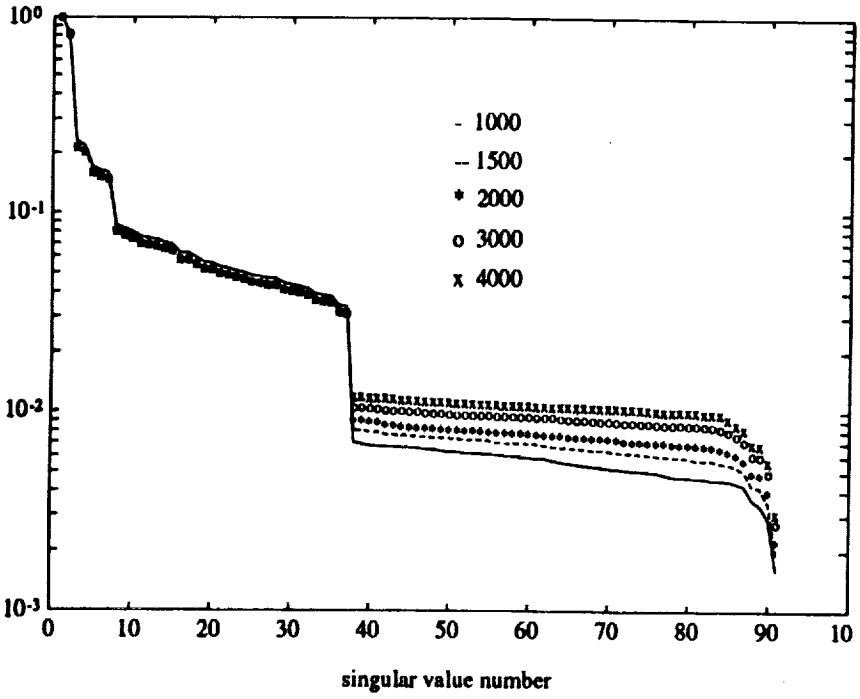

Figure 9.12 Singular values of V matrix for three-degree-of-freedom simulation

The data was generated from the three-degree-of-freedom simulation discussed in section 6. The rank of the V matrix is 37. The reason for this is as follows. The row dimension of V is $(No+Ni)p+Ni = (No)p+Ni(p+1)$. Since we have a three mode system (n=6) and if the data is clean (noise free), then $(No)p = n$. And for p=30, Ni=1, and n=6 the rank of V should be 37. Two percent random noise (based on maximum amplitude) was added to the clean data. The data consisted of ten seconds of forcing and was randomly generated (unit variance and zero mean). Observe that as the data length in the V matrix is increased, the singular values show less of a drop at the 37th singular value making it more difficult to determine the rank. A long forced response followed by a short free-decay may do better. This was another reason for generating RFF1234n, whose results will be presented later.

The above results considered a limited number of outputs (and consequently used local mode shapes). Table 9.4 presents results for Global-Local OKID. Sixty seconds of data were used to identify the frequency and damping and local mode shapes and eighty seconds for the least squares solution for the remaining mode shapes. Two points are immediately obvious. The first is the relatively poor performance of the ERA method using all 61 outputs (Hankel matrix size of 244 x 600). This can be explained as follows. Due to a limited amount of data (60 seconds), ERA has only r block rows in the Hankel matrix. By using outputs that are not all independent there is a waste of r values. The ERA method with Keydata[15] is then one solution since the independent outputs can be put to better use in the block row repetitions. Also, global mode shape information is not

lost. The other point is that GLOKID is identifying more modes for RFF1n and RFF2n for criterion 2 than OKID from Table 9.3. The reason is that while, as stated previously, the mode shapes from GLOKID are generally of lesser quality, it does not mean that all mode shapes will be of lesser quality.

It is appropriate now to discuss the results obtained using an increased forced data length followed by free-decay (i.e., RFF1234n). The forced data may help separate closely spaced modes while the free-decay may help in identifying low frequency modes. A measurement of this type may, therefore, be a good approach. But a similar response can also be produced by concatenating the responses from the individual input sequences (i.e., RFF1n, RFF2n, and RFF4n). This would have a mixture of forced and free-decay data throughout the entire data length. Each of the individual input sequences provided 50 seconds for concatenation.

Table 9.4 Number of recovered modes (based on global mode shapes)

		Number of modes		
		GLOKID-ERA		ERA
		60 sec.		60 sec.
test cases		Total modes	Target modes	Total modes
RFF1n	criterion 1	15	5	6
	criterion 2	22	8	7
RFF2n	criterion 1	15	6	7
	criterion 2	23	9	11
RFF4n	criterion 1	14	6	7
	criterion 2	18	7	8

Results are presented for 150 seconds using 20 outputs and are shown in Table 9.5. The Hankel matrix size was 520 x 1040 with p=26. The ERA method was also used with a Hankel matrix size of 600 x 1500 with the data coming from concatenation of 50 seconds of free-decay data from each of the individual input sequences.

Table 9.5 Number of modes for 150 seconds (based on local mode shapes)

	Number of modes					
	OKID-ERA				ERA	
	Concatenating		RFF1234n		Concatenating	
	Total modes	Target modes	Total modes	Target modes	Total modes	Target modes
criterion 1	35	10	41	12	28	9
criterion 2	49	11	47	12	33	10

It is obvious that RFF1234n did better than concatenation and ERA. Also, almost all of the target modes were identified (0.532 Hz was the only missing target mode, primarily because of its poor mode shape; in fact, this mode was not identified in Tables 9.3 and 9.4). This missing target mode is probably due to using only 20 outputs or the high modal density. Table 9.6 presents the lowest frequencies from RFF1234n and concatenating RFF1n, RFF2n, and RFF4n for OKID-ERA.

Table 9.6 Lowest frequencies from RFF1234n and concatenation

	damping (%)	frequency (Hz)	exact-freq. (Hz)	mac
RFF1234n	3.4198	0.1527	0.1511	0.9599
	1.6929	0.1827	0.1815	0.9535
	3.1632	0.2680	0.2767	0.9930
Concatenation	4.1143	0.2892	0.3106	0.8500

Observe that while the damping is poor, the frequencies and mode shape are excellent for RFF1234n. This would suggest that a long forced data length followed by free-decay data may give the 'best' answers although there is probably not much that can be done about the damping except possibly to increase the data length and/or filter the data. Filtering the data may help in identifying more of the low frequency modes.

9.5 Methods for Global Mode Shape Recovery

GLOKID is one method for obtaining global mode shapes. Another method is to use subset combinations with OKID and then use ERA with Keydata. That is, we remove the 20 most independent outputs from the data (after first use of Gram-Schmidt) and perform another Gram-Schmidt on this new data, which contains 41 outputs. Select a new set of 20 independent outputs which comprise a second set of data. This leaves only 21 outputs as the final data set. An OKID analysis can then be performed three times (i.e., using the first 20 outputs, then the next 20, and finally the last 21) to obtain three sets of Markov Parameters. These Markov Parameters can be used in ERA with Keydata where the first set of Markov Parameters are used in the block row repetitions. A disadvantage of this

method is that there will be three different frequency and damping estimates, which will cause a phase distortion in the Hankel matrix.

To compare these two methods, concatenate 60 seconds from each of the individual input sequences to get a data length of 1800. The parameters in GLOKID (41 outputs) consisted of p=31 and 20 outputs (of the most independent) with 1800 points in the mode shape least squares process for the other 41 outputs. The subset combination method used a p=31 for the first two OKID runs (each using 20 outputs) and 30 for the last (using 21 outputs). The Hankel matrix size in ERA with Keydata was 601 x 1200 while GLOKID (41 outputs) used 620 x 1240. It is seen in Table 9.7 that the subset combination method does better than GLOKID (41 outputs) in terms of total mode recovery. A possible explanation for this is that in the subset method each Markov Parameter set should have good mode shapes since each came from OKID. GLOKID (41 outputs), on the other hand, has only one set of Markov Parameters coming from OKID. The mode shapes at the remaining outputs must then be extrapolated using the recovered frequency and damping. And as discussed in section 9.3, there will be a global mode shape degradation. The last OKID analysis for the subset method (21 outputs) does have dependent measurements and therefore the analysis may suffer from ill-conditioning. Two methods which overcome this problem are presented. The first method (subset with SVD) uses the identified Markov Parameter set from the two OKID analyses (20 and 20 outputs) and analyzes the remaining 21 outputs with the SVD of the V matrix (due to computer memory limitations the SVD was performed on VV^T). Then the ERA with Keydata was used on the three sets of Markov Parameters. The second method (GLOKID (21 outputs))

Table 9.7 Global mode shape recovery methods using concatenated data (1800 points)

	Number of modes							
	GLOKID (41 outputs)		Subset Combination		Subset with SVD		GLOKID (21 outputs)	
	Total modes	Target modes	Total modes	Target modes	Total modes	Target modes	Total modes	Target modes
crit. 1	35	11	40	10	33	9	37	12
crit. 2	44	12	49	11	40	10	44	12

is an extension of the Global-Local concept. That is, instead of extrapolating the mode shapes to 41 outputs, ERA with Keydata is used on the first two Markov Parameters (20 and 20 outputs) to determine frequency and damping estimates. The mode shapes are then extrapolated to the remaining 21 outputs. Surprisingly, the subset combination method gives the best results although GLOKID (21 outputs) identifies the most target modes. A possible explanation why the subset with SVD did the worst out of all the methods is because the SVD was performed on VV^T instead of V. It should also be pointed out that the subset with SVD is the most computationally intensive due to the need for another SVD followed by the subset combination method (since two extra OKID analyses have to be performed) then GLOKID (21 outputs) and finally, the least expensive, GLOKID (41 outputs).

9.6 Observer Decay vs Data Length and Hankel Matrix Size

To verify the results presented in section 6.2, let us investigate the number of data per unknown in the least squares solution for the Observer Markov Parameters. Consider the case where 60 seconds from RFF1n, RFF2n, and RFF4n are concatenated (i.e., data length of 1800) with the first 20 independent outputs and a Hankel matrix size of 1 to 2 (twice as long as it is tall). Table 9.8 presents results using criteria 1 and 2. Observe that as the number of data per unknown is increased, less modes are recovered. This is expected since p and consequently $(No)p$ decrease. Also note that two data points per unknown give the 'best' results. Although the highest p value is obtained from 1.5 data per unknown, it gives less modes than two data per unknown primarily because there is less data averaging. This suggests that two data per unknown does give the optimum for a fixed data length.

As a final note, let us re-examine the role of the Hankel matrix size. For this purpose we use RFF1234n with p=18 and l=1040 (both fixed). All test cases retained 200 singular values in the Hankel matrix and are presented in Table 9.9. A Hankel matrix size of 1 to 3 appears to give the most number of modes. Certainly, the minimum size is 1 to 2. The actual size, however, depends on the available computational resources and particular problem (i.e., system order).

Table 9.8 Total number of recovered modes using OKID-ERA

data per unknown	Number of modes	
	criterion 1	criterion 2
1.5	29	39
2	38	49
3	35	42
4	25	36
5	13	23

Table 9.9 Hankel matrix size in OKID-ERA

H(0)		Number of modes	
Rows	Cols	criterion 1	criterion 2
360	360	31	36
	720	31	40
	1080	35	43
	1440	35	43

X. CONCLUSIONS

It has been shown that an optimum number of outputs exist in OKID which give the best results in terms of modal recovery (frequency and damping estimates). This is due to the fact that for a fixed data length there is a point where the values p and $(No)p$ are both optimal. In addition, not all of the noisy measurements were found to be independent. This is important since OKID requires the measurements to be as linearly independent as possible to minimize any numerical ill-conditioning. Therefore, an independent output subset was obtained from a Gram-Schmidt Orthogonalization procedure. For the SC-7 simulation, 20 out of the 61 outputs were selected as this subset. However, mode shape information was lost at the remaining 41 measurement locations. To overcome this difficulty, a new version of OKID, called Global-Local OKID (GLOKID), was developed. This new method uses the identified frequency and damping from OKID using an independent output subset and determines the local mode shapes for the remaining outputs (i.e., the outputs that were not used in OKID) using a least squares process. The global mode shapes are then obtained by appending the identified local mode shape from the least squares process to the other set of local mode shapes determined from OKID. GLOKID is shown to identify the global modal parameters.

In addition, there were several issues in the use of OKID. The first was the number of data points per unknown in the solution for the Observer Markov Parameters. Two data points per unknown was found to give adequate results for the noise level in the SC-7 simulation. Obviously, if the noise level were much higher than more data points per

unknown are required. Another issue was the accuracy of the input force on the identification process since the forces on the SSF will not be measured. Two models were used to test the accuracy. The first model was a square wave input obtained from the 'on-off' commands to the ACS thrusters. The second model used the rise and fall times from an actual ground calibration test firing of an ACS thruster. Overall, it was determined that both models identified the same total number of modes. And since the power spectra for both models were similar, it was concluded that the 'on-off' commands to the ACS thrusters can be used to create a square wave input for the purpose of system identification.

As an observation, a Hankel matrix size whose columns are twice the number of rows gave acceptable results. Of course, the more data that is included in the Hankel matrix the better the modal identification, especially for the damping estimates. This was particularly evident for the three-degree-of-freedom simulation that was considered. Also, a long forced response followed by free-decay is suggested for modal identification. The forced response may help in separating closely spaced modes while the free response may help in identifying low frequency modes. This type of excitation will also minimize the poor conditioning of the input-output matrix (V) in OKID by reducing the number of zeros.

REFERENCES

1. Widrick, T. W., "Determining the Effect of Modal Truncation and Modal Errors in Component Mode Synthesis Methods," M.S. Thesis, Dept. of Civil, Mechanical, and Environmental Engineering, George Washington University, Hampton, VA, July 1992.

2. Denman, E. D. et. al., "Identification of Large Space Structures on Orbit," ASCE Report, No. AFRPL TR-86-054, New York, NY, September 1986.

3. Pappa, R. S., "Identification Challenges for Large Space Structures," *Sound and Vibration*, Vol. 24, No. 1, April 1990, pp. 16-21.

4. Kim, H. M. and Doiron, H. H., "Modal Identification Experiment Design for Large Space Structures," AIAA paper No. 91-1183, 1991.

5. "Microgravity Performance Analysis Report," Contract No. NAS 9-18200, MDSCC, Houston, TX, March 1993.

6. Juang, J. N. and Pappa, R. S., "A Comparative Overview of Modal Testing and System Identification for Control of Structures," *Shock and Vibration Digest*, Vol. 20, No. 6, June 1988, pp. 4-15.

7. Juang, J. N. and Pappa, R. S., "An Eigensystem Realization Algorithm for Modal Parameter Identification and Model Reduction," *Journal of Guidance, Control, and Dynamics*, Vol. 8, No. 5, Sept-Oct. 1985, pp. 620-627.

8. Juang, J. N., Phan, M., Horta, L. G., and Longman, R. W., "Identification of Observer/Kalman Filter Markov Parameters: Theory and Experiments," *NASA Technical Memorandum* TM-104069, March 1991.

9. Ho, B. L. and Kalman, R. E., "Effective Construction of Linear State-Variable Methods from Input/Output Data," *Proceedings of the 3rd Annual Allerton Conference on Circuit and System Theory*, 1965, pp. 152-192.

10. Kalman, R. E., Ho, Y. C., and Narendra, K. S., "Controllability of Linear Dynamical Systems," *Contributions to Differential Equations*, Vol.1, No. 2, 1962, pp. 189-213.

11. Kalman, R. E., "Mathematical Description of Linear Dynamical Systems," *SIAM Journal on Control*, Vol. 1, 1963, p. 152-192.

12. Allemang, R. J. and Brown, D. L., "Modal Parameter Estimation Space Station Structural Characterization Experiment," Structural Dynamics Research Laboratory, University of Cincinnati, December 1989.

13. Juang, S. Z., "Equivalents of Some System Identification Methods That Use Finite Hankel Matrices," M.S. Thesis, Dept. of Civil, Mechanical, and Environmental Engineering, George Washington University, Hampton, VA, March 1992.

14. Phan, M., Juang, J. N., and Longman, R. W., "On Markov Parameters in System Identification," *Proceedings of the 9th International Modal Analysis Conference*, 1991, pp. 1415-1421.

15. Pappa, R. S., Schenk, A., and Noll, C., "Eigensystem Realization Algorithm Modal Identification Experiences with Mini-Mast," *NASA Technical Memorandum* TM-4307, Feb. 1992.

16. Longman, R. W., Lew, J. S., and Juang, J. N., "Comparison of Candidate Methods to Distinguish Noise Modes from System Modes in Structural Identification," *Proceedings of the AIAA 33rd Structures, Structural Dynamic and Materials Conference,* Dallas, TX, April 13-15, 1992, pp. 2307-2317.

17. Tolson, R. H., "Time Domain Modal Identification Methods for Application to Space Station Freedom Modal Identification Experiment," NAS1-18458, Task No. 36, George Washington University, December 1991.

18. "Modal Identification Experiment: Delta Phase B Concept Definition Study," Contract NAS9-18200, MDSCC, Houston, TX, July 1992.

19. Tanner, S., NASA Langley Research Center, Hampton, VA, Feb. 1993.

20. Martinovic, Z., AMA, Inc., Feb. 1993.

21. Popp, C., NASA Johnson Space Center, Houston, TX, Feb. 1993.

22. Golub, G. H. and Reinsch, C., "Singular Value Decomposition and Least Squares Solutions," *Numer. Math.* Vol. 14, 1970, pp. 403-420.

23. Martinovic, Z. N., "Error Analysis Applied in MDSSC-Noised Program," Memo to MIE Work Group, AMA Inc., May 1993.

APPENDIX A

We can show that $(T^{-1}AT)^{k-1} = T^{-1}A^{k-1}T$ by mathematical induction.

Step (1): show true for $k=2$

$$(T^{-1}AT)^{2-1} = T^{-1}AT$$

Step (2): assume true for $k=n$

$$(T^{-1}AT)^{n-1} = T^{-1}A^{n-1}T$$

Step (3): show truth of (2) implies truth for $k=n+1$

Now

$$(T^{-1}AT)^{n} = (T^{-1}AT)^{n-1}(T^{-1}AT)$$

But from (2)

$$(T^{-1}AT)^{n} = (T^{-1}A^{n-1}T)(T^{-1}AT) = T^{-1}A^{n}T$$

Therefore, since truth of (2) implies truth for $k=n+1$, then we conclude that $(T^{-1}AT)^{k-1} = T^{-1}A^{k-1}T$ is true for all integer k.

APPENDIX B

The following is taken from Ref. 22.

Singular Value Decomposition (SVD)

Let A be a real $m \times n$ matrix. Then there exist orthonormal matrices P (dimension $m \times m$) and Q (dimension $n \times n$) such that

$$A = PDQ^T \tag{B.1}$$

$$P^T P = I_m \ (m \times m)$$
$$Q^T Q = I_n \ (n \times n)$$

where D is $m \times n$ and has the form

$$D = \begin{bmatrix} \Sigma & 0 \\ 0 & 0 \end{bmatrix}$$

$$\Sigma = diag\{\sigma_1, \sigma_2, ..., \sigma_r\}$$

$$\sigma_1 \geq \sigma_2 \geq \cdots \geq \sigma_r \geq 0 \quad , \quad r \leq \min(m,n)$$

Eq. (B.1) is called the singular value decomposition and $\sigma_1, ..., \sigma_r$ are called the singular values. Thus if $rank[A] = k$ then $\sigma_{k+1} = \sigma_{k+2} = \cdots = \sigma_r = 0$.

The matrix P consists of the orthonormalized eigenvectors of AA^T and the matrix Q consists of the orthonormalized eigenvectors of A^TA. The diagonal elements of Σ are the non-negative square roots of the eigenvalues of A^TA if $m \geq n$ or AA^T if $m < n$.

APPENDIX C Power Spectral Density for Square Wave and Ramped Input

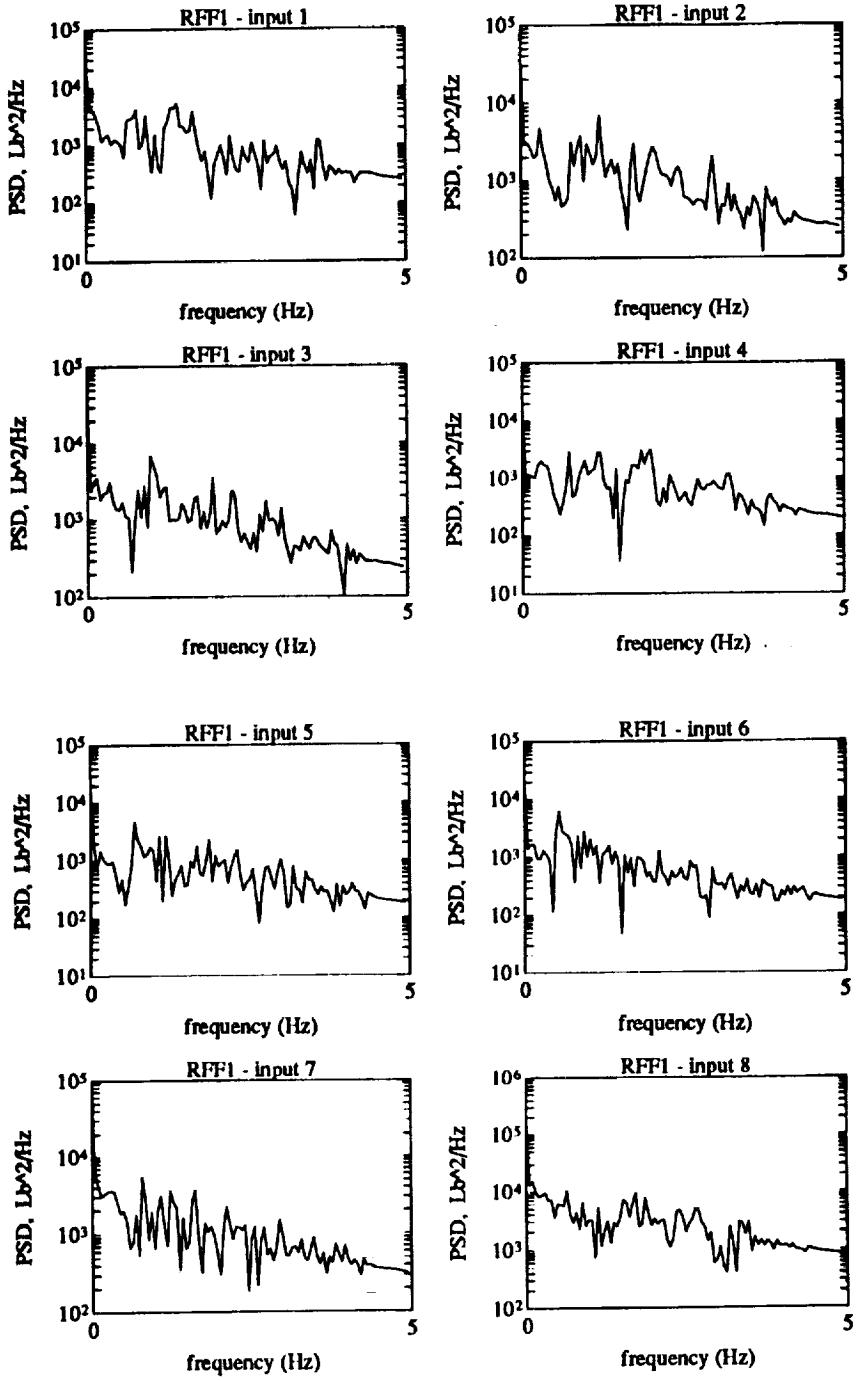

Figure C.1 PSD for RFF1 comparing square wave (solid) and ramped (dashed) input

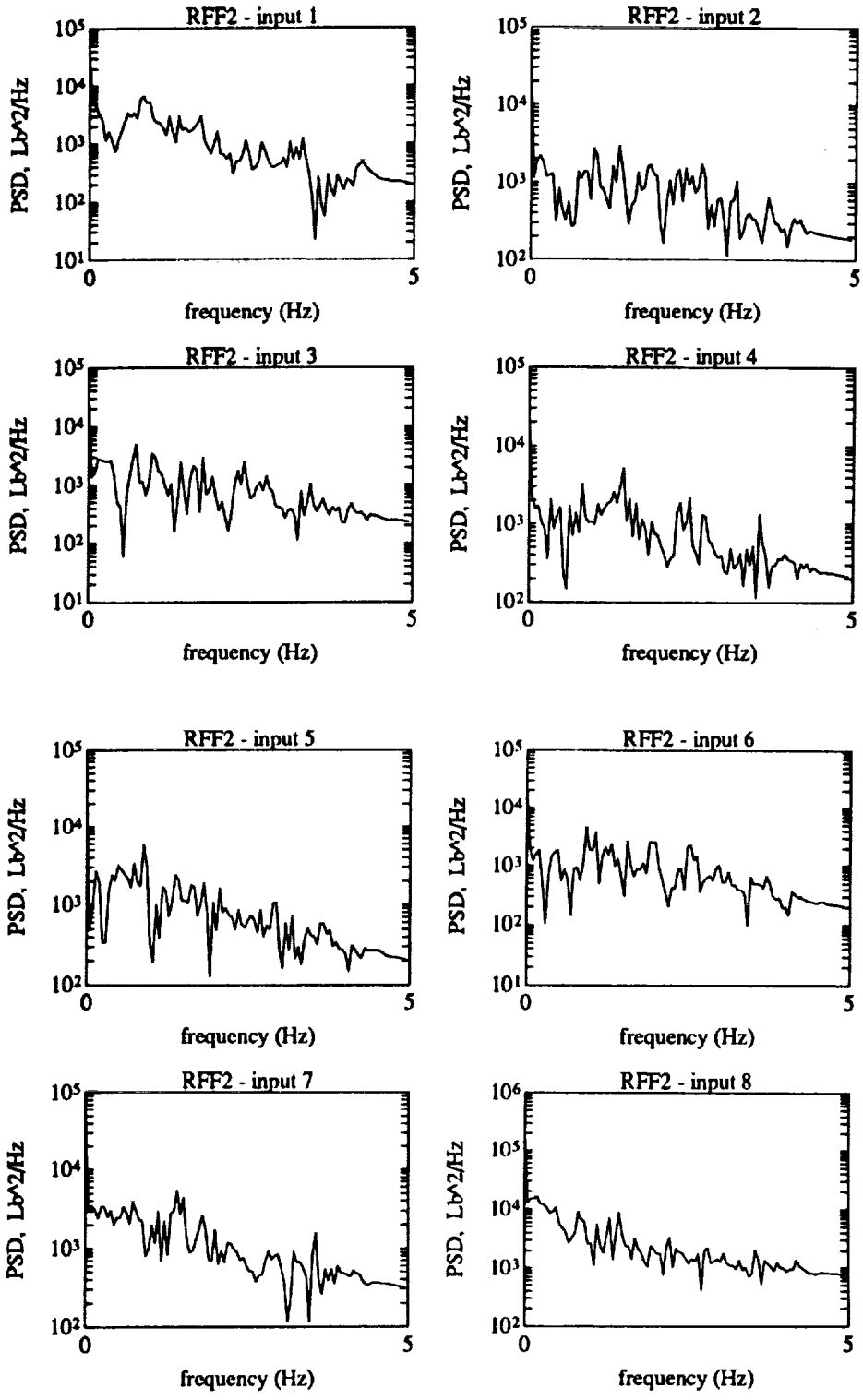

Figure C.2 PSD for RFF2 comparing square wave (solid) and ramped (dashed) input

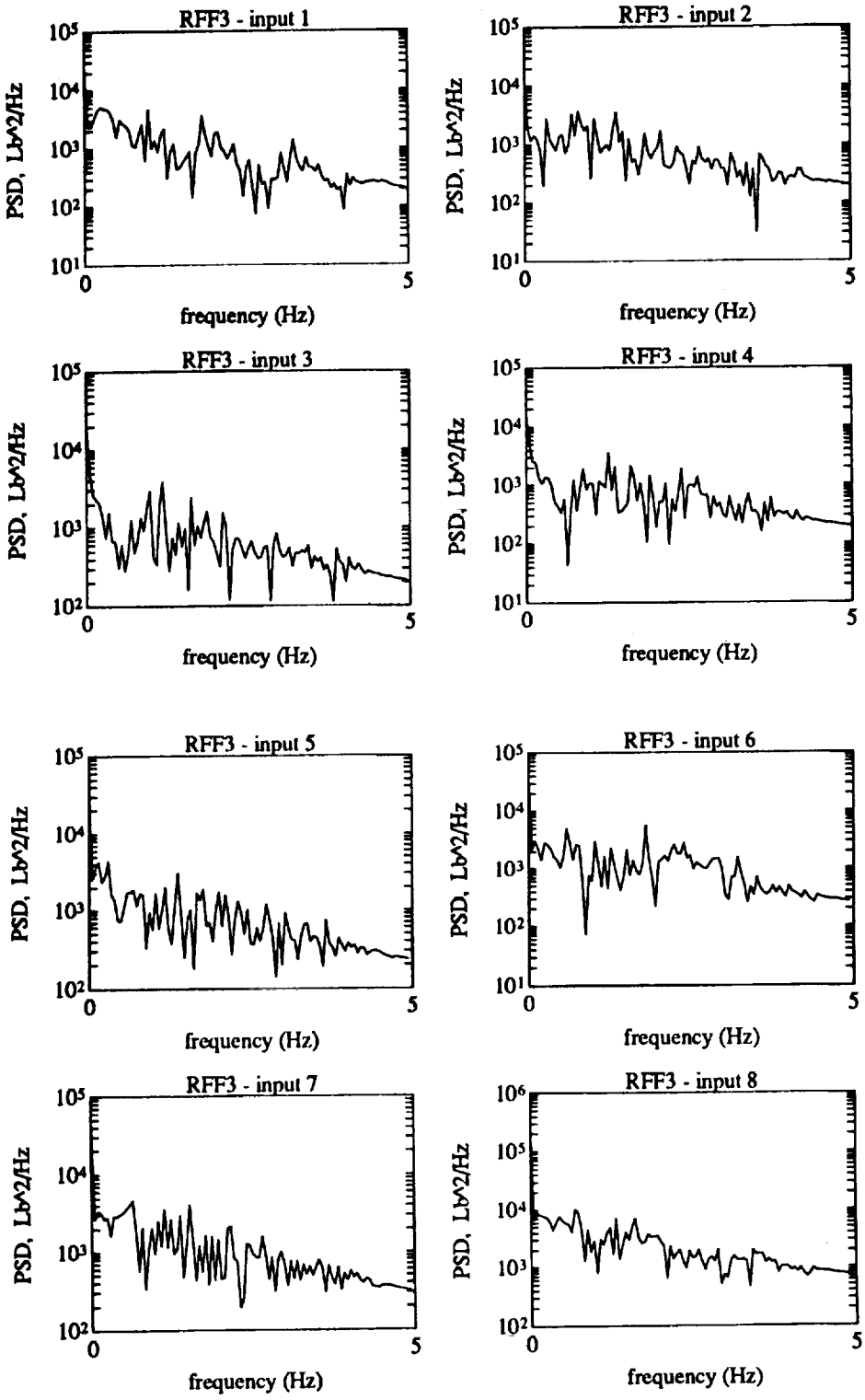

Figure C.3 PSD for RFF3 comparing square wave (solid) and ramped (dashed) input

C-2

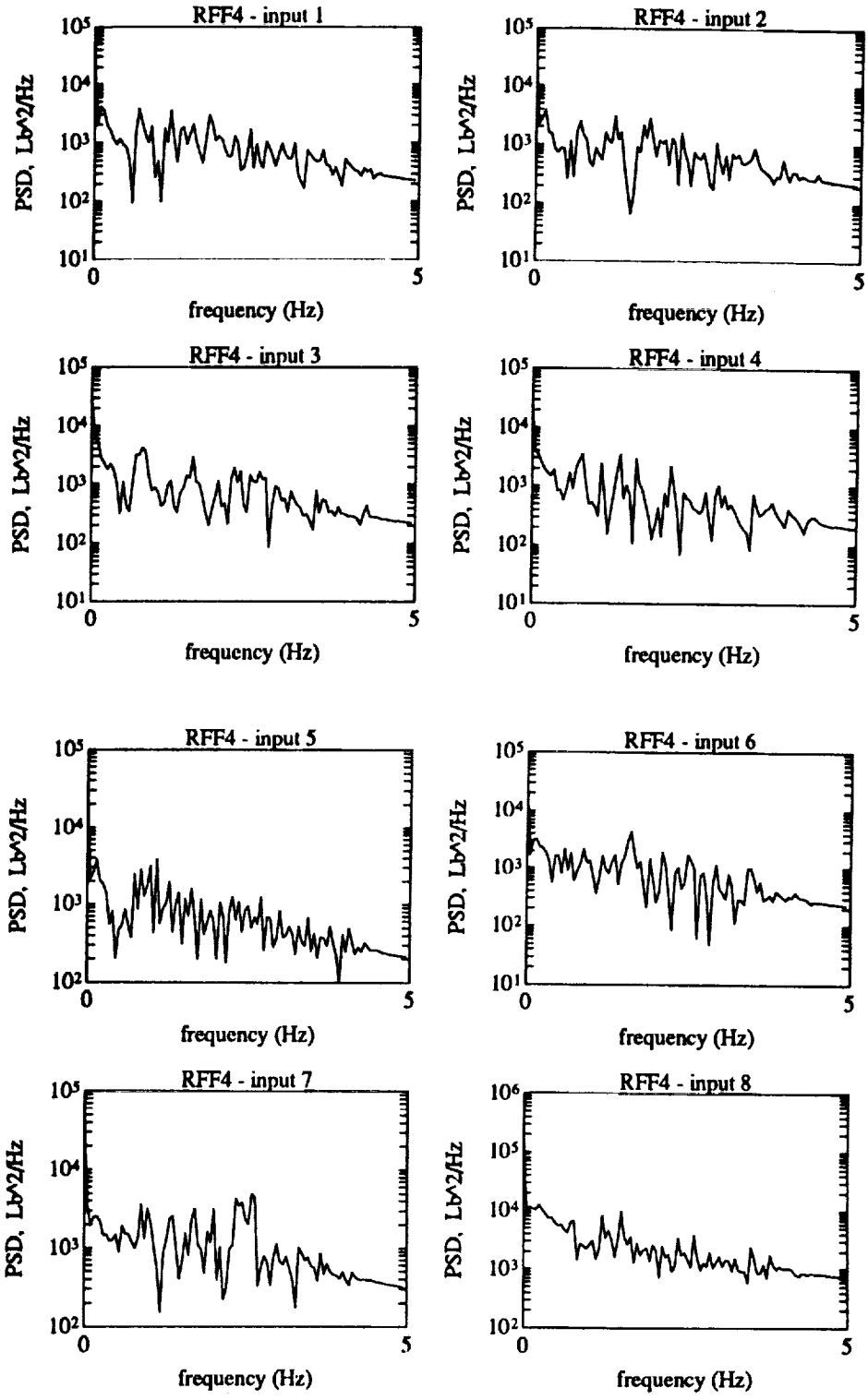

Figure C.4 PSD for RFF4 comparing square wave (solid) and ramped (dashed) input

APPENDIX D OKID-ERA Results for Square Wave and Impulse Preserved Ramped Input

Table D.1 RFF1c non-impulse preserved

damp (%)	freq (Hz)	ex-freq (Hz)	mac
1.1421	0.5314	0.5359	0.9099
1.0025	0.5670	0.5670	0.9999
1.0096	0.7458	0.7458	0.9960
0.9926	0.7925	0.7922	0.9952
0.9846	0.8078	0.8079	1.0000
1.0104	0.8239	0.8240	0.9996
1.0036	0.8604	0.8604	0.9987
0.9988	1.1337	1.1337	1.0000
1.1484	1.1926	1.1954	0.9978
1.0001	1.2227	1.2227	1.0000
0.9964	1.2553	1.2552	1.0000
1.0998	1.3221	1.3231	0.9992
0.9892	1.3668	1.3672	0.9998
0.9613	1.4650	1.4652	0.9926
0.9905	1.5028	1.5027	0.9998
1.1526	1.6468	1.6619	0.9319
1.0021	1.6781	1.6781	0.9943
1.0434	1.7253	1.7218	0.9815
0.9987	1.7399	1.7411	0.9891
0.8546	1.8207	1.8202	0.9147
1.0111	2.2328	2.2330	0.9732
0.9989	2.2505	2.2462	0.9464
1.0125	2.3592	2.3591	0.9970
1.1125	2.4816	2.4849	0.9869
1.0017	2.5889	2.5888	1.0000
0.9979	2.8142	2.8142	1.0000
1.0094	2.9888	2.9887	0.9998
1.0000	3.1223	3.1225	0.9978
1.0005	3.2789	3.2788	0.9956
1.0307	3.4719	3.4725	0.9790

Table D.1-Continued

0.9859	3.5207	3.5206	0.9963
0.9808	3.6171	3.6180	0.9893
0.9147	3.7949	3.8091	0.9614
1.0534	4.0267	4.0308	0.9435
1.0615	4.4482	4.4531	0.9788
1.0117	4.5621	4.5651	0.9820
1.0555	4.6618	4.6609	0.9844

Table D.2 RFF1c impulse preserved

damp (%)	freq (Hz)	ex-freq (Hz)	mac
1.0038	0.5670	0.5670	0.9999
1.0071	0.7458	0.7458	0.9958
0.9855	0.7924	0.7922	0.9944
0.9840	0.8078	0.8079	1.0000
1.0111	0.8239	0.8240	0.9997
1.0039	0.8604	0.8604	0.9987
0.9988	1.1337	1.1337	1.0000
1.1855	1.1927	1.1954	0.9977
1.0003	1.2227	1.2227	1.0000
0.9958	1.2553	1.2552	1.0000
1.0956	1.3221	1.3231	0.9992
0.9891	1.3668	1.3672	0.9998
0.9612	1.4650	1.4652	0.9927
0.991	1.5028	1.5027	0.9998
1.1580	1.6465	1.6619	0.9289
1.0012	1.6781	1.6781	0.9941
0.9997	1.7252	1.7218	0.9814
1.0016	1.7398	1.7411	0.9864
0.8457	1.8205	1.8202	0.9151
1.0106	2.2328	2.2330	0.9727
0.9997	2.2505	2.2462	0.9452

Table D.2-Continued

1.0128	2.3592	2.3591	0.9972
1.1073	2.4815	2.4849	0.9879
1.0018	2.5889	2.5888	1.0000
0.9979	2.8142	2.8142	1.0000
1.0091	2.9888	2.9887	0.9998
1.0000	3.1223	3.1225	0.9977
1.0006	3.2789	3.2788	0.9956
1.0311	3.4719	3.4725	0.9796
0.9828	3.5206	3.5206	0.9961
0.9868	3.6171	3.6180	0.9900
0.9193	3.7943	3.8091	0.9555
1.0523	4.0268	4.0308	0.9437
1.0609	4.4482	4.4531	0.9791
1.0175	4.5616	4.5651	0.9823
1.0537	4.6617	4.6609	0.9848

Table D.3 RFF2c non-impulse preserved

damp (%)	freq (Hz)	ex-freq (Hz)	mac
0.9721	0.5671	0.5670	1.0000
0.9844	0.7459	0.7458	0.9992
0.9685	0.7922	0.7922	0.9987
0.9129	0.8094	0.8079	0.9999
0.9844	0.8241	0.8240	0.9934
0.9840	0.8606	0.8604	0.9687
0.9997	1.1337	1.1337	1.0000
0.9986	1.2227	1.2227	1.0000
1.0073	1.2552	1.2552	1.0000
1.0107	1.3231	1.3231	0.9999
0.9734	1.3670	1.3672	0.9999
0.9700	1.4651	1.4652	0.9931
0.9886	1.5030	1.5027	0.9998
1.1807	1.6006	1.6017	0.9999

Table D.3-Continued

1.1058	1.7182	1.7218	0.9803
1.1034	1.7401	1.7411	0.9709
0.9979	2.2335	2.2330	0.9855
1.0167	2.2507	2.2515	0.9557
1.0022	2.3592	2.3591	0.9998
1.0222	2.4833	2.4849	0.9800
0.9994	2.5888	2.5888	1.0000
1.0028	2.8143	2.8142	1.0000
1.0022	2.9888	2.9887	1.0000
1.0045	3.1223	3.1225	0.9976
0.9990	3.2789	3.2788	0.9968
1.0011	3.4729	3.4725	0.9846
1.0148	3.5196	3.5206	0.9992
0.8935	3.6197	3.6180	0.9658
1.0669	3.8046	3.8091	0.9935
1.0171	4.0282	4.0308	0.9864
0.9886	4.1156	4.1104	0.9360
1.1866	4.1989	4.1967	0.9591
0.9672	4.2930	4.3193	0.9696
1.0519	4.4496	4.4531	0.9931
0.9386	4.5682	4.5651	0.9954
1.0181	4.6615	4.6609	0.9995

Table D.4 RFF2c impulse preserved

damp (%)	freq (Hz)	ex-freq (Hz)	mac
0.9732	0.5671	0.5670	1.0000
0.8057	0.6700	0.6660	0.9670
0.9850	0.7459	0.7458	0.9992
0.9701	0.7922	0.7922	0.9987
0.9091	0.8094	0.8079	0.9999
0.9849	0.8241	0.8240	0.9933
0.9837	0.8606	0.8604	0.9689

Table D.4-Continued

0.9996	1.1337	1.1337	1.0000
0.9982	1.2227	1.2227	1.0000
1.0075	1.2553	1.2552	1.0000
1.0094	1.3231	1.3231	0.9999
0.9735	1.3670	1.3672	0.9999
0.9720	1.4651	1.4652	0.9934
0.9877	1.5030	1.5027	0.9998
1.1850	1.6007	1.6017	0.9999
1.1532	1.7186	1.7218	0.9816
1.1024	1.7401	1.7411	0.9723
0.9979	2.2335	2.2330	0.9855
1.0157	2.2507	2.2515	0.9548
1.0022	2.3592	2.3591	0.9998
1.0189	2.4833	2.4849	0.9801
0.9996	2.5888	2.5888	1.0000
1.0027	2.8143	2.8142	1.0000
1.0021	2.9888	2.9887	1.0000
1.0041	3.1223	3.1225	0.9977
0.9988	3.2789	3.2788	0.9968
1.0008	3.4729	3.4725	0.9842
1.0133	3.5194	3.5206	0.9993
0.9006	3.6197	3.6180	0.9672
1.0633	3.8048	3.8091	0.9939
1.0173	4.0282	4.0308	0.9868
0.9908	4.1155	4.1104	0.9391
1.1886	4.1988	4.1967	0.9565
0.9675	4.2927	4.3193	0.9698
1.0507	4.4495	4.4531	0.9934
0.9374	4.5677	4.5651	0.9957
1.0134	4.6614	4.6609	0.9995

Table D.5 RFF4c non-impulse preserved

damp (%)	freq (Hz)	ex-freq (Hz)	mac
1.0169	0.5672	0.5670	0.9998
1.0183	0.6707	0.6660	0.9475
1.0222	0.7458	0.7458	0.9996
0.9339	0.7926	0.7922	0.9932
1.0428	0.8078	0.8079	0.9999
0.9916	0.8240	0.8240	1.0000
1.0038	0.8604	0.8604	0.9975
0.9952	0.8967	0.8967	0.9670
0.9659	1.1339	1.1337	0.9999
1.1623	1.1958	1.1954	0.9912
0.9934	1.2227	1.2227	1.0000
0.9948	1.2556	1.2552	1.0000
1.0092	1.3235	1.3231	0.9997
1.0311	1.3670	1.3672	0.9997
1.0162	1.4654	1.4652	0.9984
1.0052	1.5031	1.5027	0.9996
0.9985	1.5739	1.5739	0.9002
1.0659	1.6008	1.6017	1.0000
1.1728	2.0780	2.0857	0.9949
1.0030	2.2330	2.2330	0.9771
1.0084	2.2503	2.2515	0.9520
0.9976	2.3591	2.3591	0.9988
1.0480	2.4826	2.4849	0.9745
0.9995	2.5888	2.5888	1.0000
0.9999	2.8143	2.8142	1.0000
0.9950	2.9888	2.9887	0.9997
1.0055	3.1224	3.1225	0.9933
0.9990	3.2789	3.2788	0.9864
1.0199	3.4729	3.4725	0.9541
0.9751	3.5209	3.5206	0.9932
1.0463	3.6205	3.6180	0.9944
1.0113	4.0289	4.0308	0.9467

Table D.5-Continued

1.0725	4.1142	4.1104	0.9414
1.1709	4.1979	4.1967	0.9222
1.0588	4.4459	4.4531	0.9875
1.0013	4.6611	4.6609	0.9956

Table D.6 RFF4c impulse preserved

damp (%)	freq (Hz)	ex-freq (Hz)	mac
1.0178	0.5672	0.5670	0.9998
1.0212	0.6711	0.6660	0.9533
1.0285	0.7458	0.7458	0.9996
0.9502	0.7931	0.7922	0.9874
1.0598	0.8073	0.8079	0.9998
0.9904	0.8240	0.8240	0.9999
1.0026	0.8604	0.8604	0.9979
0.9967	0.8967	0.8967	0.9713
0.9635	1.1338	1.1337	0.9999
1.1566	1.1958	1.1954	0.9907
0.9927	1.2227	1.2227	1.0000
0.9932	1.2556	1.2552	1.0000
1.0093	1.3234	1.3231	0.9997
1.0256	1.3670	1.3672	0.9997
1.0157	1.4654	1.4652	0.9983
1.0051	1.5031	1.5027	0.9996
0.9970	1.5739	1.5739	0.9093
1.0578	1.6008	1.6017	1.0000
1.1449	2.0781	2.0857	0.9956
1.0043	2.2330	2.2330	0.9798
1.0057	2.2503	2.2515	0.9548
0.9976	2.3591	2.3591	0.9987
1.0487	2.4825	2.4849	0.9746
0.9993	2.5888	2.5888	1.0000
1.0006	2.8142	2.8142	0.9999

Table D.6-Continued

0.9951	2.9888	2.9887	0.9998
1.0040	3.1224	3.1225	0.9962
0.9992	3.2789	3.2788	0.9868
1.0128	3.4729	3.4725	0.958X
0.9741	3.5207	3.5206	0.9940
1.0475	3.6205	3.6180	0.9943
1.0134	4.0288	4.0308	0.9456
1.0693	4.1140	4.1104	0.9417
1.1747	4.1979	4.1967	0.9265
1.0606	4.4460	4.4531	0.9882
0.9905	4.6605	4.6609	0.9945

APPENDIX E Power Spectral Density for Square Wave and Zero-Order Hold Ramped Input

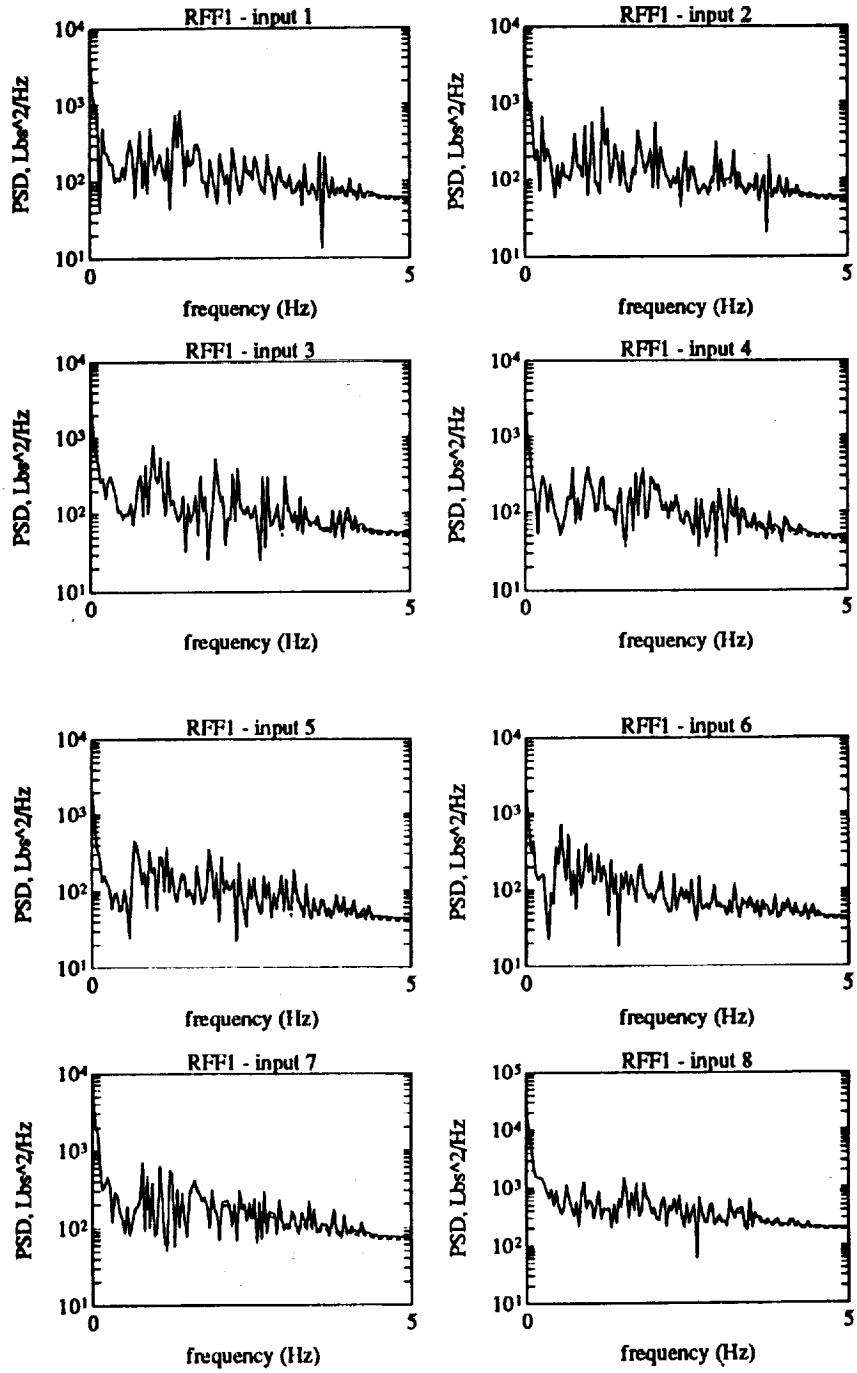

Figure E.1 PSD for RFF1 comparing impulse (dashed) and non-impulse (solid) preserved input

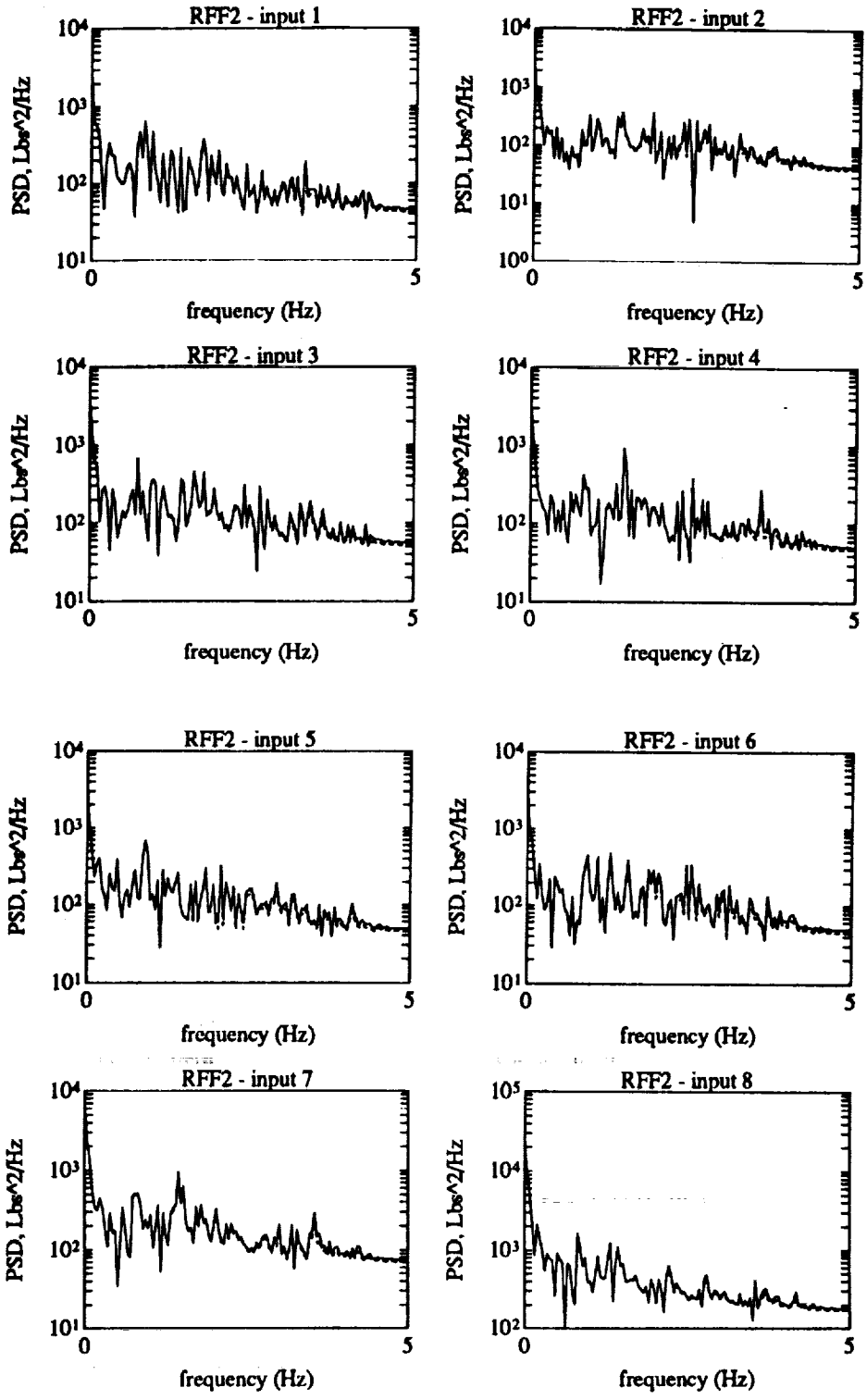

Figure E.2 PSD for RFF2 comparing impulse (dashed) and non-impulse (solid) preserved input

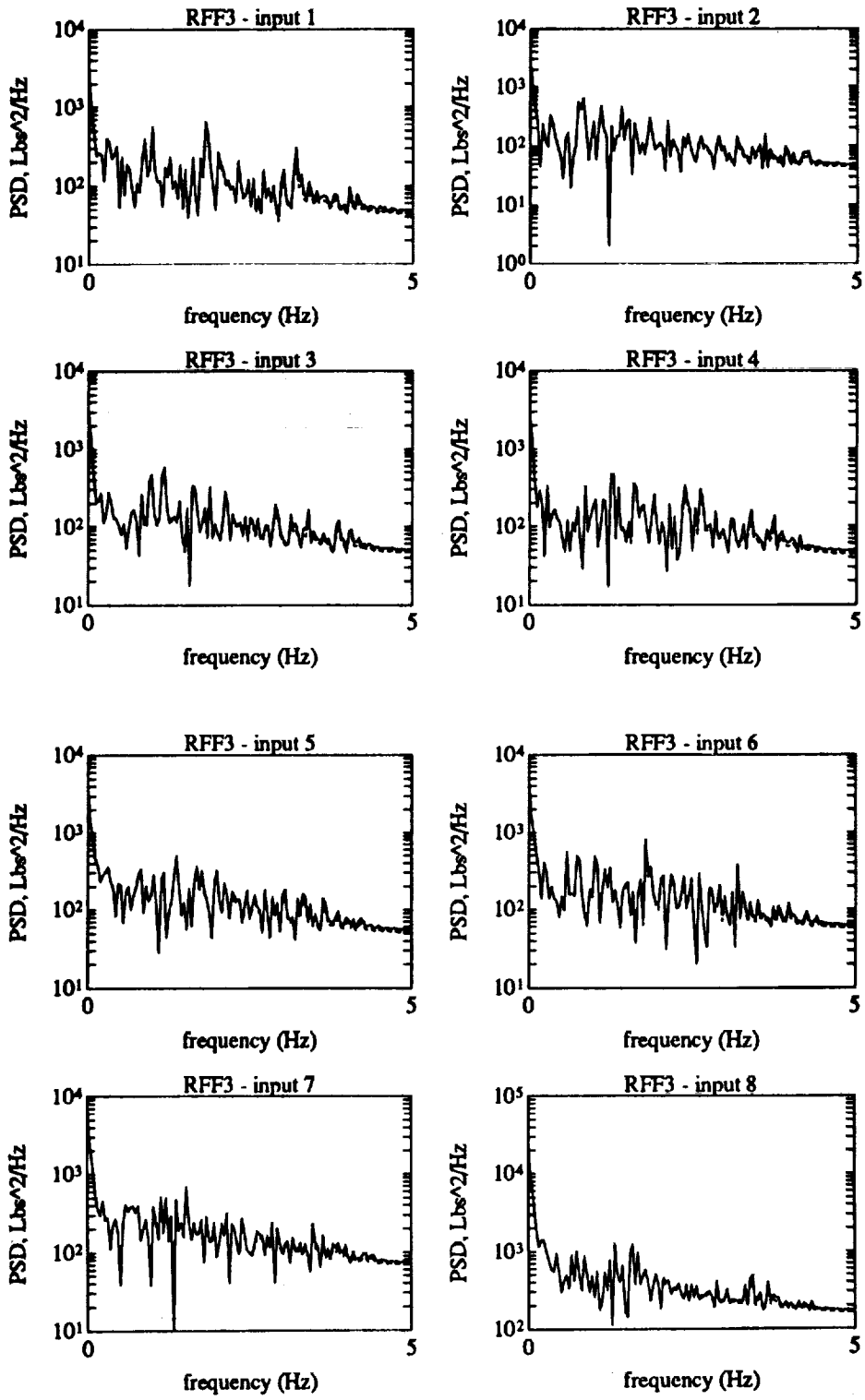

Figure E.3 PSD for RFF3 comparing impulse (dashed) and non-impulse (solid) preserved input

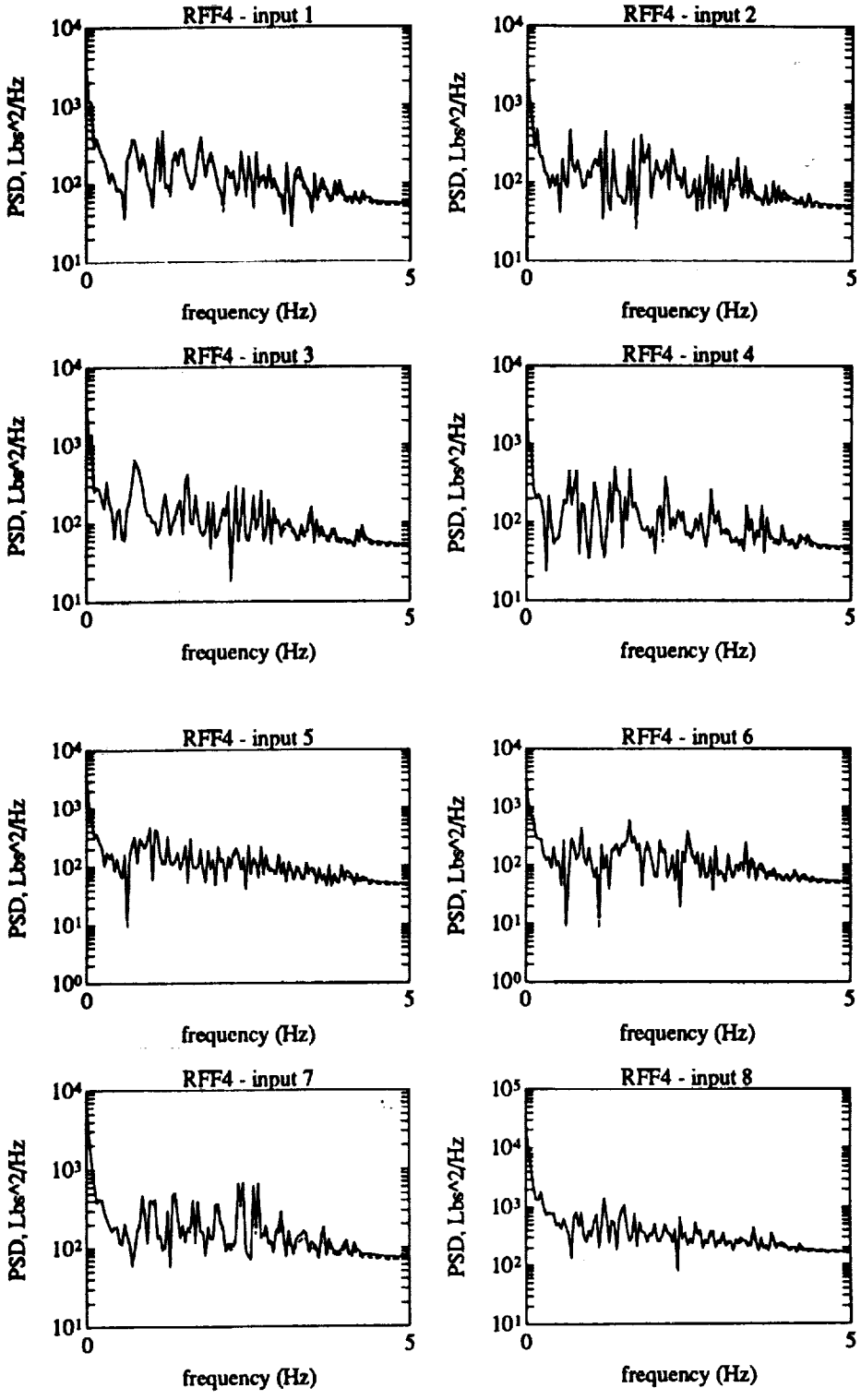

Figure E.4 PSD for RFF4 comparing impulse (dashed) and non-impulse (solid) preserved input

APPENDIX F Power Spectral Density for Square Wave and Thruster Model Input

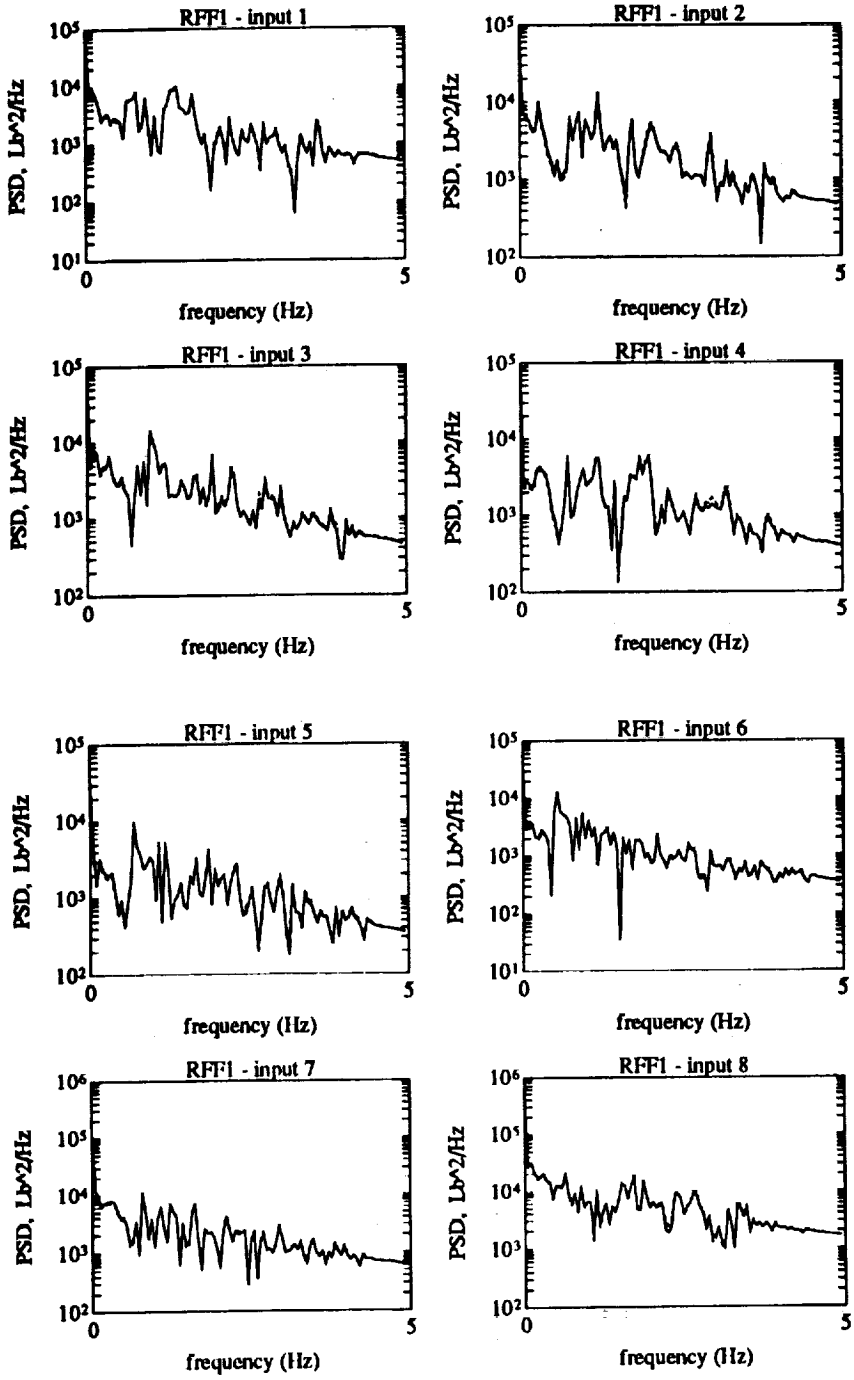

Figure F.1 PSD for RFF1 comparing impulse (dashed) and non-impulse (solid) preserved input

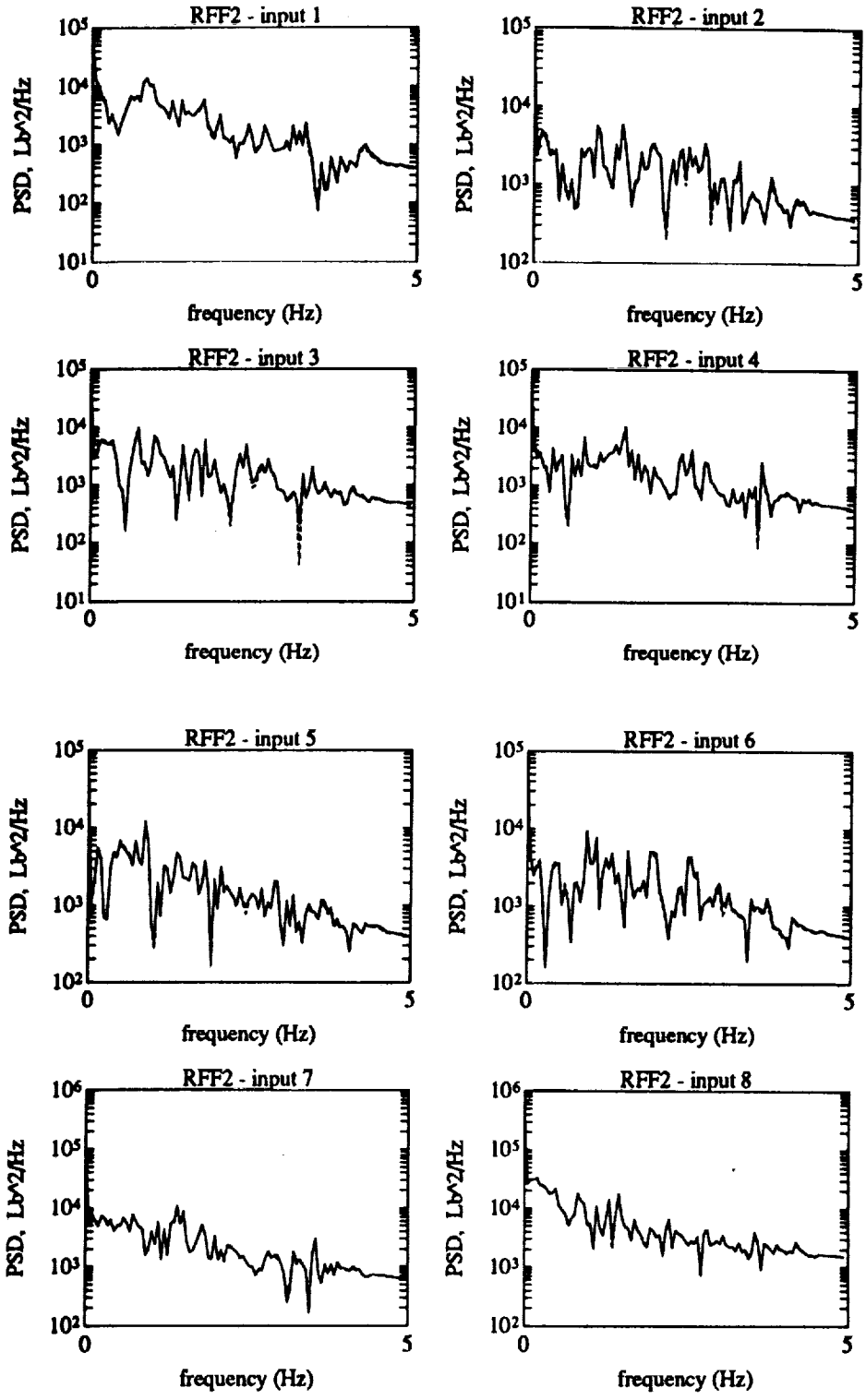

Figure F.2 PSD for RFF2 comparing impulse (dashed) and non-impulse (solid) preserved input

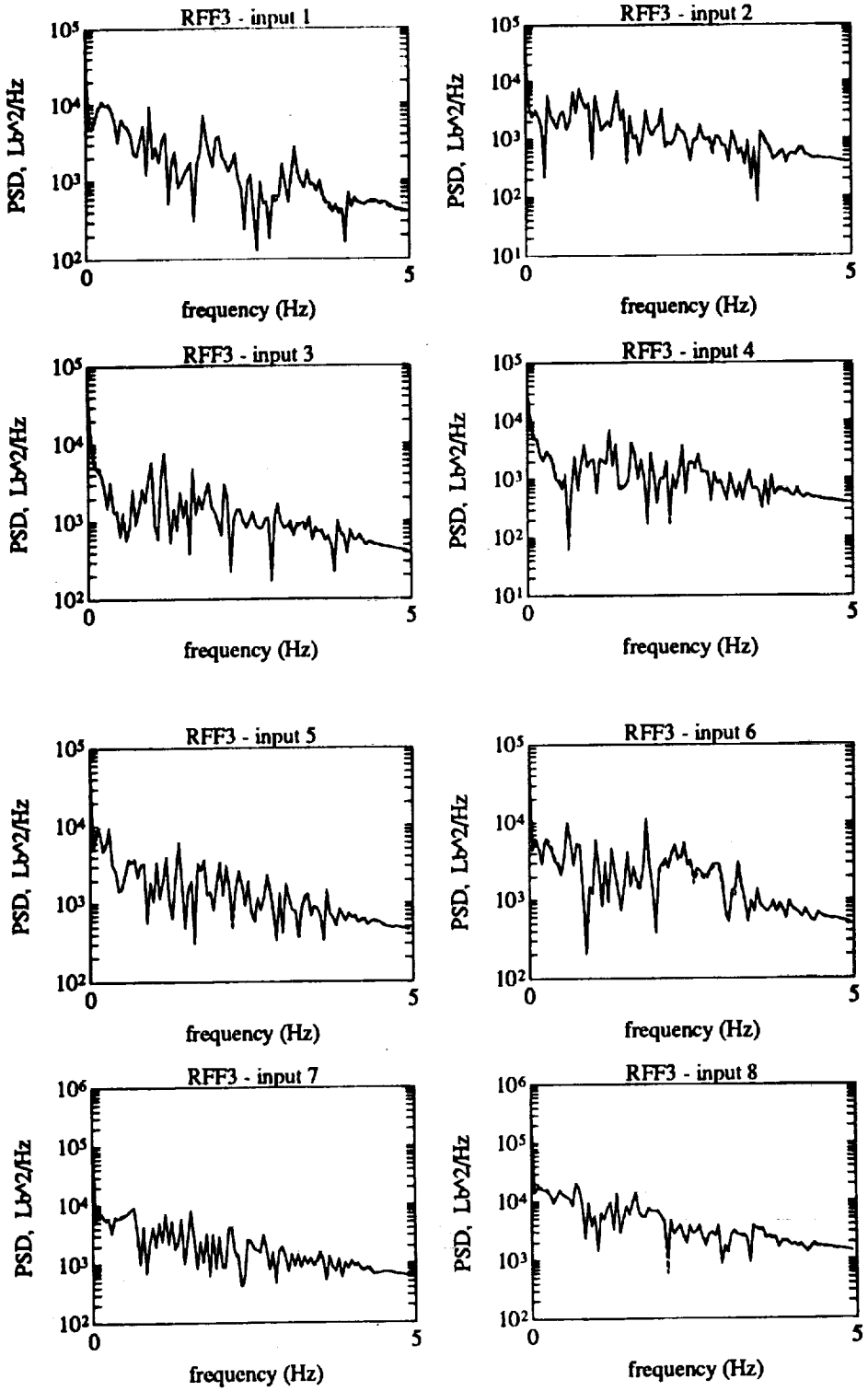

Figure F.3 PSD for RFF3 comparing impulse (dashed) and non-impulse (solid) preserved input

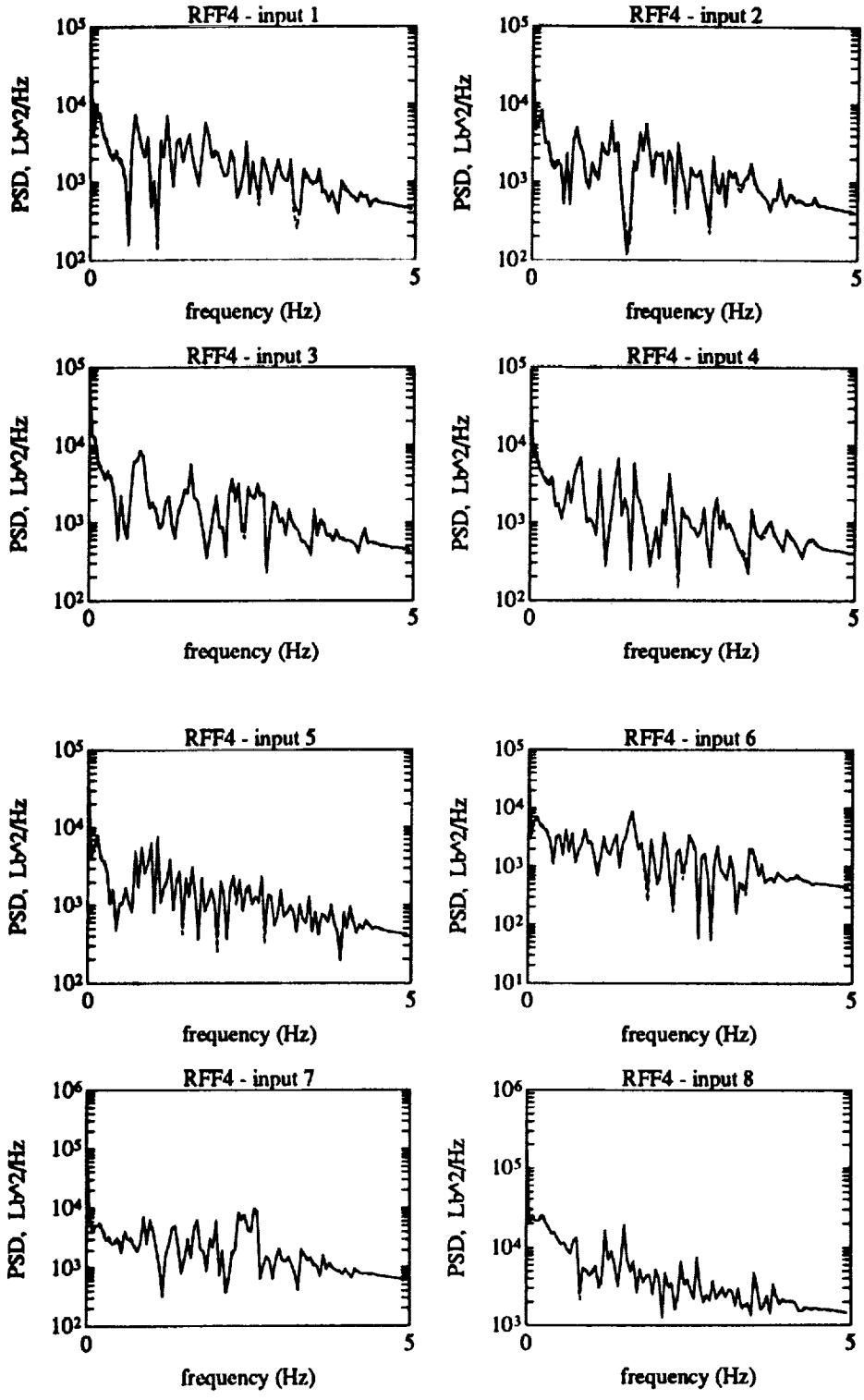

Figure F.4 PSD for RFF4 comparing impulse (dashed) and non-impulse (solid) prescrved input

APPENDIX G OKID-ERA Results for Square Wave and Thruster Model Input

Table G.1 Recovered modes using criterion 1 for RFF1c

non-impulse preserved			impulse preserved			exact
damp (%)	freq (Hz)	mac	damp (%)	freq (Hz)	mac	freq (Hz)
1.0580	0.5369	0.9485	---	---	---	0.5333
1.0482	0.5673	0.9998	0.9921	0.5671	1.0000	0.5670
0.9457	0.6710	0.9068	---	---	---	0.6660
0.9545	0.7457	0.9970	0.9930	0.7457	0.9992	0.7458
1.0106	0.7923	0.9924	0.9872	0.7924	0.9989	0.7922
1.0255	0.8073	0.9999	1.0318	0.8078	1.0000	0.8079
1.0213	0.8242	0.9959	0.9945	0.8240	0.9994	0.8240
0.9943	0.8604	0.9820	1.0018	0.8604	0.9985	0.8604
0.9820	1.0012	0.9825	0.9489	1.0021	0.9798	1.0033
0.9944	1.1337	1.0000	0.9993	1.1337	1.0000	1.1337
0.9943	1.1958	0.9939	0.9557	1.1954	0.9998	1.1954
0.9916	1.2231	1.0000	0.9969	1.2227	1.0000	1.2227
1.0011	1.2552	1.0000	1.0043	1.2553	1.0000	1.2552
1.0036	1.3239	0.9951	1.0499	1.3239	0.9986	1.3231
1.0066	1.3668	0.9998	1.0062	1.3673	0.9999	1.3672
1.0343	1.4675	0.9258	---	---	---	1.4652
1.0227	1.5030	0.9997	1.0049	1.5030	0.9997	1.5027
0.9958	1.6015	0.9999	0.9627	1.6020	0.9999	1.6017
0.9153	1.6784	0.9937	1.0032	1.6782	0.9960	1.6781
---	---	---	1.0617	1.7204	0.9940	1.7218
---	---	---	0.9927	1.7407	0.9904	1.7411
1.0646	1.7498	0.9383	1.0640	1.7603	0.9689	1.7610
1.1829	1.7943	0.9846	0.9933	1.7970	0.9386	1.7956
1.0737	1.9012	0.9236	---	---	---	1.8905
---	---	---	1.0681	1.9472	0.9538	1.9463
1.0070	2.0307	0.9994	0.9907	2.0299	1.0000	2.0297
1.1295	2.0902	0.9902	1.1163	2.0857	0.9985	2.0857

Table G.1-Continued

---	---	---	1.0163	2.1155	0.9672	2.1163
1.0092	2.2331	0.9590	---	---	---	2.2330
0.9751	2.2500	0.9479	0.9989	2.2503	0.9506	2.2515
1.0301	2.3598	0.9896	0.9903	2.3590	0.9959	2.3591
1.0083	2.4834	0.9817	1.0000	2.4831	0.9866	2.4849
0.9858	2.5898	1.0000	0.9933	2.5888	1.0000	2.5888
0.9979	2.8135	0.9999	1.0099	2.8142	0.9998	2.8142
0.9655	2.9879	0.9990	0.9895	2.9887	0.9998	2.9887
1.0709	3.1232	0.9953	1.0046	3.1232	0.9877	3.1225
1.9718	3.2777	0.9960	0.9836	3.2791	0.9822	3.2788
1.0407	3.4734	0.9823	---	---	---	3.4725
0.9325	3.5190	0.9185	1.0386	3.5209	0.9539	3.5206
0.8670	3.6168	0.9909	0.8466	3.6204	0.9843	3.6180
---	---	---	1.0817	3.6856	0.9877	3.6905
0.9053	3.8098	0.9991	0.9889	3.8100	0.9992	3.8091
1.0171	3.8635	0.9936	1.1408	3.8648	0.9949	3.8930
0.9135	4.0293	0.9389	---	---	---	4.0308
1.0150	4.0676	0.9347	---	---	---	4.0592
---	---	---	0.9901	4.3206	0.9986	4.3193
0.8561	4.3681	0.9694	1.1166	4.3859	0.9934	4.3812
0.8674	4.4045	0.9487	---	---	---	4.4215
---	---	---	0.9397	4.4501	0.9946	4.4531
---	---	---	0.9686	4.5579	0.9098	4.5651
0.9629	4.6448	0.9939	1.0252	4.6504	0.9884	4.6609

APPENDIX H Output Ranking From Gram-Schmidt Orthogonalization

Table H.1 Ranking (output no.) of outputs from Gram-Schmidt

RFF1n	RFF2n	RFF4n	RFF1234n	Concatenation
46	46	46	46	46
53	53	29	2	53
29	28	39	59	51
56	34	51	32	2
49	55	58	52	28
42	12	13	53	58
57	52	2	61	29
28	37	28	29	55
2	39	14	39	22
32	29	53	56	41
47	9	40	55	39
39	41	20	41	59
61	47	47	28	61
41	24	55	4	47
59	40	41	47	3
52	48	3	49	20
3	54	56	3	43
33	3	48	43	49
34	2	43	58	56
30	43	1	34	19
1	44	19	19	1
44	1	44	44	34
58	17	34	1	44
48	30	30	30	52
43	51	52	48	30
51	49	49	51	48
36	32	36	36	36
50	50	50	50	50
37	19	22	37	40

Table H.1-Continued

40	22	25	25	25
35	15	42	17	37
22	25	37	24	24
23	20	45	23	45
25	42	24	22	17
18	45	23	45	42
55	36	15	20	23
45	5	31	42	32
24	13	9	13	9
38	10	32	15	5
9	27	11	5	15
7	7	59	9	18
13	23	61	21	13
20	11	18	18	7
5	18	27	27	57
15	59	5	57	11
11	61	7	7	27
27	21	21	11	21
21	35	35	35	35
31	38	38	38	38
8	57	57	26	26
10	8	10	8	8
16	26	8	10	60
60	58	16	60	4
4	4	60	16	10
26	14	12	4	16
12	16	26	14	14
14	6	4	12	12
19	60	17	33	33
17	56	33	31	54
54	31	6	54	31
6	33	54	6	6

APPENDIX I Data Acquisition Errors

The following is taken from Ref. 23. The data acquisition errors (noise model) consisted of the following

Sampling Delay Error

Scale Factor Error

Electrical Noise

Bias Error

Digitization Error

All random numbers were generated with a normal distribution. Measurements were converted to g's before adding noise. That is, the multiplying factor was 1/386 since the measurements were in in/sec^2.

Sampling delay error was randomly generated for each output by using the time delays given in Table I. Response at delayed time (noise data) was obtained by linearly interpolating the response at the undelayed time (i.e., clean data).

Table I Sampling delay errors

Bus time uncertainty	0-1 milli sec.
BIU time uncertainty	+/-0.05 milli sec.
Local MDM time uncertainty	+/-0.15 milli sec.
MDM channel skew	0-1.5 milli sec.

Scale factor error was randomly generated for each output by using Table II.

Table II Scale factor errors

Temperature variation in accelerometer	+/-1.5%
MDM Signal conditioning card	+/-0.5%
Accelerometer internal axis misalignment	+/-0.1%
Mounting misalignment with Space Station coordinate system	+/-0.0004%
Repeatability over 3 years	+/-0.278%
A/D nonlinearity	+/-0.5%

The response at each time was multiplied with the sum of the scale factor errors and this number was added to the response itself.

Electrical noise was randomly generated for each output with a maximum amplitude of 10 micro g. This signal was then filtered with a band pass filter allowing only -1 to 5 Hz components to remain. The Root Mean Square (RMS) value was computed for this filtered noise signal. The filtered noise signal was divided by the RMS value and this new noise signal was added to the response.

Bias error was randomly generated and added to each output by using Table III.

Table III Bias errors

Temperature	+/-1 milli g
Launch stress	+/-0.1 milli g
Repeatability over 3 years	+/-2.8 milli g

Digitization error was performed using Table IV.

Table IV Digitization errors

Ranges (milli g)	Resolution (milli g)
1.28	0.002
7.83	0.006
27.5	0.018
86.5	0.054

REPORT DOCUMENTATION PAGE

Form Approved
OMB No. 0704-0188

1. AGENCY USE ONLY (Leave blank)	2. REPORT DATE	3. REPORT TYPE AND DATES COVERED
	August 1993	Contractor Report

4. TITLE AND SUBTITLE
System Identification for Space Station Freedom Using Observer/Kalman Filter Markov Parameters

5. FUNDING NUMBERS
G NAG1-1416
WU 590-14-31-01

6. AUTHOR(S)
Michael Papadopoulos and Robert H. Tolson

7. PERFORMING ORGANIZATION NAME(S) AND ADDRESS(ES)
Joint Institute for Advancement of Flight Sciences
The George Washington University
Langley Research Center, Hampton, VA 23681-0001

8. PERFORMING ORGANIZATION REPORT NUMBER

9. SPONSORING/MONITORING AGENCY NAME(S) AND ADDRESS(ES)
National Aeronautics and Space Administration
Langley Research Center
Hampton, VA 23681-0001

10. SPONSORING/MONITORING AGENCY REPORT NUMBER
NASA CR-191521

11. SUPPLEMENTARY NOTES
Originally published as Master of Science Thesis by the first author.
NASA Technical Monitor: Raymond G. Kvaternik

12a. DISTRIBUTION/AVAILABILITY STATEMENT
Unclassified - Unlimited
Subject Category 18

12b. DISTRIBUTION CODE

13. ABSTRACT *(Maximum 200 words)*

The Modal Identification Experiment (MIE) is a proposed experiment to define the dynamic characteristics of Space Station Freedom. Previous studies have emphasized free-decay modal identification. The feasibility of using a forced response method (Observer/Kalman Filter Identification (OKID))is addressed. The interest in using OKID is to (1) determine the input mode shape matrix which can be used for controller design or control-structure interaction analysis, and (2) investigate if forced response methods may aid in separating closely spaced modes. A model of the SC-7 configuration of Space Station Freedom was excited using simulated control system thrusters to obtain acceleration output. It is shown that an 'optimum' number of outputs exists for OKID. To recover global mode shapes, a modified method, called Global-Local OKID, was developed. This study shows that using data from a long forced response followed by free-decay leads to the 'best' modal identification. Twelve out of the thirteen target modes were identified for such an output.

14. SUBJECT TERMS	15. NUMBER OF PAGES
Space Station Freedom, modal identification, system identification	122
	16. PRICE CODE A06

17. SECURITY CLASSIFICATION OF REPORT	18. SECURITY CLASSIFICATION OF THIS PAGE	19. SECURITY CLASSIFICATION OF ABSTRACT	20. LIMITATION OF ABSTRACT
Unclassified	Unclassified	Unclassified	